Alma Mater Studiorum – Università di Bologna

DOTTORATO DI RICERCA IN

Scienze Ambientali: Tutela e Gestione delle Risorse Naturali

XXV Ciclo

Settore Concorsuale di afferenza: 04 / A3 – Geoscienze
Settore Scientifico disciplinare: GEO / 05 – Geologia Applicata

THE INFLUENCE OF FRACTURES ON VULNERABILITY TO POLLUTION OF A CARBONATE AQUIFER: MONTE CONERO (ITALY)

Tesi presentata da: Dott.ssa Elizabeth Noemí Díaz General

Coordinatore:
Prof. Enrico Dinelli

Tutore:
Prof. Giovanni Gabbianelli

Relatore:
Prof. Marco Antonellini

Esame finale anno 2013

PREFACE

About the author.

Elizabeth is an international student at the University of Bologna thanks to the exchange program Erasmus Mundus External Cooperation Windows. She comes from Chile where she was graduated with the professional title of Civil Engineer in Geography and the academic degree of Bachelor in Sciences of Engineering at the University of Santiago of Chile. This professional formation has specialized to Elizabeth in the area of the Geosciences, specifically focused on territorial planning, GeoInformatics and Geographic Information Systems (SIG), and Environmental Assessment. Her undergraduate thesis was developed in the area of the planning of the protection activities in a National Park through the development of a tool for the decision making.

ABSTRACT

The carbonate outcrops of the anticline of *Monte Conero* (Italy) were studied in order to characterize the geometry of the fractures and to establish their influence on the petrophysical properties (hydraulic conductivity) and on the vulnerability to pollution. The outcrops form an analog for a fractured aquifer and belong to the *Maiolica* Fm. and the *Scaglia Rossa* Fm. The geometrical properties of fractures such as orientation, length, spacing and aperture were collected and statistically analyzed. Five types of mechanical fractures were observed: veins, joints, stylolites, breccias and faults. The types of fractures are arranged in different sets and geometric assemblages which form fracture networks. In addition, the fractures were analyzed at the microscale using thin sections. The fracture age-relationships resulted similar to those observed at the outcrop scale, indicating that at least three geological episodes have occurred in *Monte Conero*. A conceptual model for fault development was based on the observations of veins and stylolites. The fracture sets were modelled by the code FracSim3D to generate fracture network models. The permeability of a breccia zone was estimated at microscale by and point counting and binary image methods, whereas at the outcrop scale with Oda's method. Microstructure analysis revealed that only faults and breccias are potential pathways for fluid flow since all veins observed are filled with calcite. According this, three scenarios were designed to asses the vulnerability to pollution of the analogue aquifer: the first scenario considers the *Monte Conero* without fractures, second scenario with all observed systematic fractures and the third

scenario with open veins, joints and faults/breccias. The fractures influence the carbonate aquifer by increasing its porosity and hydraulic conductivity. The vulnerability to pollution depends also on the presence of karst zones, detric zones and the material of the vadose zone.

Key words:

- Carbonate fractured aquifer
- Mechanical fracture types
- Petrophysical properties
- Fault development conceptual model
- Discrete Fracture Networks (DFNs)
- Vulnerability to pollution

TABLE OF CONTENTS

CHAPTER 1: INTRODUCTION

Monte Conero, *Le Marche*, Italy, the area of interest for this research is a coastal aquifer consisting of carbonate rocks, immersed in a natural area of value for the biodiversity and for tourism (Parco del Conero, 2011). It is surrounded by agricultural fields on one side (Regione Le Marche, 2010) and by the Adriatic Sea on the other side. This territory has been affected by violent tectonic episodes during its geologic past and, as a consequence, the aquifer is intensely fractured making it more vulnerable to groundwater pollution (Fagundo *et al.*, 2002; Evans *et al.*, 2005; Cherubini, 2008). Carbonate aquifers are also very sensitive to changes in recharge patterns (Worthington & Ford, 2009). In addition, fractures in carbonate rocks are prone to preferential dissolution creating so-called karstic aquifers (Birk *et al.*, 2003).

Rock fractures typically form patterns that reflect the stress history and geologic history of the area. In this study fractures are studied through a geometric characterization on carbonate outcrops of, *Monte Conero* (*Le Marche* Region, Italy, Figure 1-1), with particular emphasis on the qualitative and quantitative analysis of mechanical types of fractures. All mechanical types of fractures (veins, joints, stylolites, etc) are important because they are related to each other mechanically and geometrically. The fractures determine to a large extent the hydraulic conductivity of the aquifer because they can be either barriers or pathways for movement such as veins and stylolites (Antonellini & Aydin, 1994; Mollema & Antonellini, 1998; Aydin, 2000; Agosta *et al.*, 2007; Schultz & Fossen, 2008). Understanding the relationships between the mechanical origin of the fractures and its current distribution will help to better quantify the sensitivity of fractured carbonate aquifers to pollution and to better manage these kinds of aquifers.

Figure 1-1: View of the *Monte Conero* from Sirolo(sud)

This research seeks to study the influence of fractures on vulnerability to pollution in the carbonate aquifer of *Monte Conero*. We analyzed the fracture distribution and its influence on petrophysical properties of the aquifer. Fractures were measured in fieldwork elaborating fracture maps and using compass surveying. Porosity and permeability of rock were estimated with theoretical models based on observation of microscopic data and on fracture network model elaborated from discrete fractures. A conceptual model about fault development was built from observations of the fracture age-relationships. The changes of the petrophysical properties were analyzed in three scenarios and the vulnerability to pollution was estimated for each one using an index.

The specific objectives are:

1. To characterize the fractures and the hydrogeology of a fractured carbonate aquifer (*Monte Conero*)
2. To identify the relationship between mechanical types of fractures.
3. To study the relation between the spatial distribution of the fractures, the tectonics and the lithology in the study area.

4. To establish the influence of fractures on the petrophysical properties of the aquifer (porosity, permeability, hydraulic conductivity).
5. To determine the aquifer vulnerability of Monte Conero to pollution coming from above.

Previous field based studies about fractured aquifers and reservoirs were focused on particular rock type, for example porous sandstones with fault and compaction band development (Antonellini & Aydin 1994; 1995. Antonellini *et al*, 1994; Mollema *et al*., 1996) or on Dolomite with the development of joint-zones (Mollema & Antonellini, 1999; Antonellini & Mollema, 2000) or on deformation in carbonates which consider various generations of stylolites, faults and fractures (Berkowitz, 2002; Tondi *et* al., 2006; Petracchini *et al*., 2012). Studies on fractured carbonate aquifers (as opposed to carbonate petroleum reservoirs) are often focused on the relation between dissolution and fractures as in karst terrains occurs (e.g. Kaufmann & Braun, 2000; Worthington & Gunn, 2009; Worthington & Ford, 2009). Other authors have tried to relate the distribution of all different types of fractures to a particular setting such as a fold or fault-realted fold (e.g. Mollema & Aydin (1997); Petracchini *et al*., 2012; Shackleton et al. 2011). According to these last studies it is important to consider all types of fractures to be able to understand fluid flow in a fractured aquifer since they all may contribute in different ways to fluid flow circulation. Therefore, in this study, we also have studied all types of fractures in relation to the lithology and the setting for our analysis since it provides a most realistic approach for fluid flow in a fractured aquifer.

Natural rock fractures exposed above the earth's surface or hidden below are typically studied with techniques such as analysis of outcrops, fracture maps, windows scale in outcrops, areal images, thin sections, stereological techniques, geophysical

approaches, drill holes, core samples, or trace testing (Berkowitz, 2002). We have studied fractures by outcrop analysis in which field data, such as fracture type, orientation, length, spacing and aperture were surveyed.

The conceptual understanding of fracture media involves the assumption of a fractured rock mass as a homogeneous, anisotropic porous medium (Oda, 1985) with anisotropic permeability due to fractures (Snow, 1969) and dual porosity, in the case of porous rocks like sandstone. The complexity of fracture geometry is idealized in several ways. One single rock fracture may be idealized as a smooth parallel plane model of constant aperture and infinite extent (Baghbanan & Jing, 2007; Bear *et al*. (ed.), 1993; Snow, 1969; Xu & Dowd, 2010) alternatively; fractures may be described as disks. The geometry of a typical racture surfaces can also be described with fractal properties and the power law (Baghbanan & Jing, 2007; Berkowitz, 2002).

The process of fluid flow in fractured media has been addressed vastly from the petroleum engineering perspective with the scope of exploring and producing from fractured petroleum reservoirs (Baghbanan & Jing, 2007). In this field, the transport problem has been studied for oily contaminants, solutes or reactive. But fractured reservoirs also are of interest to others disciplines such as hydrology, mining engineering, storage of CO_2 and the use of geothermal energy. One conceptual model of a fractured aquifer is structured by the anisotropic Darcy's law (Snow, 1969; Worthington & Gunn, 2009). Petrophysical properties, potential flow and flow properties data are incorporated in the fractured aquifer models. The approach for the flow analysis uses flow equations where the principle of mass balance is applied (Chen *et al*., 2006).

The Reynolds equation (Yeo & Ge, 2005), which is derived from a “local cubic law” (Snow, 1969) is a quantitative way of describing fluid flow in single fractures. However, questions remain about the applicability of this equation in rough geometries, since this was formulated for smoothened surfaces. Other studies propose the use of methods to quantify fluid flow, such as drawing a sphere, and nuclear magnetic resonance imaging (Baghbanan & Jing, 2007; Berkowitz, 2002).

One line of models that may simulate flow and transport in networks of highly interconnected fractures incorporate the concept of Representative Elementary Volume (REV). In these models, the individual fractures are not considered individually but their effect on petrophysical properties is averaged over a particular rock volume of choice. The size of the representative elementary volume depends on the scale of the factures and faults (Baghbanan & Jing, 2007; Bear *et al*. (ed.), 1993). These models can be deterministic or stochastic (based in random fields and probability distributions). Stochastic models are of various kinds such as Monte Carlo analysis, ‘black box’ formulations and/or hierarchical conceptualizations (e.g. fractal and percolation concepts) (Baghbanan & Jing, 2007; Bear *et al*. (ed.), 1993). Deterministic models are preferred for their better quantification of many flow and transport phenomena and, therefore, they can account directly for the effect on individual fractures (Baghbanan & Jing, 2007).

The numerical method of Finite Element is typically used for flow analysis in rock masses (Oda, 1986), it allows to better representation of the irregularity of the fracture, compared, for example, with the method of Finite Differences (Fetter, 2001). This type of approach allows to consider the fracture aperture as a variable.

In this research we have studied the flow through the petrophysical properties using the Oda's conceptual model developed during 1985-1986 and derived from the anisotropic Darcy's law (Harstad *et* al, 1996). Modelling approaches have been done integrating Discrete Fracture Network and the Oda's method. In this field of fracture modelling, since the late 1970's the concept of discrete fracture networks was introduced and since then several of codes have been developed to represent them numerically (e.g. Dershowitz *et al.*, 1993; Pashin *et al.*, 2008; Xu & Dowd, 2010; Massart *et al.*, 2010). Because it is impossible to characterize every single fracture, modelling of fracture networks with Discrete Fracture Network (DFN) models (Xu and Dowd, 2010; Jing, 2003) may be used, combining stochastic modelling, Monte Carlo simulations and fracture properties measured for example on outcrops of rocks. FracSim3D, elaborated by Xu & Dowd (2010), is one of the available programs in this subject and is the code used in this study, which offers representations in two and three dimensions and statistical tools for the analysis of the results.

To provide input for the DFN, a part of this research was focused on fracture geometry characterization and identification and characterization of discrete fractures which form pathways for fluid flow (Dershowitz *et al.*, 2004).

Vulnerability to pollution in aquifers is typically evaluated using conceptual models which are materialized in an index and represented on cartography. These models are based on variables that represent the properties of the aquifer that influence the vulnerability (Vías *et al.*, 2010). Some of these models are: DRASTIC, SINTACS, GOD, among others (Polemio *et al.*, 2009). The application of these indexes has a place in territorial management and decision making, but recently has been introduced in the earth sciences (e.g. Corniello *et al.*, 2004; Alvino *et al.*, 1998; Ducci, 2010; Marsico *et al.*, 2004;

Yu *et al.*, 2010). Due to the complex nature of fracture aquifers, their vulnerability is not easily assessed. However, some authors such as Denny *et al.* (2007) have tried to incorporate to these indexes the influence of fractures through the addition of variables, such as length, orientation and intensity of fractures, using methodologies applicable only at macro-scale. We have decided to use the DRASTIC index (Aller *et al.*, 1985), because we consider that is one of the most complete indexes. We keep the original characteristics of the index for our analysis rather than the modified version for fractures (Denny *et al.*, 2007), since our study area is too small and characteristics as fracture length, orientation and intensity are already considered into DFN models. Models of vulnerability to pollution have been applied to evaluate the vulnerability to saltwater intrusion and pesticides.

This research aims to contribute in the understanding of fractured carbonate aquifers by is analyzing all types of fractures in carbonate outcrops and defining its relative importance to fluid flow. Both Discrete Fracture Networks and Vulnerability Assessment have been studied previously only by a single group of fractures; we intend to establish observations for a best application of them according to the type of fracture in carbonate aquifers. The fracture distributions have not previously been documented in the outcrops of Monte Conero and therefore the results of this study may contribute also to the knowledge of this particular area. Studies of Monte Conero are scarce especially those related to hydrogeology (Nanni & Vivalda, 2009; Nanni, 2011). Despite the fact that the fresh water present in the *Monte Conero* aquifer is not used for human consumption, this aquifer is important in naturalistic term sunder the tutelage of the Natura 2000 Network (Regione Le Marche, 2011). The area has an important environmental value, and therefore it is essential to keep it free of pollution. The outcrops of *Monte Conero* are representative for many carbonate outcrops in the Appenines as well as for carbonate aquifers and reservoirs below ground. They are well conserved and well exposed thus

Monte Conero is a good analogue for carbonate fracture aquifers and reservoirs. This study aims to contribute in the science of predicting the location of potential barriers or migration pathways in fractured carbonate aquifers.

According to the objectives of our research, this thesis is structured in 6 chapters:

- *Chapter 1: Introduction.* The Problem and objective of the research and the state of the art of the topics involved in this study are described in this section.
- *Chapter 2: Description of the Study Area.* The geological and hydrological settings of the study area are described in this chapter.
- *Chapter 3: Fracture Characterization*. The observations made on outcrops and on thin sections are described in this chapter. The characteristics and properties of the different types of fractures, the systematic sets and their geometrical relationships are described. The discussion of this chapter is focused on the analysis and relation of fractures in terms of their geological formation, their geological age and their contribution to the development of faults.
- *Chapter 4: Modelling of the Fracture Network Geometry.* The fracture data are analyzed quantitatively using the code FracSim3D for the generation of Discrete Fracture Networks (DFNs) models. The resulting models are used to estimate the petrophysical properties of the aquifer employing the Oda's method.
- *Chapter 5: Assessment of the Vulnerability to Pollution of the Aquifer*. The fracture characterization and the aquifer characteristics are integrated into the vulnerability model DRASTIC and represented in thematic maps in order to evaluate the vulnerability of the aquifer in different scenarios.
- *Chapter 6: Conclusions*. In this section final conclusions about the research are drawn.

CHAPTER 2: DESCRIPTION OF THE STUDY AREA

The study area is located in *Le Marche* region, in the centre of Italy along the coast of the Adriatic Sea to the south of Ancona (Figure 2-1). The research is focused on *Monte Conero*, a limestone promontory 572 metres high and with an estimated surface area of 3500 metres by 2500 metres. This is the only location along the Adriatic Sea from Venice to the *Puglia* region with a steep cliff coast. Since 1987, the land is protected as a Regional Park that extends over 6,011 ha. but tourism and agriculture is allowed in the area. In the past the area has been subjected to strong tectonic activity causing folding and fracturing of the sedimentary layers and the aquifer. Surface runoff is intermittent and groundwater is still poorly studied. In the following sections the geological and hydrological aspects of *Monte Conero* are described.

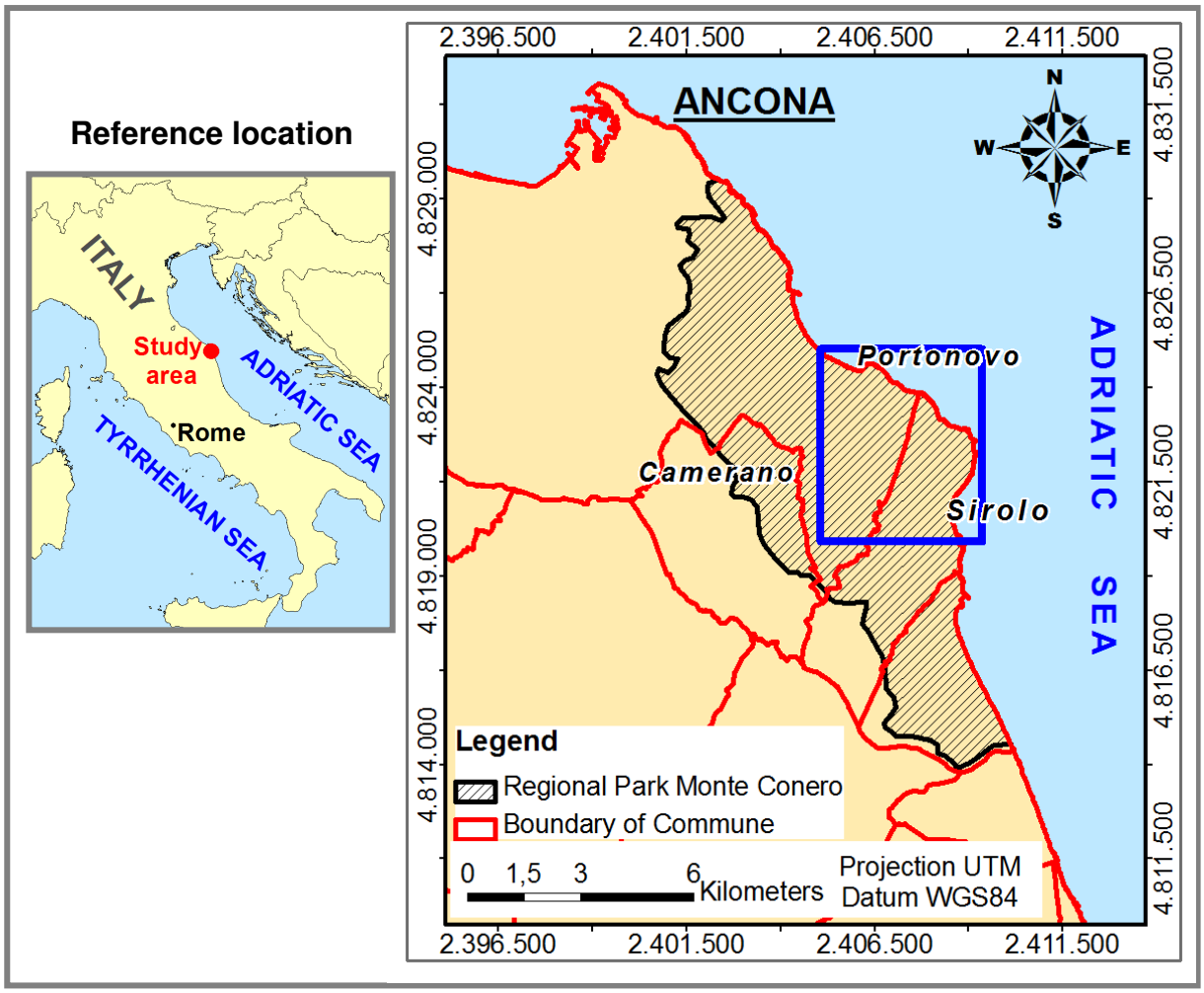

Figure 2-1: Location of the Study Area. Base cartograohy courtesy of *Istituto Superiore per la Protezione e la Ricerca Ambientale di Le Marche* and ESRI database

2.1 Geological Setting

2.1.1 Sedimentological characteristics

The geological formations of the *Monte Conero* were principally formed by marine sedimentation (Montanari & Sandroni, 1995). It was a slow process of sedimentation of pelagic calcareous mud with a large number of remains of unicellular planktonic microorganisms. In addition in an environment with stagnant seawater – there was also accumulation and preservation of organic matter resulting in the deposits of marls (limestone with clay). Later, the pelagic sedimentation was becoming increasingly more

calcareous and thinner. In the Eocene the pelagic mud was mixed with clay minerals of continental origin. After the beginning the compression regime (see Section 2.1.2), in the Lower Pliocene, the sedimentation was characterized by sandy turbidites. In the Upper Miocene the sedimentation was characterized by evaporites. Many layers are characterized with lenses and nodules of flint enclosed in the limestone, they have been formed by concentrations of amorphous silica derived from the deposit of microorganism of silica, such as radiolarians (Montanari & Sandroni, 1995).

a. <u>Sedimentological sequence</u>

The *Conero*'s rock formations are part of the second half of the Umbria-Marche stratigraphic succession, ranging from the *Maiolica* Fm. (Early Cretaceous) until Plio-Pleistocene deposits (Figure 2-2)**.** In the Umbria-Marche stratigraphic sequence a part of the succession are the *Maiolica* Fm., the *Marne a Fucoidi* Fm., the *Scaglia Bianca* Fm. and the *Scaglia Rossa* Fm. (Bortolotti *et* al, 1994; Montanari & Sandroni, 1995). However, in the *Monte Conero* the stratigraphic sequence is different from the rest of the territory of the Apennines Umbria-Marche (Montanari & Sandroni, 1995). The *Marne a Fucoidi* Fm. has a smaller thickness (10 m v/s 60 m). The *Scaglia Bianca* Fm. has typically a thickness of 80-100 metres, but in the *Monte* Conero this formation and the boundary between the *Scaglia Bianca* Fm. and *Scaglia Rossa* Fm. – known as *Bonarelli* level with a typical thickness of 1 metre, are completely absent. Therefore, between the *Scaglia Bianca* Fm. and *Scaglia Rossa* Fm. there was a *hiatus* or a stratigraphic gap. Probably, a big submarine landslide caused by an earthquake has removed the sediment of these formations moving them to the deepest parts of the ancient sea basin (Montanari & Sandroni, 1995).

The geological succession of the *Monte Conero* is composed as follows:

Table 2-1: Geological Formation of the *Monte Conero* from Coccioni *et al.* (1997)

	Formation	Age	Description
1	*Maiolica*	Barremian – Aptian	Limestones with lenses and flint nodules and sporadic interlayers of marl and clay
2	*Marne a Fucoidi*	Aptian	Alternations of silty clay, clay marls and calcareous marls with flint nodules and in lenses
3	*Scaglia Bianca*	Upper Albian	Calcari giallo-grigiastri
4	*Scaglia Rossa*	Turonian – Lutetian	Limestones and marly limestone with nodules of flint, with interlayers of marl-limestone and interbedded limestone debris
5	*Scaglia Variegata*	Lutetian – Priabonian	Alternation of marly limestones and calcareous marls polychrome
6	*Scaglia Cinerea*	Priabonian – Aquitanian	Marl, calcareous marl and marl clay variously alternating
7	*Bisciaro*	Aquitanian – Burdigalian	Calcareous marl and marly limestone with interbedded volcaniclastic
8	*Schlier*	Burdigalian – Messinian	Marl and calcareous marl with limestone-marl levels
9	*Peliti euxiniche*	Lower Messinian	Clay marly-silty, in places bituminous, with thin interbeds of sandsone
10	*Gessoso-solfifera*	Middle Massinian	Solfiferi limestone, bituminous clays and gypsum
11	*Di Tetto*	Middle-Upper Messinian	Clay marly-siltu with thin sandstone intercalations
12	*A Colombacci*	Upper Messinian	Marly clays intercalated with sandstones and limestones evaporate horizons
13	*Orizzonte del Trave*	Upper Messinian	Calcarenites and sandstones more or less cemented
14	Pelitic-sandy lithofacies	Pliocene	Marly-silty clays
15	Pelitic lithofacies	Middle Pliocene	Marly silty clays
16	Pelitic lithofacies	Lower Pleistocene	Marly clay more silty toward the top
17	Pelitic-sandy lithofacies	Lower Pleistocene	With lenses bioclastic and conglomerates
18	Sandy-conglomerate lithofacies	Lower-Middle Pleistocene	Of transition with a guide layer interbedded silty pastropods and red paleosol
19	Slope deposits		-
20	Fluvial-torrential fan deposits		-
21	Alluvia deposits of the valley floor		-
22	Coastal deposits	Today	-

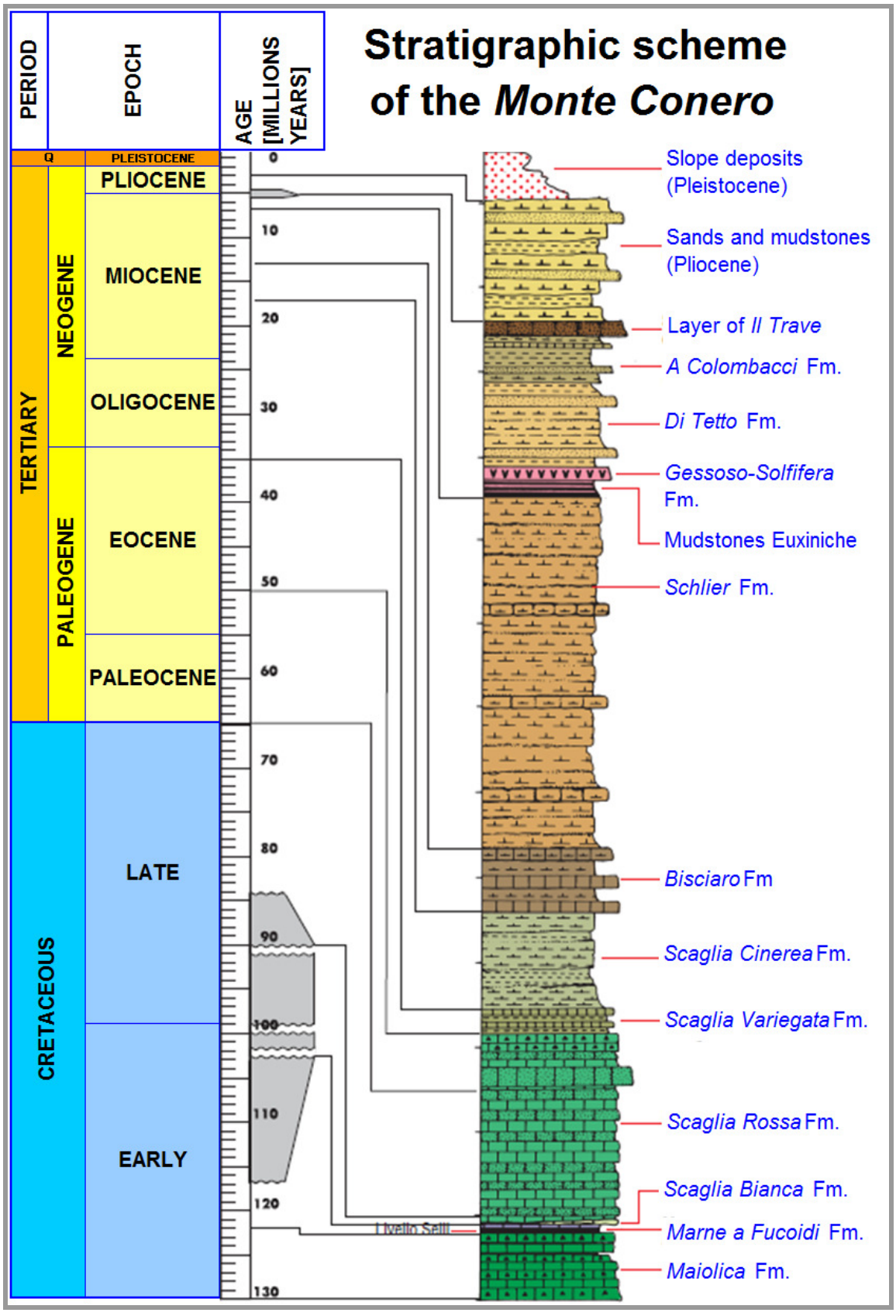

Figure 2-2: Stratigraphic succession of *Monte Conero*. Modified of Parco del Conero (2011)

The outcrops in the *Monte Conero* principally belong to the *Maiolica* and *Scaglia Rossa* Formations; thus, our attention will be focused on them. Between these two formations occurs the *Marne a Fucoidi* Fm. which is principally composed of marl and marly-clay, and with a thickness from 45 to 90 metres plays an important role in the aquifers of *Monte Conero*.

a. ***Maiolica*** **Formation**

The *Maiolica* is the older formation present in the *Monte Conero* and has geological successions which cross the Jurassic-Cretaceous boundary. It is characterized by well-defined layers composed of micritic white limestone of thin grains and irregular lenses and nodules of gray-black flint. The nodules have a relatively round shape and they have dimensions ranging from 3 cm to 14 cm. The thickness of flint lenses is about 12 cm (Figure 2-4). Younger layers are intercalated between white limestone and thin dark clay levels (black shale, Figure 2-3) which are increasing in frequency and thickness going upwards in the stratigraphic column (Montanari & Sandroni, 1995; Bortolotti *et al.* 1994). The thickness of the formation, Figure 2-5, varies between 20 and 400 metres (Bortolotti *et al.*, 1994).

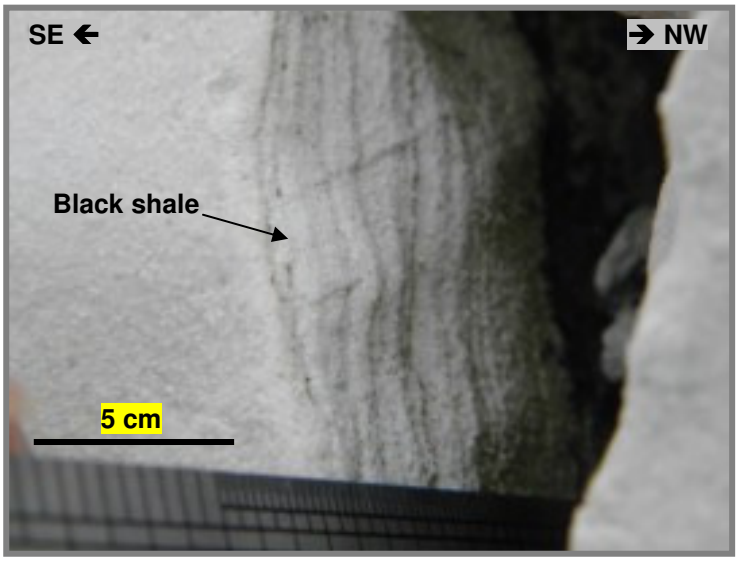

Figure 2-3: Alternation of dark clay levels (black shale)

The orientation of the sedimentary layers of the *Maiolica* Fm., exposed along the coastal area between the *Scoglio della Vela* and the *Spiaggia dei Gabbiani* (Figure 2-12), have an average dip-direction of 47º and an average dip-angle of 48º. The rest of the *Maiolica* outcrops show almost vertical layers with a dip-angle ranging between 85º and 90º (area between the *Spiaggia dei Gabbiani* and the *Spiaggia delle due Sorelle*).

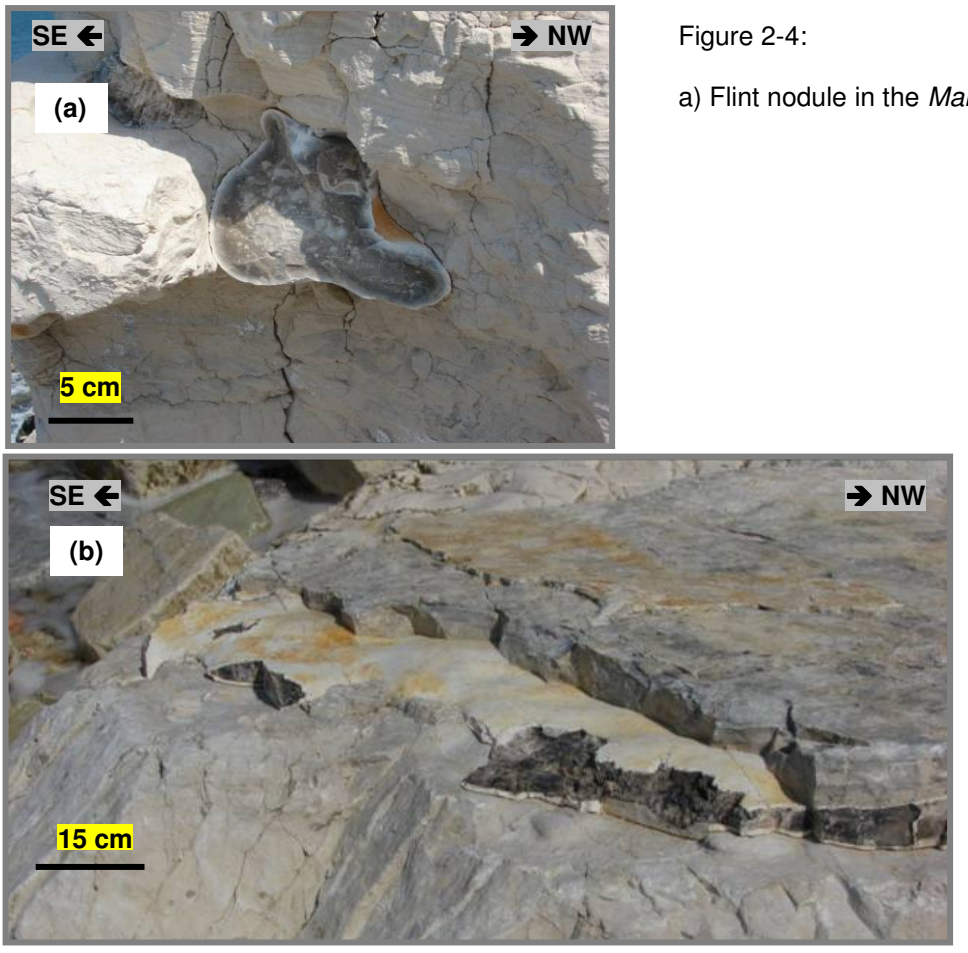

Figure 2-4:

a) Flint nodule in the *Maiolica* Fm.

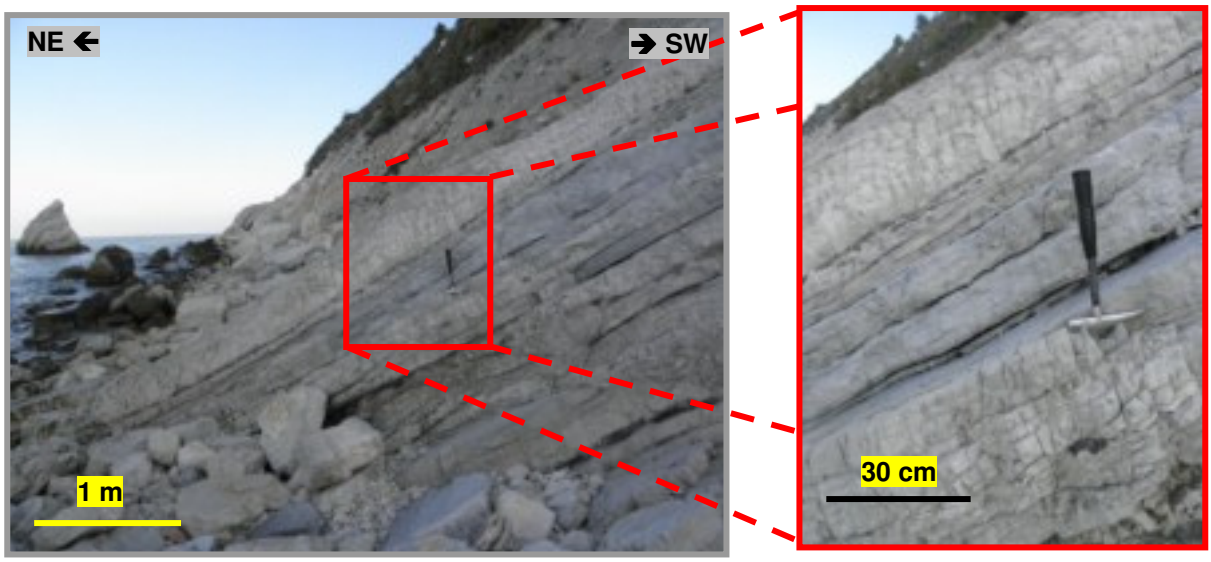

Figure 2-5: Differences in the appearance and thickness of layers in the *Maiolica* Fm.

b. *Scaglia Rossa* Formation

The *Scaglia Rossa* Fm. is part of the *Scaglia* unit (*Bianca*, *Rossa*, *Variegata* and *Cinerea*) and consists typically of rose and red limestone layers. However, in the *Monte Conero*, some intervals of the *Scaglia Rossa* Fm. have not undergone the process of oxidation and therefore have a white colour. The complete *Scaglia* unit has geological successions in the Mesozoic-Cenozoic boundary and Paleocene-Eocene boundary (Figure 2-2) and it is composed of well-defined layers of limestones and marly-limestones. The *Scaglia Rossa* Fm. is composed of micritic limestone with alternation of marl and flint layers. Marl layers have a thickness of about 5 cm. Flint nodules are brown and dark red colour (Figure 2-7); they

Figure 2-6: Thickness of layers of the *Scaglia Rossa* Fm.

usually are elongated, with widths of about 8 cm and lengths three times this value. The lenses usually are ellipsoid shape with shorter side range from 3 cm to 10 cm. According to the flint present in the formation, *Scaglia Rossa* may be divided in 4 subcategories (Bortolotti *et al.*, 1994):

- R1: limestone with flint
- R2: red limestone without flint
- R3: red marly-limestone without flint
- R4: red limestone with flint, which represents the boundary with the *Scaglia Variegata* Fm.

The formation thickness ranges from 200 to 400 metres (Bortolotti *et al.*, 1994), and the layer thickness is rather homogeneous and varies between 10 and 15 centimetres (Figure 2-6).

The average orientation measured along the coastal outcrops of the *Scaglia Rossa* Fm., from the *Spiaggia Sassi Neri* to the boundary with the *Maiolica* Fm. (Figure 2-12), is 151/18º (dip-direction/dip-angle). Layers measured in the hinterland, areas of *Fonte d'Olio* and *Poggio d'Ancona* (Figure 2-12) averaged a dip-direction of 179º and 8º of dip-angle. The layers are deformed as folds and undulations on a scale of meters in diverse several outcrops (Figure 2-8).

Figure 2-7:
a) Flint nodule in the *Maiolica* Fm.
b) Flint lens in the *Maiolica* Fm.

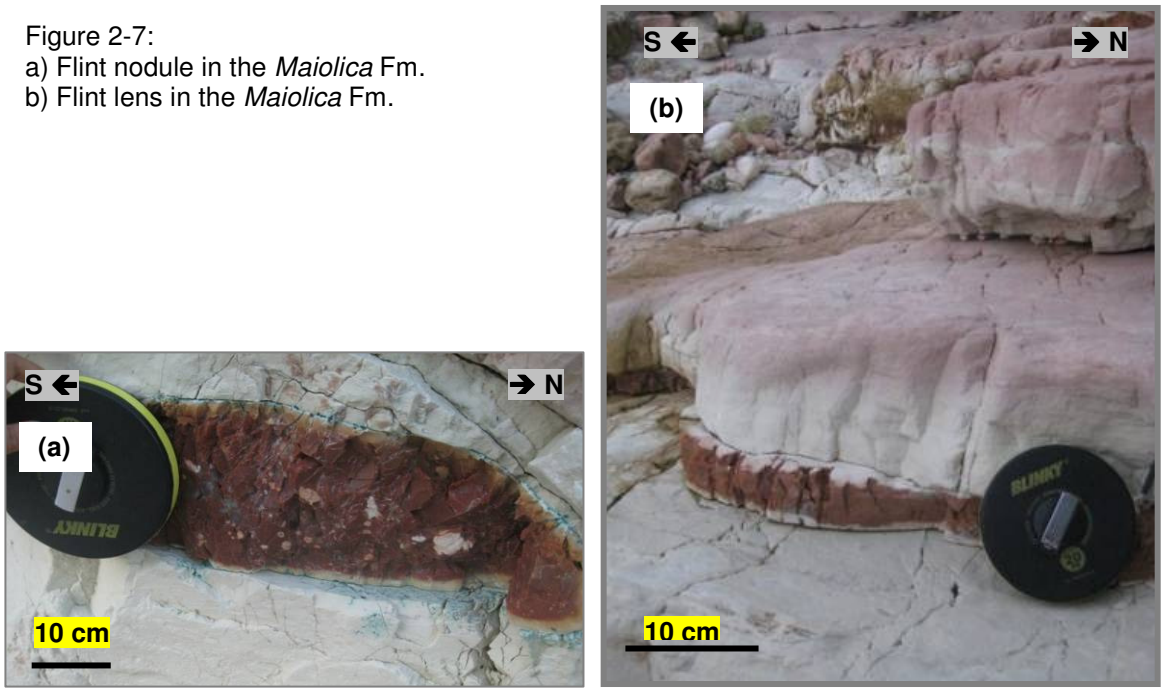

Figure 2-8: Deformed layers in the *Scaglia Rossa* Fm.

c. Landslides

Landslides in the *Monte* Conero are very typical (Alexander, 1984), the best known is the large landslide dated to the prehistoric times that gave rise to the Bay of Portonovo (Cumin, 1936; Angeli, 1991; Angeli *et al.*, 1992). The entire coastal zone is characterized for marine erosion and landslides (

Figure **2-9**); therefore, many outcrops in *Portonovo* but especially in *Sirolo* (Coccioni *et al.*, 1997) are covered by detritus from a previous landslide. Currently, this process is so dynamic in this Park that we could witness the changes on the landscape week after week. This erosion softens fractures and rocks, making the hillsides of these areas more unstable. Despite being the same material and type of rock, those of the hinterland appear to be less hard than those on the coast, showing them more fragile to touch and wind. In the hinterland, the rocks are eroded only by rain water but the roots of vegetation are developing along the fractures, which also weaken this part of *Conero*'s hillslopes. For these reasons we decided to start and to put the focus of our research on the coastal area, where the outcrops have smooth polished surfaces and are more accessible for measurements, maps and photographs.

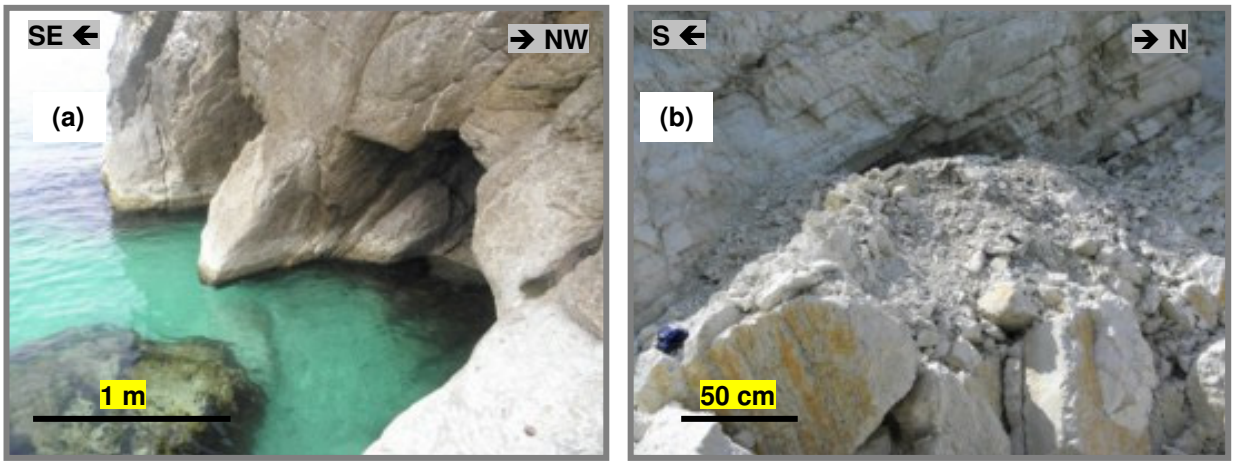

Figure 2-9: a) A cave eroded by sea in *Portonovo.* b) A case of landslide in *Sirolo.*

d. Karst areas

Carbonate rocks are usually characterized by the dissolution of layers which generate karst geomorphologies (Cucchi *et al.*, 2001). The *Monte Conero* is not the exception. Karst geomorphologies were observed in the hinterland of the *Scaglia Rossa*

Fm. In outcrops of *Fonte d'Olio* small caves with openings of about 30 centimetres were observed (Figure 2-10). In addition, sinkholes in scale of metres were observed on the ground of the area of *Fonte d'Olio* and near to the boundary between the *Marne a Fucoidi* Fm. and the *Scaglia Rossa* Fm. in *Sirolo* (toward the top of *Monte Conero*). These sinkholes are like the schemes shown in Figure 2-11, with the centre of the hole covered by soil and vegetation.

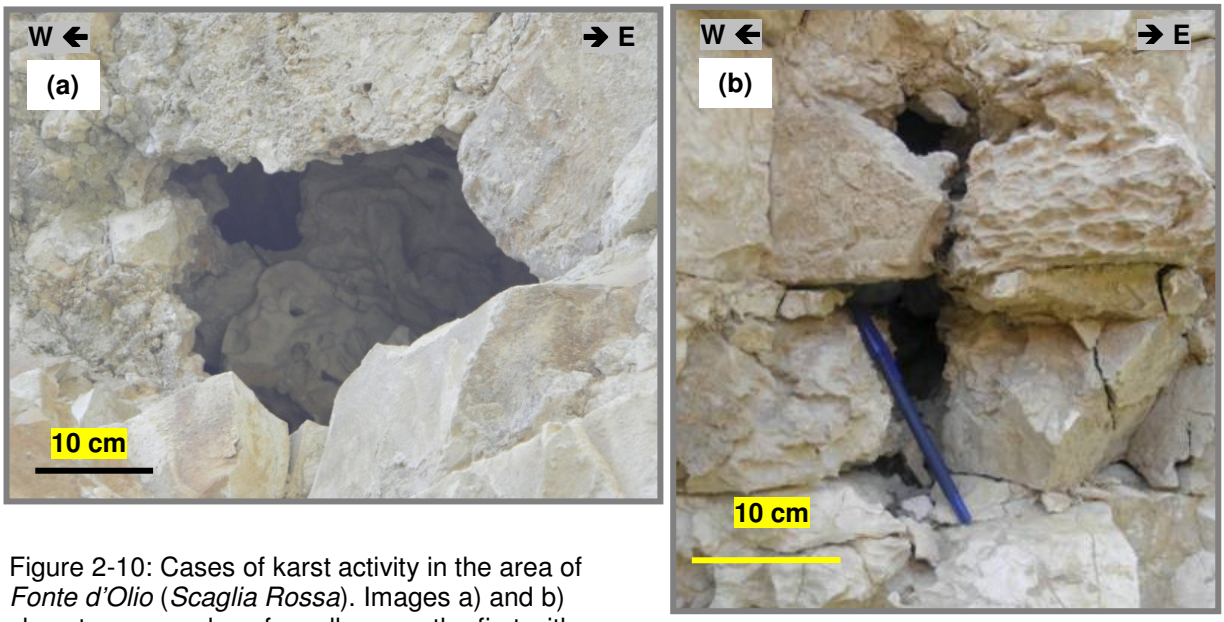

Figure 2-10: Cases of karst activity in the area of *Fonte d'Olio* (*Scaglia Rossa*). Images a) and b) show two examples of small caves, the first with a radial opening and the second with a elongated opening.

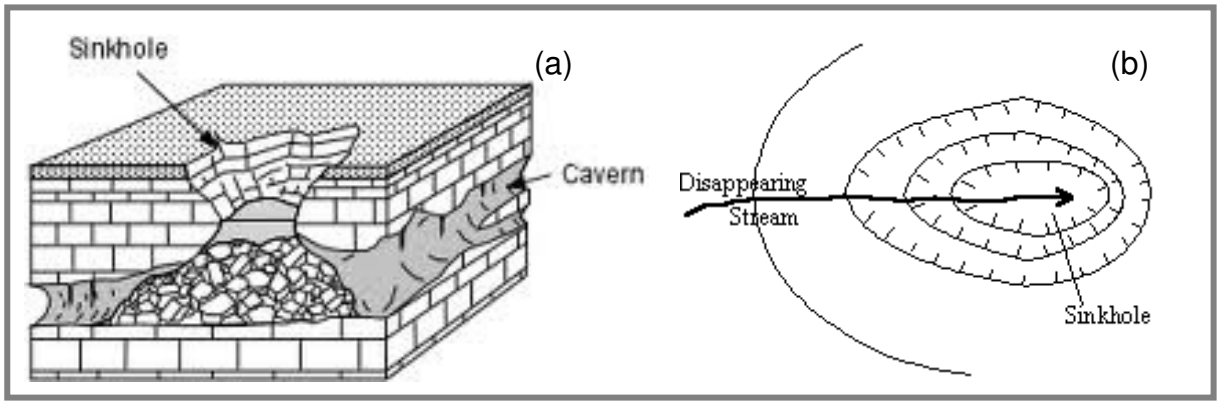

Figure 2-11: Schemes of a sinkhole. a) A frontal three-dimensional view. b) A superficial view.
Source Image a: http://earthsci.org/processes/struct/subside/sinkhole2.gif
Image b: http://www.sonoma.edu/users/f/freidel/remote/karst.gif

Therefore, based on our observations and in the absence of surface runoff, we might expect that there is a karst network in the underground of *Monte Conero* with other entries covered by lush vegetation. A karst network is a very important factor in terms of fluid flow, since the aperture here can reach values in a scale of metres becoming an aquifer more vulnerable (Cherubini, 2008).

2.1.2 Structural characteristics

The *Monte Conero* is an anticline that was developed about 5 million years ago, during the Lower Cretaceous age, as a result of a compressive force from the southeast (**¡Error! No se encuentra el origen de la referencia.**3), that is, Apennine vergence (Montanari and Sandroni, 1995). This tectonic phase caused the formation of an asymmetric fold. The folds oriental limb trends NE and has a layer dip between 70ºand 85º while its occidental limb dips 22º (Figure 2-12). The fold axis has an average trend of N 138º (Cello and Coppola, 1984).

The *Conero* anticline is intersected by a strike-slip fault system and diverse non-systematic normal faults that have a spacing of tens to hundreds of meters and a fault length measured along strike of hundreds of meters (Figure 2-13). The strike-slip faults are predominantly sinistral faults, orientated at high angle to fold axis (Cello & Cappola, 1984; Coccioni *et al.*, 1997), dividing and moving rock blocks without generate important changes in the axis orientation (Cello & Cappola, 1984). Sinistral faults trend N 90-100 while dextral faults trend N 30-40 (Cello & Cappola, 1984). According to Fancelli & Radrizzani (1964), the offset along the sinistral strike slip faults range from 100 to 200 metres. Cello & Cappola (1984) point out that the structures in the coastal zone of Ancona

province originally would have been a single structure formed by the *Conero* anticline, the *Varano* anticline, the *Tavernelle* syncline, the *Ancona* monocline and the *Polverigi* anticline. The study of Cello & Cappola (1984) indicate that the stress field during the Pliocene tectonic phase was dominated by σ_1 in direction SW-NE

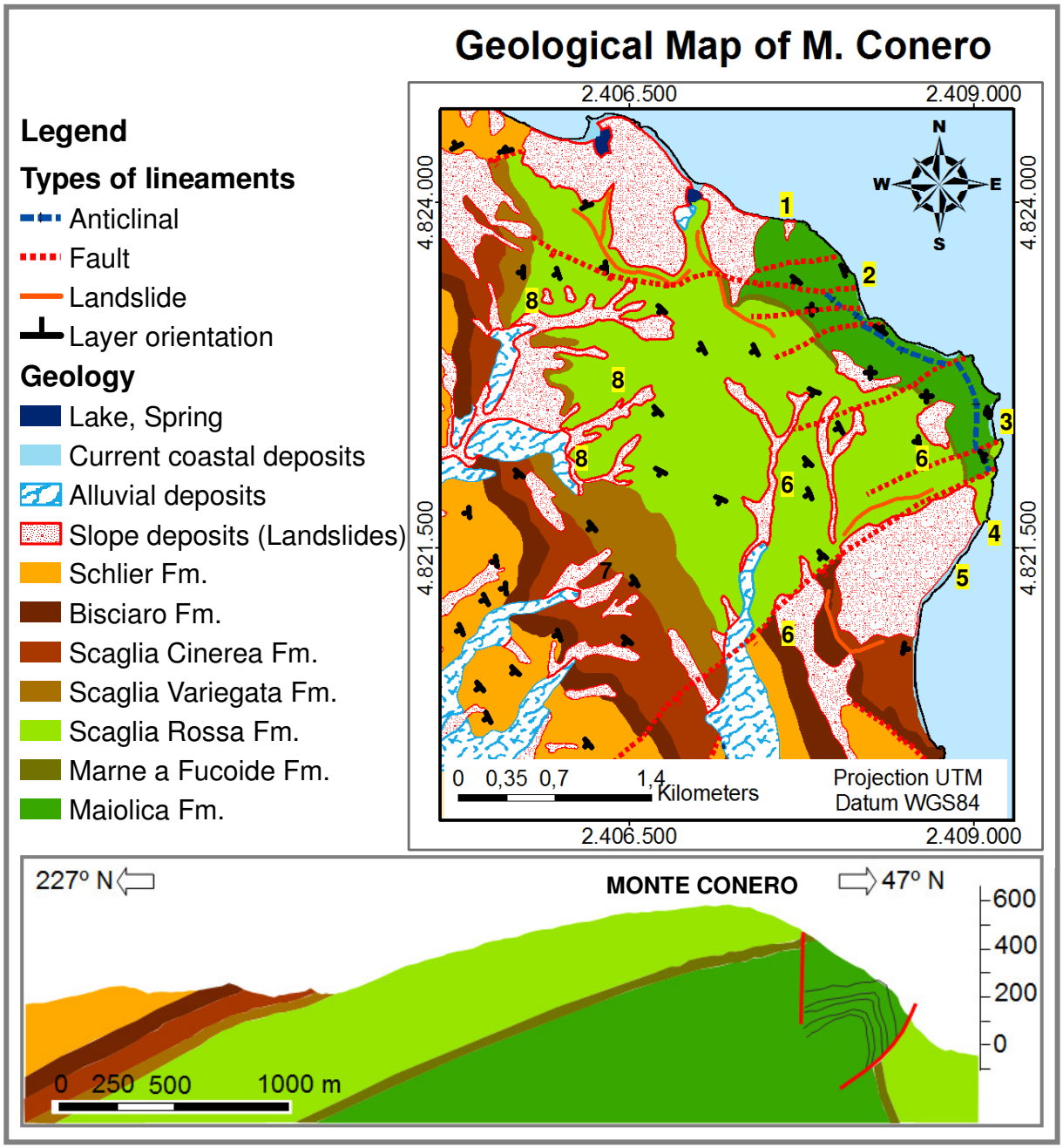

Figure 2-12: Geological map and profile of the *Monte Conero*. Referential points/areas: 1) *Scoglio della Vela* (*Portonovo*). 2) *Spiaggia dei Gabbiani.* 3) *Spiaggia delle Due Sorelle.* 4) Boundary *S. Rossa-Maiolica.* 5) *Spiaggia Sassi Neri* (*Sirolo*). 6) *Fonte d'Olio.* 7) *Massignano*'s quarry. 8) *Poggio d'Ancona* Source: Modified of Coccioni *et al.* (1997)

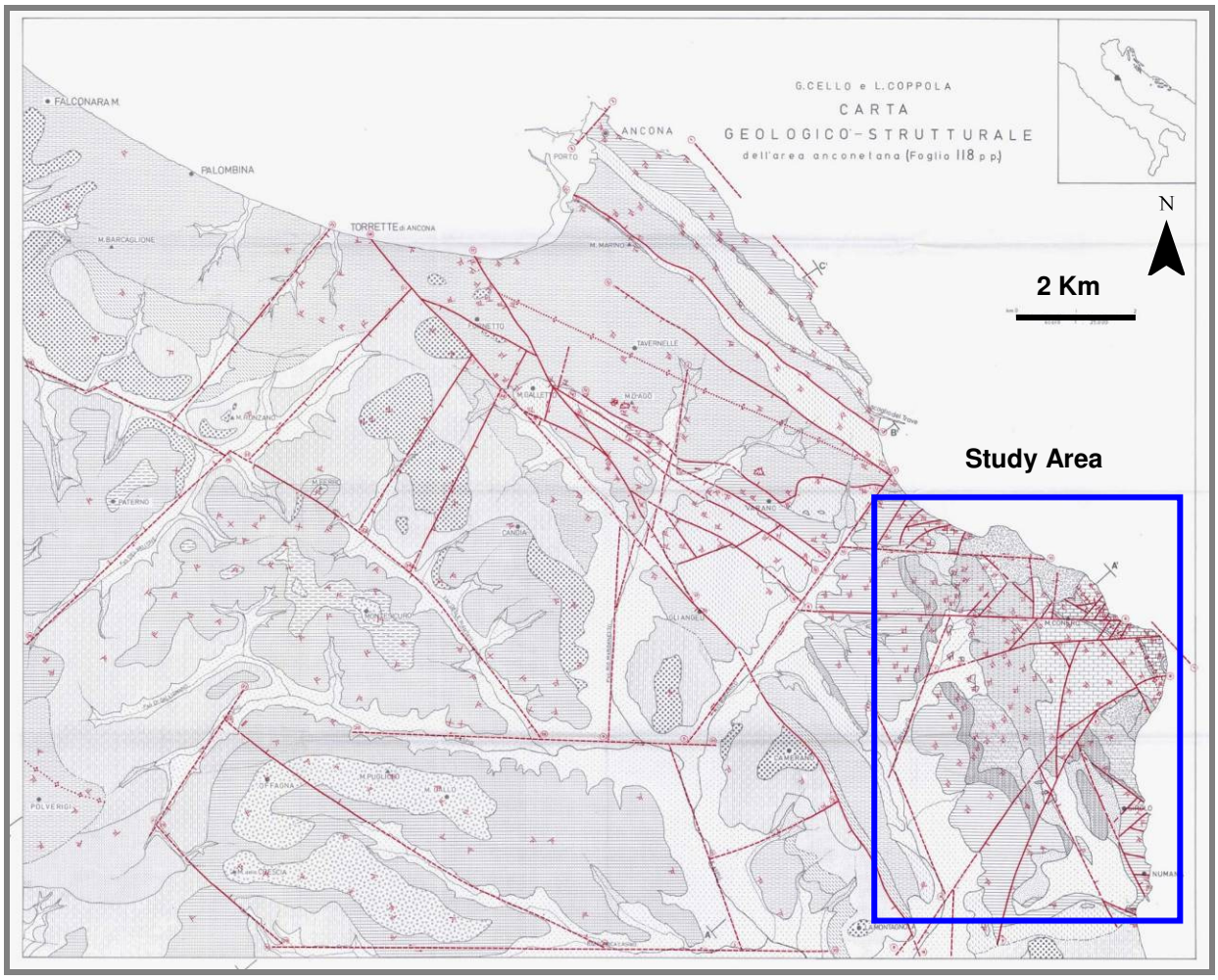

Figure 2-13: Geological lineaments of the regional context of the *Monte Conero*. Scale map 1:25000
Source: Cello & Coppola (1984). http://www.egeo.unisi.it/carte.php?idserie=194

Tectonic history

The Apennine Umbria-Marche was formed 230 million years ago (in the Upper Triassic) characterized by extensional tectonic regimes and calm periods. Likewise, the sedimentological series of the Apennine Umbria-Marche was affected by subsidence, submarine landslides and repeated closures of the Strait of Gibraltar. The deformation of the Umbria-Marche basin starts due to the compressive activity, which was developed gradually from west to east from the Lower Miocene (18 millions years ago), generating folds and large thrust belt structures (Figure 2-15), which formed mountain chains (Alberti *et al.*, 1998; Argnani, 1998). Only 5 millions years ago (in the Lower Pliocene) the area of the *Monte Conero* was affected by the compressive tectonic regime that was characterizing the Umbria-Marche basin causing the emergence of the *Monte Conero.*

During the Quaternary (from 1.7 million years ago to today), during periods of glaciations and low sea stand, the surrounding

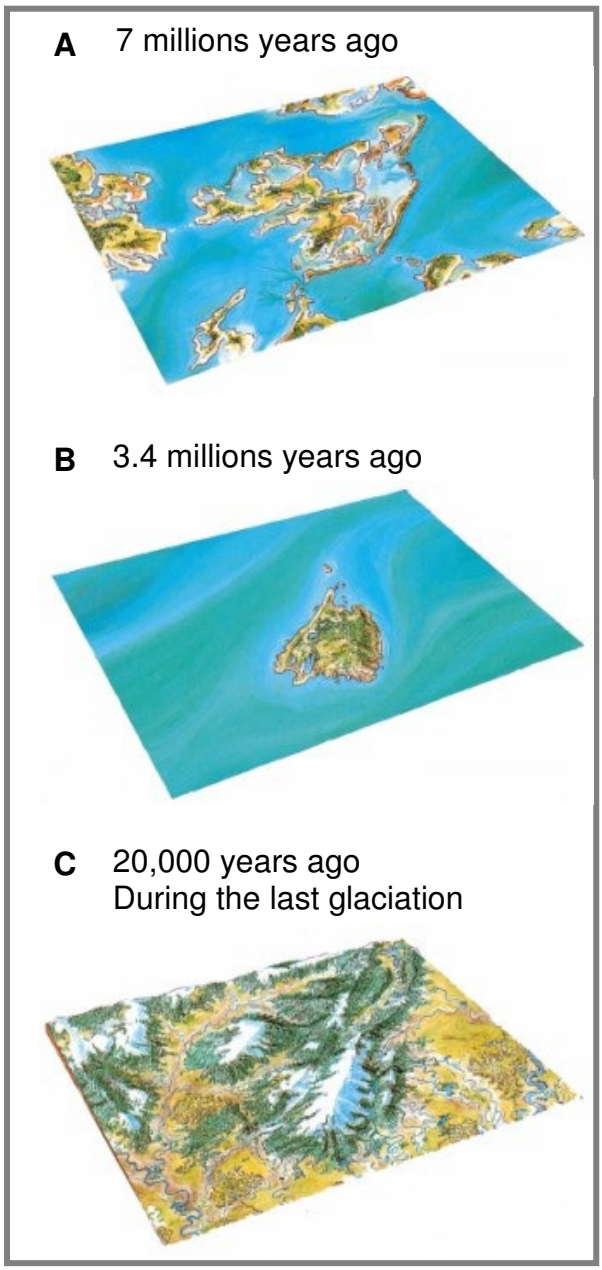

Figure 2-14: Geological Evolution of the Monte Conero. A. The area was characterized by lagoons and extensive lagoons with shallow water. B. Probably an island during the Upper Pliocene. C. The rainwater, trapped as ice at the poles, the Alps and the Apennines, caused a lowering of the level of the Mediterranean Sea about 100 metres, causing the retreat of the Adriatic Sea and giving space to a vast alluvial plain. Part D and E fallow in the next page.
Source: Parco del Conero (2011).

areas of the *Monte Conero* emerged, while during interglacial periods *Monte Conero* stood outs as an island in the middle of submerged land (**¡Error! No se encuentra el origen de la referencia.**4).

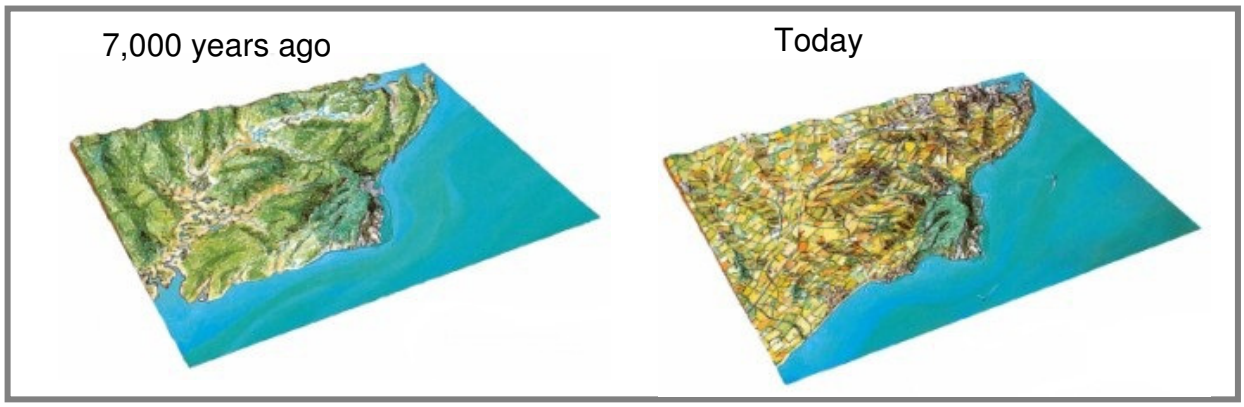

Figure 2-14 (continuation): Geological Evolution of the Monte Conero. D. The sea flooded and covered with swamp long stretches of coast (the valleys of the Musone, Aspio and the area where today stands Ancona) and began the erosion of the cliffs of the *Monte Conero*. E. The slow process of erosion that began around 10,000 years ago, and still ongoing shaped coastline and sculpted the white cliffs of the *Conero.* In the surrounding hinterland the landscape has been modified by human activities such as reclamation of marshes and wetlands, damming and alteration of rivers, reforesting, urbanizing and industrializing hills and valleys. Parco del Conero (2011).

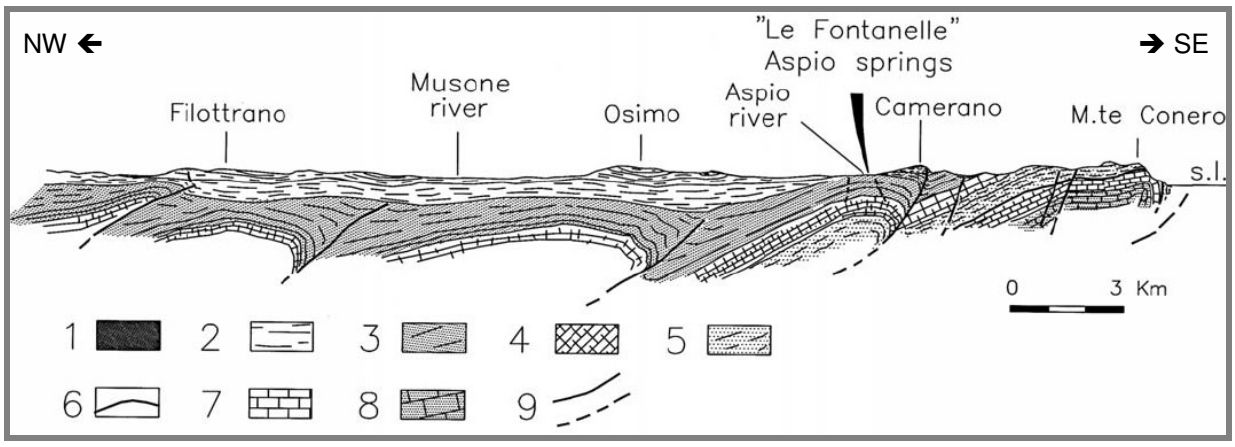

Figure 2-15: Schematic geological cross section through the Marche foredeep, between Esino and Musone rivers. 1-2) Plio-pleistocene sequence pelitic e pelitic-arenaceous (2) and arenaceous-conglomerate (1) late-orogenic sequence of Plio-Pleistocene; 3) Messinian and Pliocene syn-orogenic sequence; 4-5-6-7-8) Mesozoic-Cenozoic limestone sequence consisting of: *Scaglia Cinerea*, *Bisciaro* and *Schlier* (4), *Scaglia* Formations (5), Marne a Fucoidi (6), Maiolica (7) and Calcare Massiccio (8); (9) Overthrusts and faults. Source: Nanni & Vivalda (2005)

2.2 Hydrological Setting

2.2.1 Hydrological context of Monte Conero

Monte Conero is part of the Coastal Basin between the *Esino* and *Musone* Rivers (Figure 2-16). The *Aspio,* the *Musone* and the *Potenza* rivers are the principal waterways of perennial nature and with variable seasonal regime in the area of *Ancona* (Fancelli & Radrizzani, 1964).

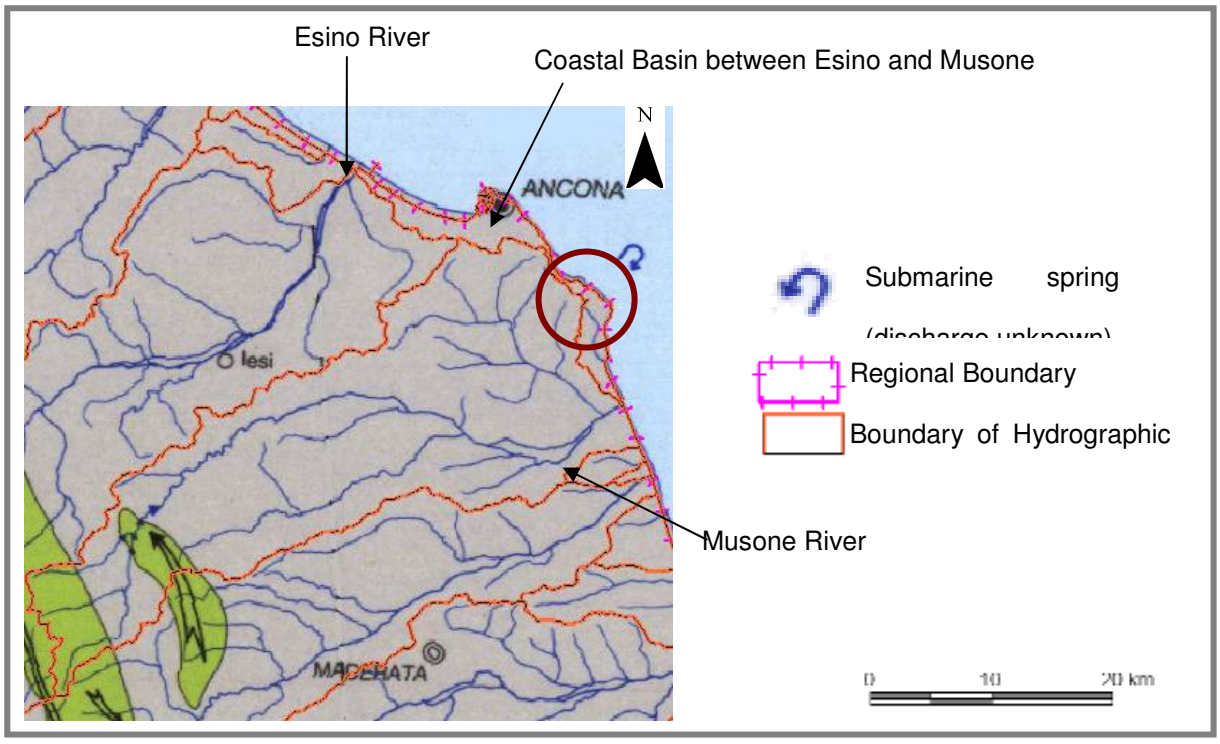

Figure 2-16: Hydrological context of Monte Conero (Regione Marche, 2008).

The western side of the *Conero* is crossed by a network of small basins (Figure 2-17), many of which flow into the ditch of *I Molini* which flows to the south, and ends between the coastal towns of *Numana and Marchelli*. The regime of these waterways is torrential and their recharge depends exclusively of rainwater (De Grandis, 1995).

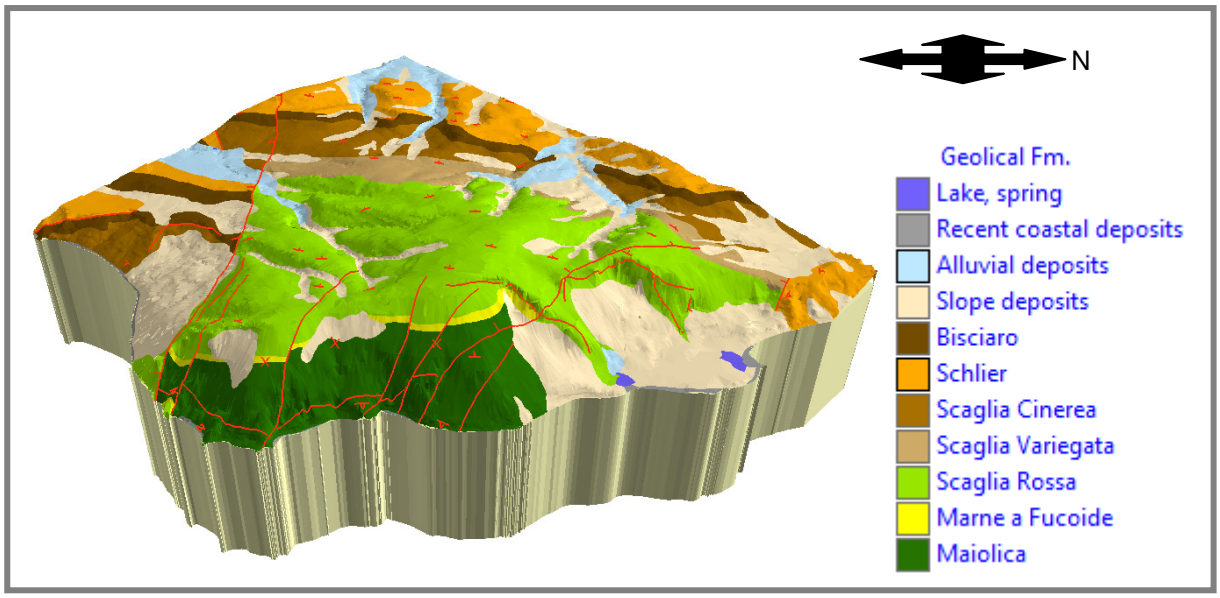

Figure 2-17: Physical geography of *Monte Conero*, where it is possible to distinguish the topography and hydrogeological basins in relation with the geological formations (based on Coccioni *et al.*, 1997, ARPAM, 2011)

The *Monte Conero* together with the *Cingoli* anticline (Petracchini *et al.*, 2012) are part of the outer basin of the *Le Marche* dorsal. They are considered as structures hydraulically covered with *Miocene* deposits at low permeability (Nanni & Vivaldi, 2009). The hydrogeological characteristics vary in accordance with the lithology of the outcrops.

The hydrogeological structure of the *Maiolica* consists mainly of limestones and marly-limestones from the *Marne a Fucoide* Fm (Regione Marche, 2008; Nanni & Vivalda 2009). The permeability of the complex is linked to the fracturing and is increased by karst phenomena (Bocchini & Fontana, 1983).

The hydrogeological structure of the *Scaglia* is formed by the most calcareous part of the *Marne a Fucoide* Fm. and the marly-limestone succession of the *Scaglia Bianca*, *Rossa* and *Variegata* (Pignocchi, 1991; Regione Marche, 2008; Nanni & Vivalda, 2009). The aquifers of the *Scaglia Rossa* are supported by the *Marne a Fucoide* lithotypes at low-permeability at the bottom and the *Scaglia Cinerea* lithotypes at the top (Regione Marche,

2008; Nanni & Vivalda, 2009). The permeability of the *Scaglia* complex is high for fracturing and fracturing (Pignocchi, 1991; Nanni & Vivalda, 2009); the karstification here is little known and is represented by vertical and horizontal ducts poorly developed (Nanni & Vivalda, 2009).

In both hydrogeological structures the infiltration is always higher than the runoff (Nanni & Vivalda, 2009).

The continental detrital deposits with high porosity exposed in *Portonovo* bay are the deposits *Monte Conero* with significant high porosity and permeability (Coccioni *et al.*, 1997; Conti, 1998). This area was formed by a large landslide in prehistoric times (Manfredi, 1987; Conti, 1998) and is characterized by two coastal lakes: "*Lago Grande*" and "*Lago Piccolo*" separated by 672 metres, as it is shown in Figure 2-18. This figure also shows the distribution of the 5 private wells and one spring existing in the area in 1997, which allowed the characterization of some of the hydrological aspects of the area (Conti, 1998) as described in the next section (Section 2.2.2, page - 31 -). Currently, these wells and spring as well as other wells around *Monte Conero* are inoperative due to the generation of the aqueduct (Nanni, 2011; ISPRA, 2011).

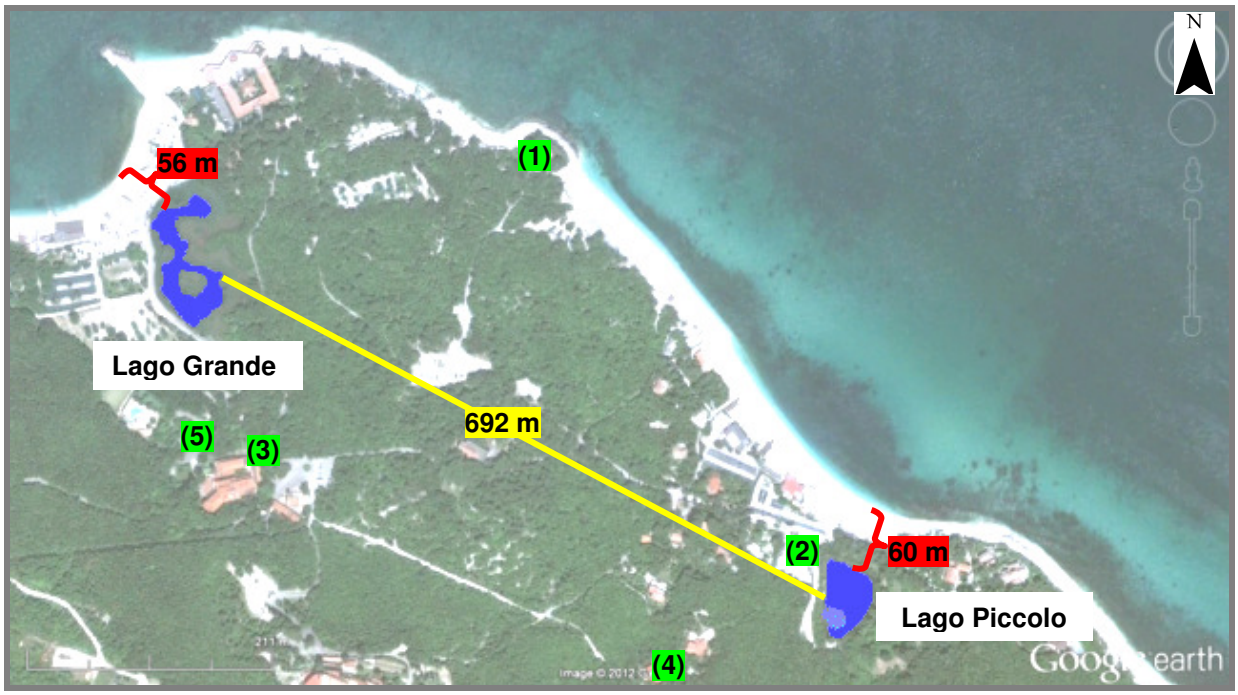

Figure 2-18: Relative position of the *Lago Grande* and *Lago Piccolo*, and wells and spring I 1997. The number in yellow indicates the distance between both lakes. Numbers in red indicate the minimal distance between the lakes and the coastaline. Image and distances measured from Google Earth 2012. Numbers in green indicate the position of wells and spring in 1997 according to Conti (1998): 1) Well "Torre", 2) Well "Parcheggio", 3) Well "La Fonte", 4) Well "Internazionale", 5) Spring.

The *Lago Grande* is located at 56 metres from the coastline (Figure 2-18 and Figure 2-19) and, according to Conti (1998), the maximum depth of the lake in 1997 was less than 100 cm in the profile oriented in direction WE and 172 cm in the direction NS. According to the study of Turroni (1995), the bottom lake sediments are composed of fetid silt in the first 27-30 cm depth and clayey silt from 30 to 70 cm depth (Conti, 1998).

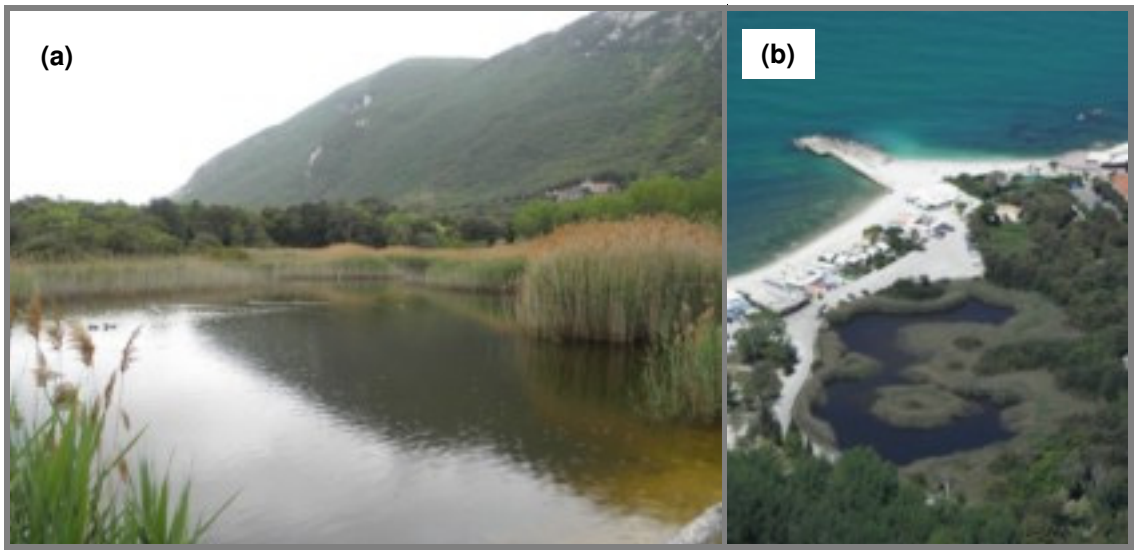

Figure 2-19: *Lago Grande*, *Portonovo*. a) View from the edge E-SE of the lake. b) View from the top of *Monte Conero*

The *Lago Piccolo* is located at 60 metres from the coastline (Figure 2-18 and Figure 2-20) and the maximum depths registered by Conti (1998) were 200 cm in the direction WE and 222 cm in the direction NS. The sediments on the bottom of the lake are composed clayey-silt up to a depth of 31 cm (Turroni, 1995).

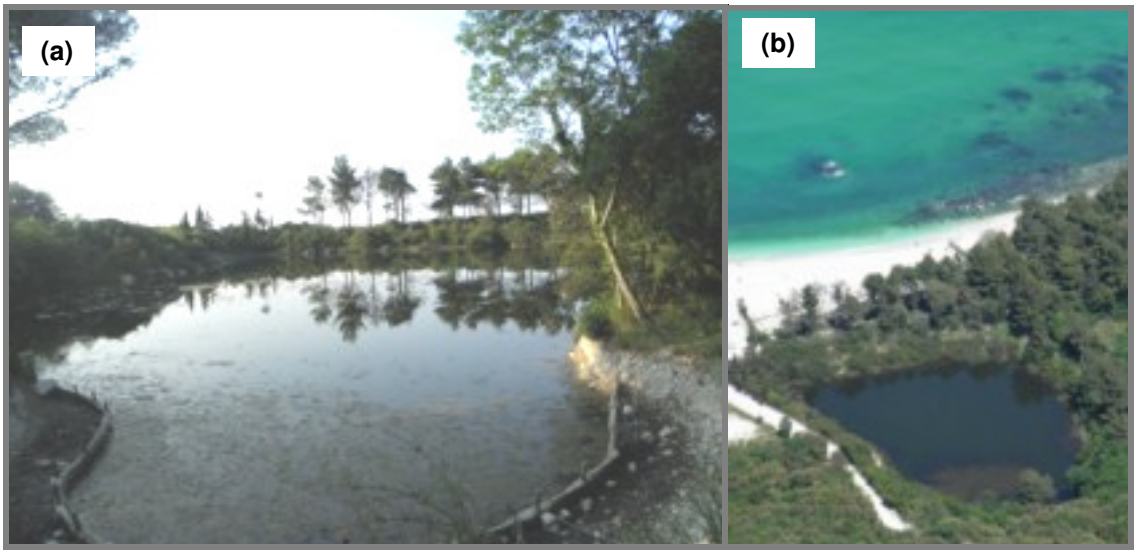

Figure 2-20: *Lago Piccolo*, *Portonovo*. a) View from the edge S-SW of the lake. b) View from the top of *Monte Conero*

The areal surface of both lakes has decreased over the years mainly due to human intervention and the introduction of touristic activities (Conti, 1998). Several of

measurements made during summer months in different years are proof of that (Cumin, 1936; Moretti *et al.*, 1982 and Conti, 1998). The *Lago Grande* changed its areal surface from 18,000 m^2 in 1936, to 14,000 m^2 in 1973, to 6,700 m^2 in 1997; whereas in the *Lago Piccolo* the decrease of the areal surface was from 14,000 m^2 in 1936, to 4,000 m^2 in 1972 and 2,790 m^2 in 1997.

2.2.2 Characterization and estimation of parameters of the aquifer

a. Groundwater Circulation

We have based the characterization of the groundwater circulation of *Monte Conero* on the characteristics of the springs in the area reported in different studies. The springs in *Monte Conero* and in the surrounding areas are not capable of sustaining a river system (Manfredi, 1987) and although they are numerous in the *Ancona* Province, have an insignificant flow (less than 1 lt/s) and a seasonal regimen flow (Fancelli & Radrizzani, 1964; Nanni & Vivalda, 2009).

Figure 2-21: Spring found in the area of *San Lorenzo*, in the geological boundary of the *Scaglia Variegata*, *Cinerea* and a fault.

The springs that emerge from the *Maiolica* Fm. exposed in the Conero and elsewhere in the region are generally recharged by small aquifers formed in the suspended and less fractured levels or on lithotypes with lower permeability (Nanni & Vivalda, 2009).

Instead the springs that emerge from the *Scaglia* Fm. typically are located at the bottom the waterways which affect the slopes and often they emerge close to the *Marne a Fucoidi* aquiclude. Also, the springs in this complex may emerge in the particular structural conditions of the *Scaglia Cinerea*. This is the case of the spring observed in Monte Conero during our fieldwork in the year 2011 (Figure 2-21), which is located in the lithostratigraphic boundary between the *Scaglia Variegata* Fm. and the *Scaglia Cinerea* Fm. According to Coccioni *et al.* (1997) this is a zone intersected by a fault. According to Capari *et al.* (2006) this spring together with a similar spring located towards the south of the observed spring, are the only two documented springs in the area of *Monte Conero.* Both springs have a seasonal regime with unknown discharge (Capari *et al.*, 2006) like the only submarine spring along the coastal of the *Maiolica* Fm. (Regione Marche, 2008). The existence of this submarine spring suggests the presence of a karst system in the *Scaglia Rossa* Fm. (Fleury *et al.*, 2007).

In 1998, Conti (1998) measured the flow of a spring located in *Portonovo* (Figure 2-18, number 5). The average flow was of 3.8 lt/min, with a minimum of 2.8 lt/min registered in summer and a maximum of 5 lt/min in winter. This spring is currently nonexistent.

The research of Nanni and Vivalda (2009) revealed that the springs from the hydrogeological structure of the *Maiolica* and *Scaglia* of the Marche carbonate dorsal are recharged by a double circulation, one fast of macro-fractures and karst, and one slow of micro-cracks. The last circulation controls the base flow on the aquifers that recharge the springs.

In this study, we assume on the basis of Nanni and Vivalda (2009) that the *Monte Conero* is composed of at least two aquifers separated by the aquiclude of the *Marne a Fucoidi.* The upper most aquifer discharges in the hinterland and that the lower aquifer discharges under the Adriatic Sea and in the coastal lakes. In fact, Nanni (1983) suggests that the underground flow is directed towards the two coastal lakes. It is possible that another aquifer exists at depth below sea level.

We have used the model LocClim (Local Climate Estimator) elaborated by the Food and Agriculture Organization (FAO, 2002) to calculate an estimate of the natural recharge of the aquifers. LocClim calculates among others, evapotranspiration rates based on climate data registered at weather stations. We considered the following weather stations *Macerata*, *Falconara* and *Ancona* for data of temperature; *Falconara* and *Ancona* for precipitation data; and *Ancona* for potential evapotranspiration. LocClim calculated an average temperature of 13.6 [ºC], an average maximum temperature of 17.22 ºC, and an average minimum temperature of 10.94 [ºC] (Graphic 2-1). The monthly mean precipitation is of 64.71 [mm] and it is relatively constant during the year seasons, the minimum precipitation level occurs during January (51.2 mm) and the maximum during August (83.5 mm). The mean evapotranspiration is of 70.72 [mm], which is higher than the precipitation so casuing a hydrological deficit of -6.01 [mm], in the summer months (from May to September, Graphic 2-2). The maximum deficit occurs during July, when the temperature is the highest (27.6 ºC). These data are consistent with the seasonal regime of the springs, which have a higher discharge during the winter months. Since the amount of monthly precipitation is relatively constant during the year; the high evapotranspiration rates in summer controls the reduced spring flow in that period.

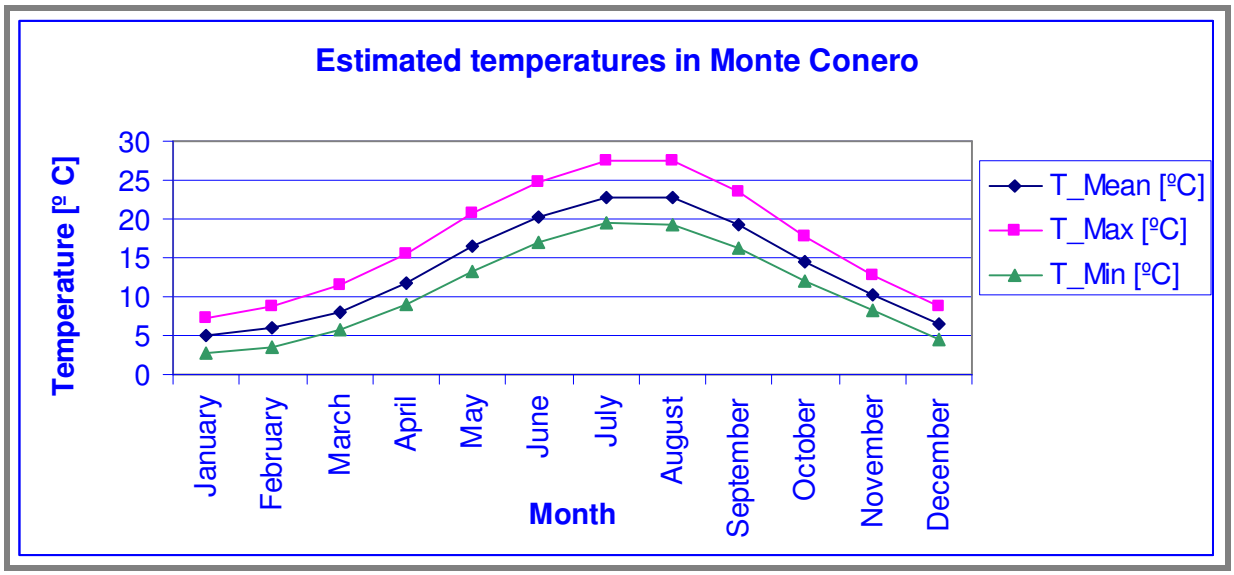

Graphic 2-1: Minimum, maximum and mean temperatures estimated for Monte Conero by LocClim (FAO, 2002)

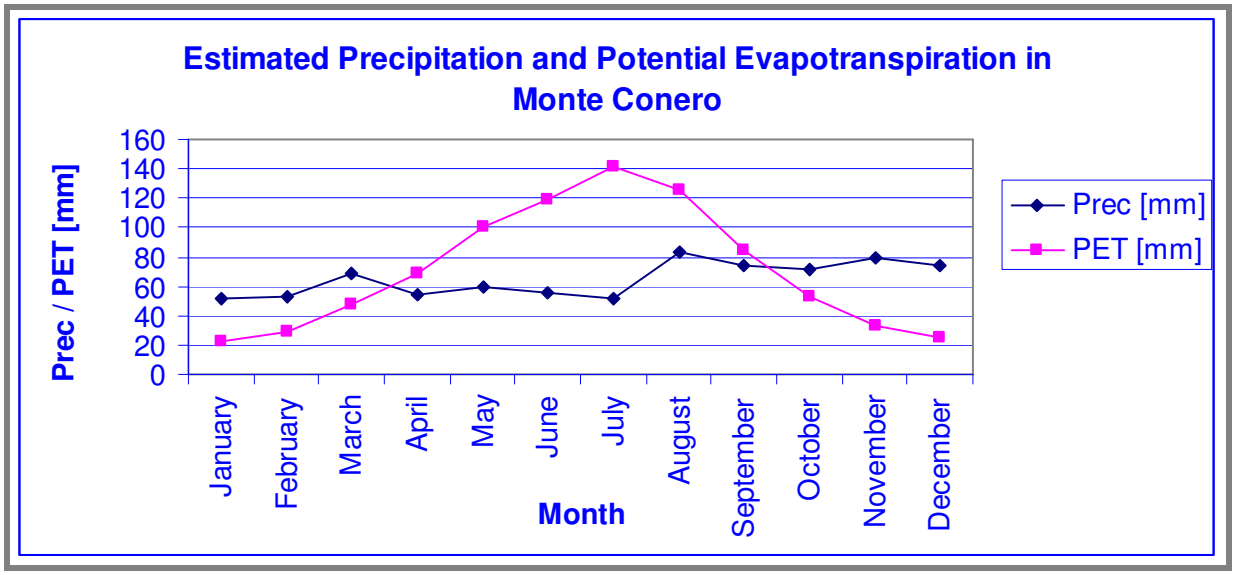

Graphic 2-2: Precipitation and potential evapotranspiration estimated for Monte Conero by LocClim (FAO, 2002)

b. <u>Depth to the water table level</u>

The only reference of the water table level in *Monte Conero* is the work of Conti (1998) who reports the values of the water table in the zone of *Portonovo* based on the measurements in 4 private wells (Figure 2-18 and Graphic 2-3), from July 1997 to May 1998. The water table in the two wells that are located close to the lakes ("*La Fonte*", "*Torre*" and "*Parcheggio*") occurs at greater depths than in the well farther away from the

lakes ("*International*"). The average water table level is at 2.1 metres during the summer and at 1.3 metres during the winter. The *International* well shows values with a constant trend which averages 44 cm. According to Conti (1998), the water table is not influenced by the superficial morphology and the underground flow is directed towards the *Lago Piccolo*.

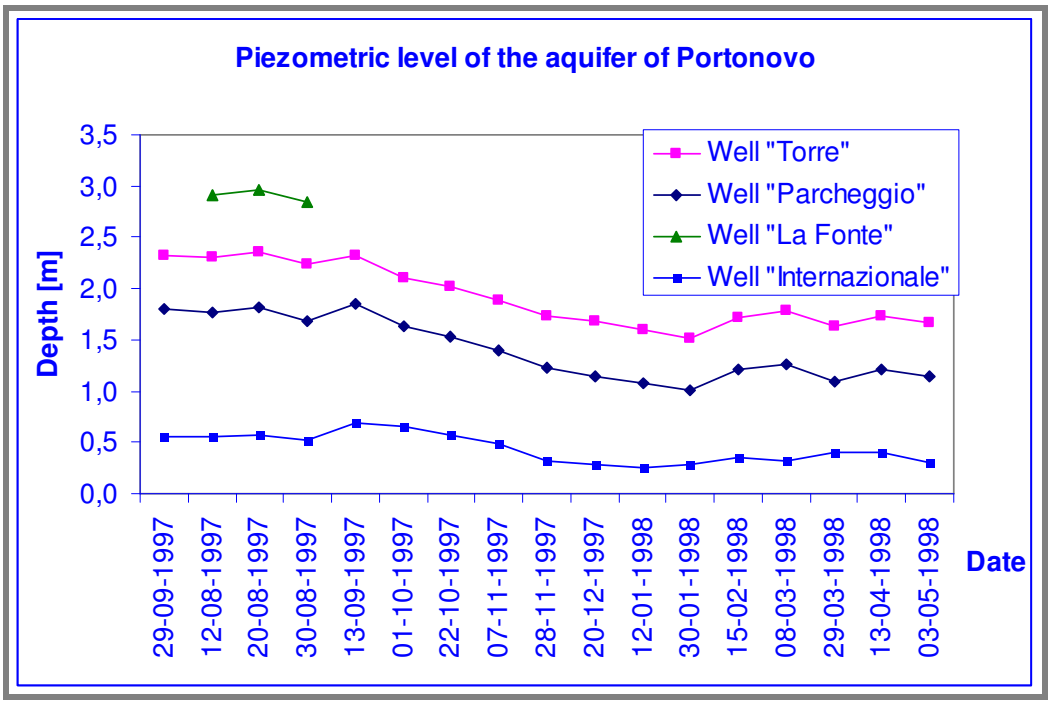

Graphic 2-3: Piezometric level of the aquifer of Portonovo (Conti, 1998)

To obtain another estimation of the depth of the water table of *Monte Conero* the equation of Ghyben-Herzberg (1889; 1901) for an elongated island has been used (Oude Essink, 2001). This equation relates the amount of natural recharge, the width of the recharge zone, the hydraulic conductivity the density difference between salt and fresh water to the depth of the saltwater - freshwater interface in a coastal setting, for a particular geometry. Also the height of the water table can be calculated. The following figure shows the parameters of the equation:

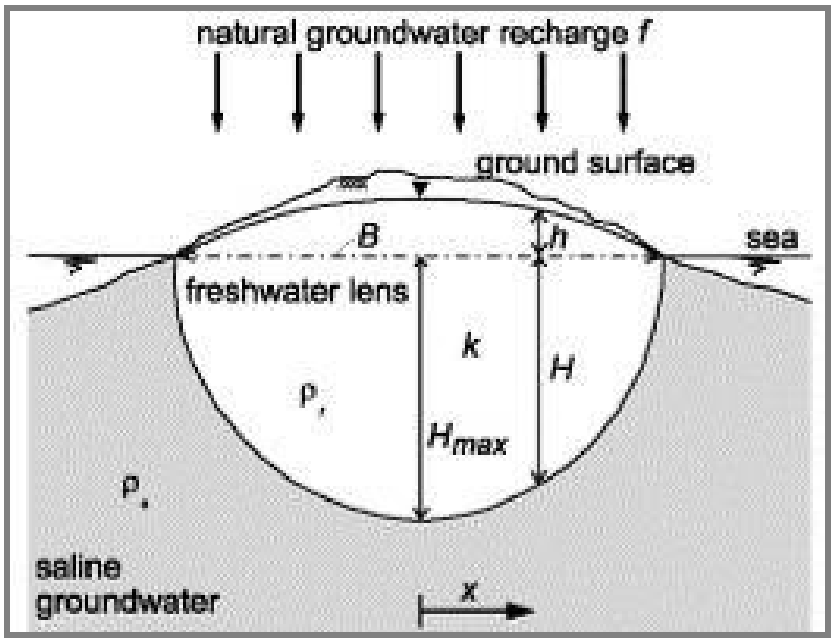

Figure 2-22: Parameters of the aquifer in the Ghyben-Herzberg (1889; 1901) equation, the case of an elongated island (Oude Essing, 2001)

We have assumed that *Monte Conero* may be represented by an island model since this has an arranged as an isolated geological complex. In addition, the model has the following assumptions:

- The system is homogeneous
- There is a horizontal fresh water flow
- There is no saline water flow
- There is no hydrodynamic dispersion

The equation is composed as follows:

$$H = \sqrt{\frac{f \cdot (0.25 \cdot B^2 - x^2)}{k \cdot (1+\alpha) \cdot \alpha}}$$ Equation 2-1

Where,

H : depth of the fresh-salt interface below mean sea level [Length]

f : natural groundwater recharge [Length Time^{-1}]

x : horizontal position (distance from the axis of symmetry) [Length]

B : width of the island [Length]

k : hydraulic conductivity [Length/Time]

α : relative density difference defined by:

$$\alpha = (\rho_{salt} - \rho_{freshwater}) / \rho_{freshwater}$$ Equation 2-2

h : piezometric head of fresh water with respect to mean sea level [Length]. It is defined as:

$$h = \alpha \cdot H$$ Equation 2-3

The natural groundwater recharge (f) was considered as the total annual positive difference between precipitation and potential evapotranspiration, based on the LocClim data (See Section 2.2.2 and Graphic 2-2, page - 34 -), that is $182[mm/year] = 5.76 \cdot 10^{-9}[m/s]$ during the months from October to March.

The width of the island (B), *Monte Conero*, was considered as 3500 [m], whereas the hydraulic conductivity (k) was taken to be 5 x 10^{-5} [m/s]. This value for the hydraulic conductivity is an average value derived from the literature, considering the characteristics of the rocks of *Monte Conero*. For a limestone 7.8 x 10^{-8} [m/s] (Davis, 1969) and for limestone with karst 0.0001 [m/s] (Herczeg *et al.*, 1997)

The density of the Adriatic Sea, based on an electrical conductivity of 46.6 [mS/cm] at 22.8 [ºC] measured during May 2011, is 1.017 (Kg/m^3). Thus, using the Equation 2-2: $\alpha = (1.017 - 1.000) / 1.000 = 0.017$

Lastly, the equations 2-1 and 2-3 for the parameters of depth of the fresh-salt interface below mean sea level (H) and piezometric head of fresh water with respect to mean sea level (h), respectively, were programmed in Excel. The results are shown below.

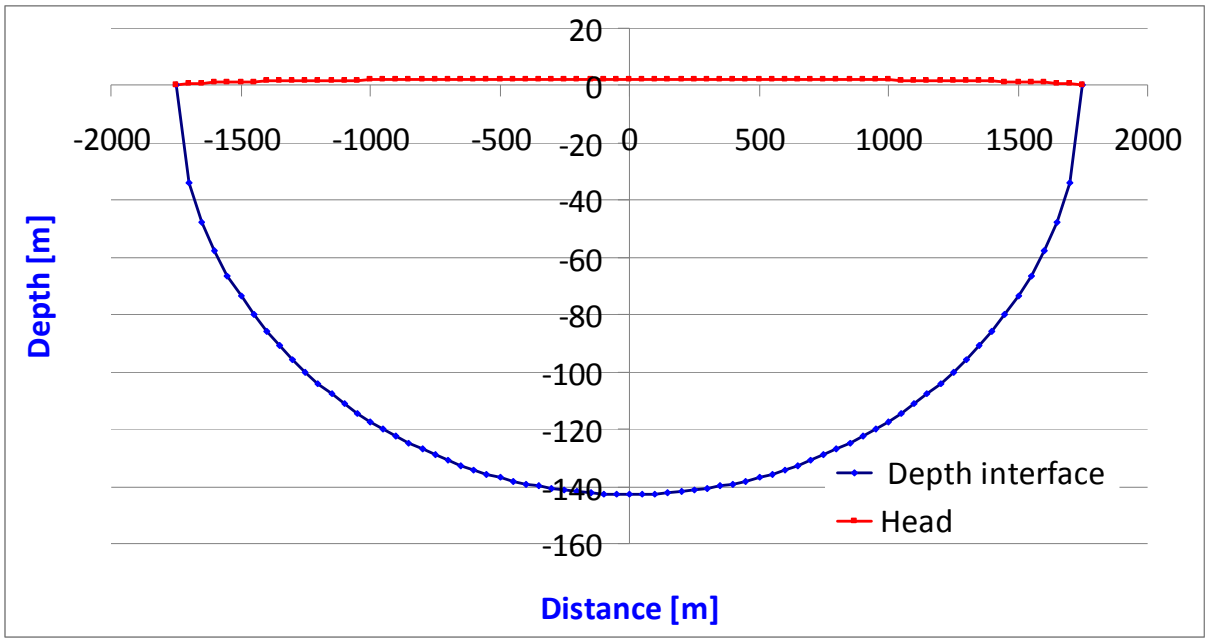

Graphic 2-4: Estimation of depth of the fresh-salt interface and the piezometric head of freshwater in *Monte Conero* using the Ghyben-Herzberg (1889; 1901) equation

In Graphic 2-4 it is possible to appreciate that the piezometric level has a little elevation from the sea level, with a maximum of 2.43 [m] in the centre of the island and decreasing gradually toward the boundaries. The maximum depth of the freshwater lens is about 140 metres.

c. Saltwater Intrusion

Since *Monte Conero* is along the coast, there is the potential for saltwater intrusion into its aquifers. A saltwater wedge underlies fresh water aquifers in all coastal aquifers, also those that are in a natural state (for example Vacher, 1988; Antonellini *et al.*, 2008).

The salt water is separated from the freshwater by a so called mixing zone of barckish water. The depth to the mixing zone is influenced by many natural factors such as the amount of recharge, as well as by human interventions such as drainage or pumping.

Salt or brackish water is indeed present in Monte Conero: the two lakes of *Portonovo* are filled with brackish groundwater that is above a layer of saltwater (Colosimo & Crescenti, 1973; Conti 1997).

Below follows an overview of measure electrical conductivity in the lakes, encountered in the literature. Both lakes are filled with brackish water, being, at present, the *Lago Piccolo* that has electrical conductivities with values that are close to those of seawater (the electrical conductivity of the Adriatic Sea in May 2011 was of 46.6 [mS/cm] at 22.8 ºC). The average superficial electrical conductivity of the *Lago Piccolo* varied throughout time (Table 2-2). During the summer of 1982 it was 10.78 [mS/cm] (Marelli, 1982) and in 1994 it was 22.7 [mS/cm] (Turroni, 1994). During August 1997 the average electrical conductivity was 14 [mS/cm] at an average temperature of 28 ºC (Conti, 1998). In November 1997, the superficial electrical conductivity was 7.8 [mS/cm] at 12.7 ºC and at bottom it was of 12.1 [mS/cm] at 14.3 ºC (Conti, 1998). In May 2011 we measured a superficial electrical conductivity of 30.38 [mS/cm] at 25.9 ºC.

In the *Lago Grande* the values of electrical conductivity are relatively constant over the years (Table 2-2). In this lake were registered electrical conductivities of 8.12 [mS/cm] in 1982 (Marelli, 1984) and 3.75 [mS/cm] in 1994 (Turroni, 1994). Toward the end of the summer of 1997, the lake had an average and superficial electrical conductivity of 6.45 [mS/cm] at an average temperature of 27.6 ºC (Conti, 1998). In November 1997, the superficial electrical conductivity was of 2.1 [mS/cm] and at bottom was of 5.2 [mS/cm] at

13.2 ºC (Conti, 1998). In May 2011 we registered a superficial electrical conductivity of 11.4 [mS/cm] at 24.2 ºC

Table 2-2: Electrical Conductivities registered in different periods

Source	Year / season	Depth	Lago Piccolo		Lago Grande	
			Elect.Cond.	T º	Elect.Cond.	T º
			[mS/cm]	[º C]	[mS/cm]	[º C]
Marelli, 1984	1982 summer	superficial	10,78	no data	8,12	no data
Turroni, 1994	1994 summer	superficial	22,70	no data	3,75	no data
Conti, 1998	1997 August	superficial	13,97	28,30	6,41	28,40
Conti, 1998	1997 August	superficial	14,12	27,60	6,44	27,20
Conti, 1998	1997 September	superficial	no data	no data	6,49	27,30
Conti, 1998	1997 November	superficial	7,84	12,70	2,09	13,00
Conti, 1998	1997 November	bottom	12,11	14,30	5,23	13,30
fieldwork	2011 May	superficial	30,38	25,90	11,40	24,20

The data shown in Table 2-2 shows that the recharge of rainwater during the winter months (Section 2.2.2, part a, Graphic 2-2). This could be associated to the diminution of the electrical conductivity in the lakes. The results of Conti (1998) suggest that the lakes would be in contact with the brackish-salt water, since on the bottom the values of electrical conductivity are within the theoretical ranges for this parameter. In 2011, the highest value of electrical conductivity was registered at the surface of the lakes.

The following graphic shows the values reported by Conti (1998) for the wells of the area of *Portonovo* (Figure 2-18 of Section 2.2.1).

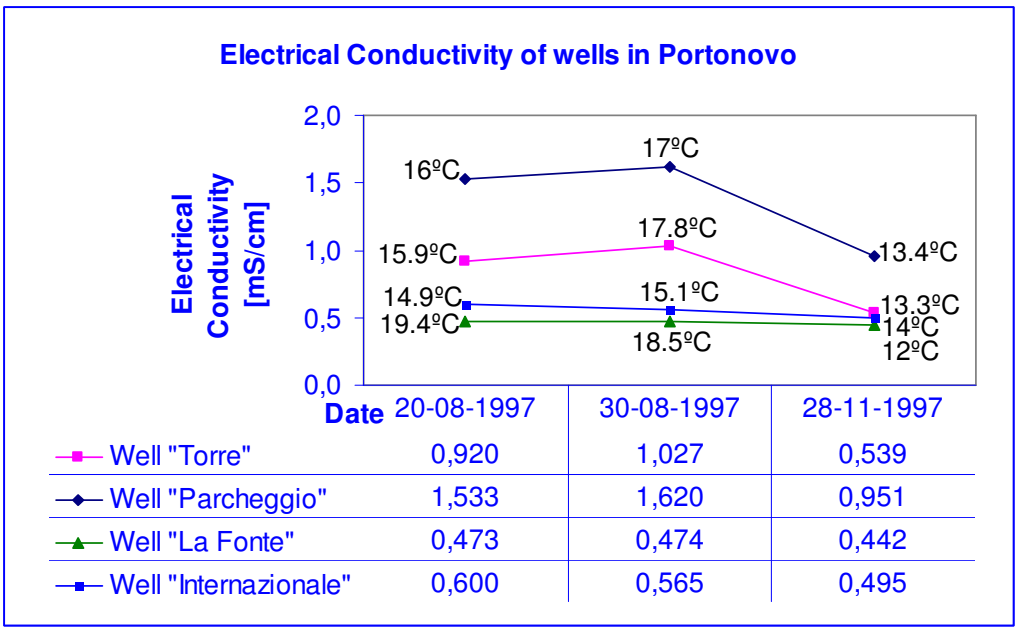

Graphic 2-5: Variation of the Electrical Conductivity in the aquifer of Portonovo. The numbers on the points in the graphic indicate the temperature of the water during the measurements. (based on Conti, 1998)

The spring of *Portonovo* is located in close to the well "*La Fonte*" (Figure 2-18 of Section 2.2.1) and has practically the same values of this well, whereas its temperature is 14.5 ºC. As in the case of the lakes, for the wells and spring the recharge of rainwater generates a diminution of the electrical conductivity levels.

In the hinterland, the spring of *San Lorenzo* shown a low electrical conductivity (665.9 [$\mu S / cm$] at 18.7 [ºC]), as a signal that in this area there is not saltwater intrusion.

d. Conceptual Model of the aquifer

On the basis of the information described above a conceptual hydrogeological model of the *Monte Conero* was elaborated (Figure 2-23). The permeability (by fracturing) of the geological formation of the *Maiolica* and Scaglia *Rossa*, the absence of permeability of the *Marne a Fucoidi* and the characteristic of the discharge points (springs and lakes), defined the presence of two parallel aquifers. These two aquifers are also explained by the

values of the electrical conductivity as indicator of saltwater intrusion. In the spring of the hinterland, the value of the electrical conductivity was considerably lower than the spring along the coast, probably due to the folding of the impermeable layer of the *Marne a Fucoidi* which acts as a barrier of protection to the aquifer from saltwater intrusion. However, we have considered the theory of Ghyben-Herzberg which defines the presence of three different strata of water, since the *Marne a Fucoidi* Fm. may present a small permeability by fracturing.

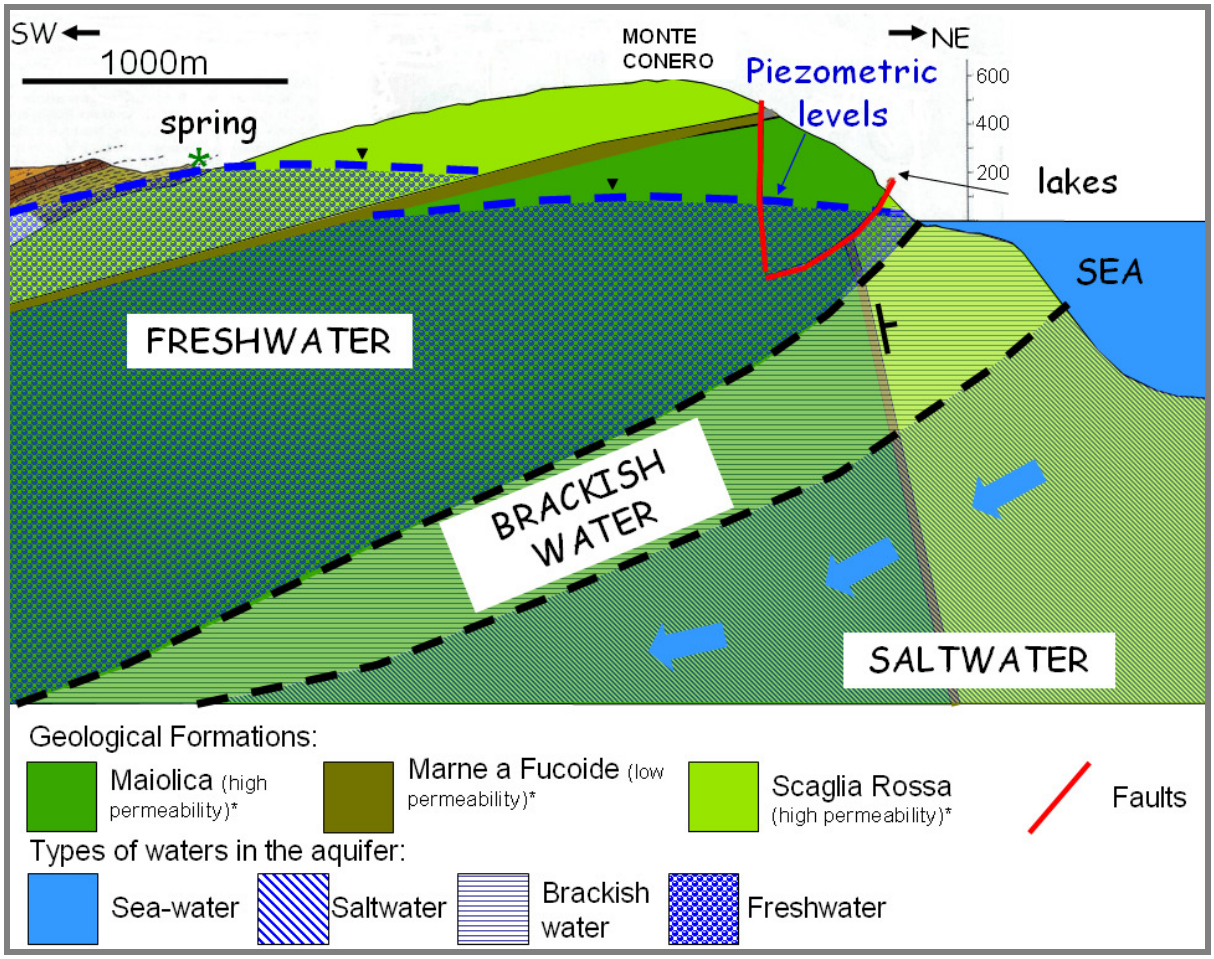

Figure 2-23: Conceptual hydrogeological model of the *Monte Conero*

CHAPTER 3: FRACTURE CHARACTERIZATION

3.1 Introduction

We studied outcrops in different structural positions of *Conero*'s anticline trying to find relationships between fracture patterns and structural position and thus the folding process. The localities of *Portonovo* and *Sirolo* were studied along the coast. In the hinterland the sector of *Fonte d'Olio* and the localities of *Massignano* and *Poggio d'Ancona* allowed us to study of this part of the fold. The carbonate outcrops studied are of the regional geological formations. The *Maiolica* Formation is exposed only in the *Portonovo* area while the *Scaglia Rossa* Formation crops out in the others localities. In the area of *Sirolo* the *Scaglia Variegata* Formation is also present (Figure 3-1).

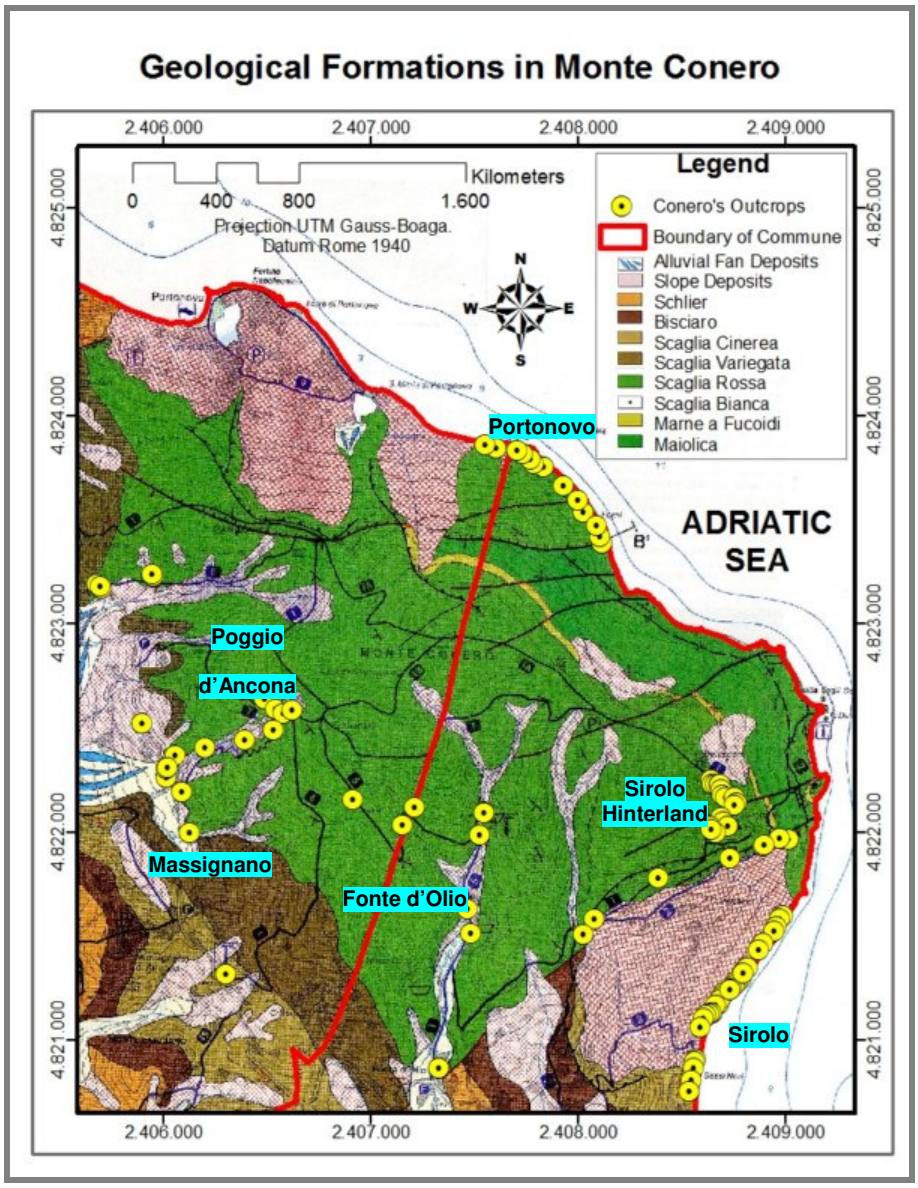

Figure 3-1: Geological Fms. on *Monte Conero*. The yellow marks show the geographical position of the outcrops visited. Based on Coccioni *et al.* (1997).

In this study we make reference to different concept of Structural Geology. In particular, we consider:

- Fracture: "Structure defined by two surfaces, or a zone, across which a displacement discontinuity occurs" (Aydin, 2000, p. 798). There are three modes of fractures, as is shown in Figure 3-2.

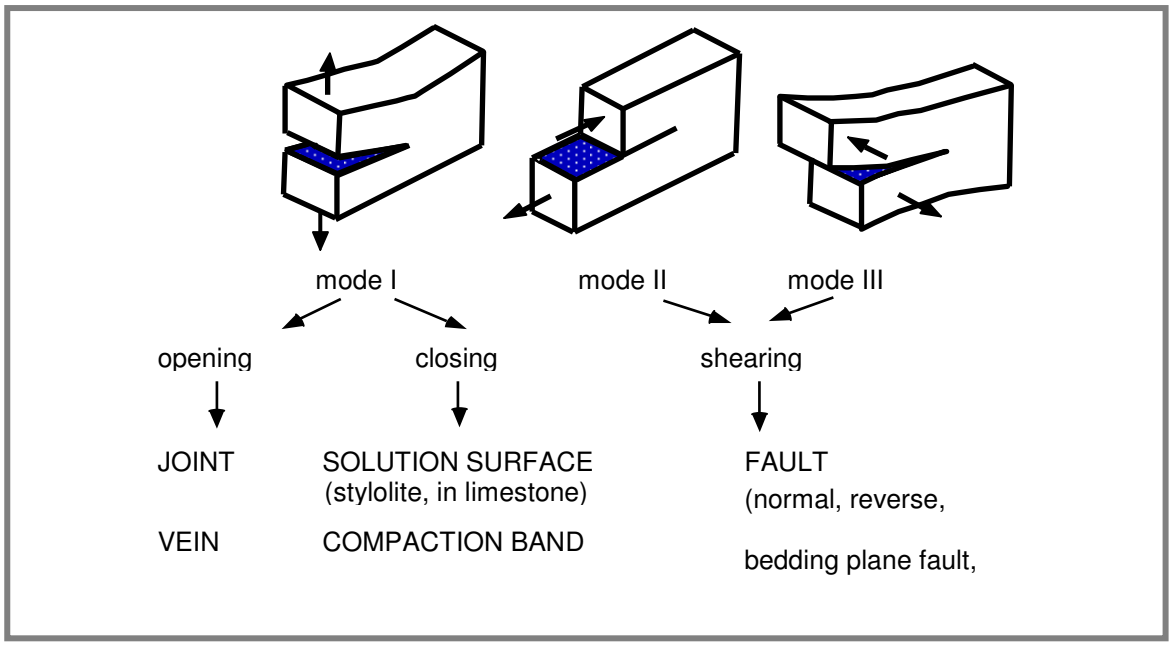

Figure 3-2: Modes of mechanical fractures

- Fault: “Planar or zonal structure across which appreciable shear displacement discontinuities occur” (Billings, 1972, p. 174). There are different types of faults according to the shear displacement, as is shown in Figure 3-3.

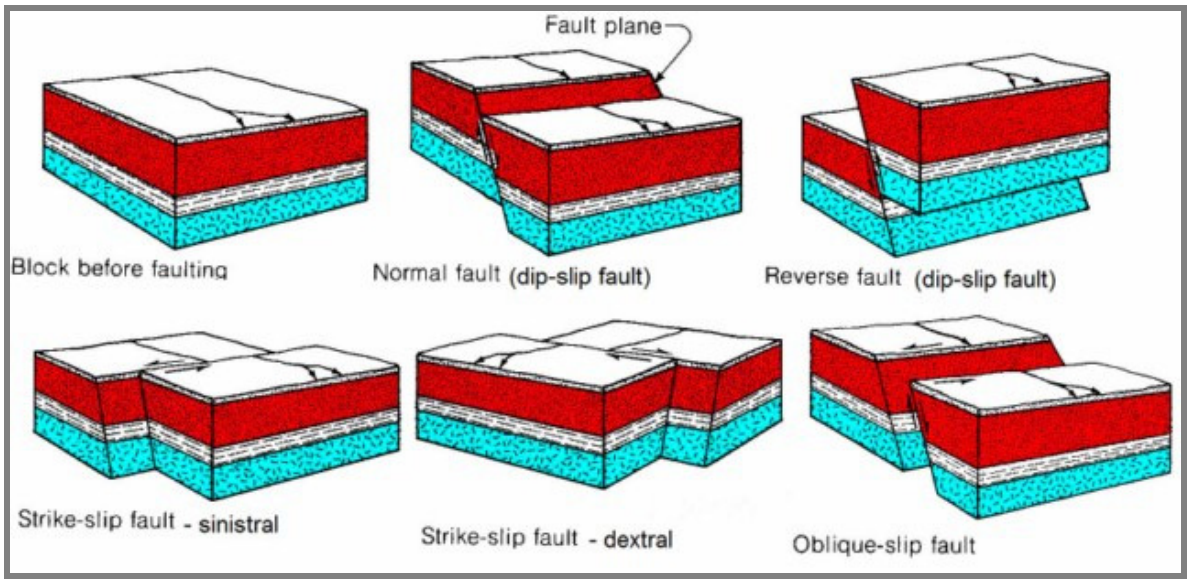

Figure 3-3: Types of Faults

- Vein: It is the same type of joint but typically filled with some mineral.
- Joint: “Fracture having field evidence for predominantly opening displacements between their opposing walls” (Pollard and Aydin, 1988)
- Stylolite: It is caused by pressure solution.

The classification of stylolites according to the pure geometry is composed of (Park & Schot, 1968): (1) Simple or primitive wave-like type, (2) Sutured type, (3) Up-peak type (rectangular type), (4) Down-peak type (rectangular type), (5) Sharp-peak type (tapered and pointed), (6) Seismogram type.

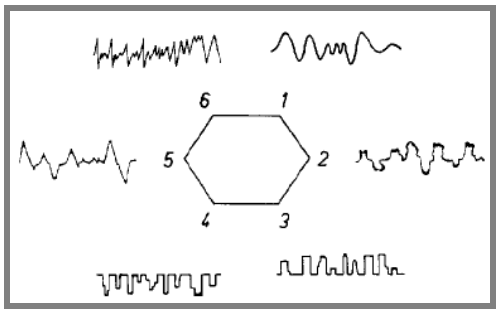

Figure 3-4: Classification of stylolites according to geometry

The classification of stylolites in relation to the bedding plane is composed of (Park & Schot, 1968): (1) Horizontal stylolites, (2) Inclined stylolites, (3) Horizontal-inclined (vertical)-crosscutting stylolites, (4) Vertical stylolites, (5) Interconnecting network stylolites, (6) Vertical-inclined (horizontal)-crosscutting stylolites.

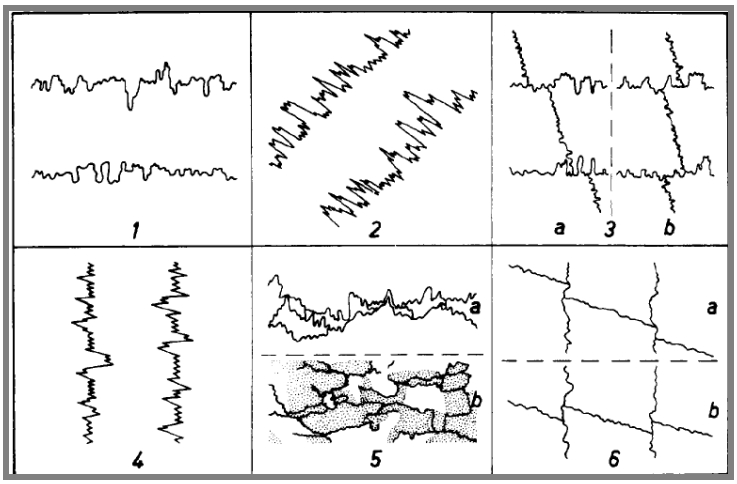

Figure 3-5: Classification of stylolites in relation to the bedding

- Breccia or breccia zone: It is the area generated due to the displacement of the planes of a fault.
- Set of fractures: It is composed of fractures with similar proprieties, commonly the orientation.
- Stress: According to the direction the component of the stress, different fractures may be generated (Figure 3-6).

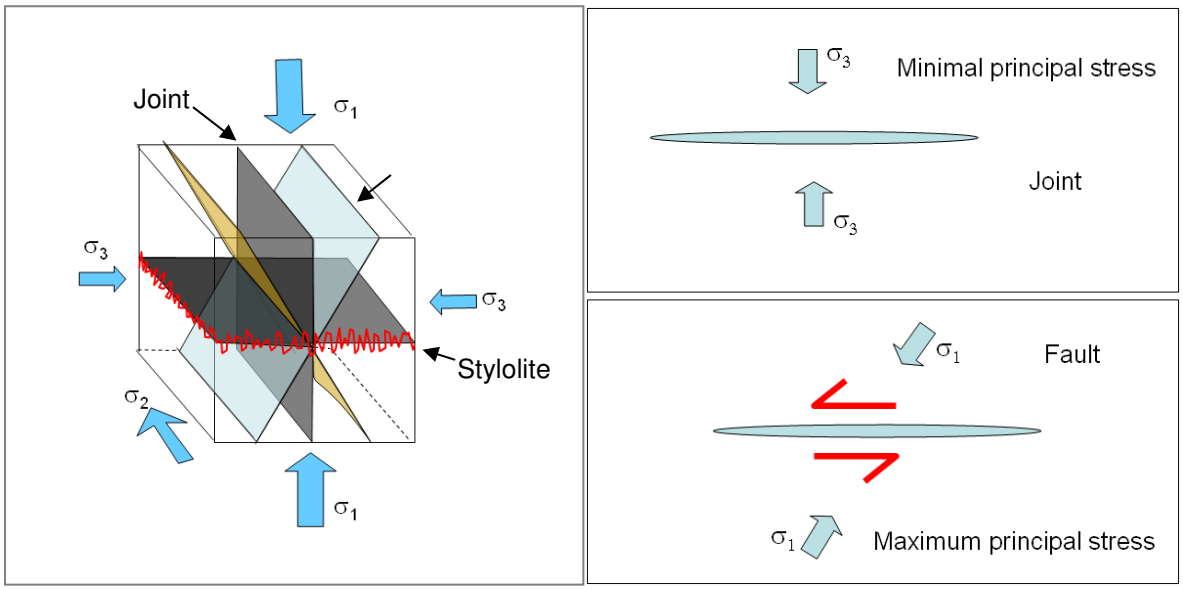

Figure 3-6: Fractures generated according to the stress components

- Joints are perpendicular to s3
- Stylolites are perpendicular to s1
- Faults at 25°-40° angle to s3

3.2 Methods

The fracture sets were defined on the basis of the mechanical type of fractures, their orientation and their arrangement in the outcrops. This was done for both geological formations that were studied: The *Maiolica-* and *Scaglia Rossa formation*. The *Maiolica* Formation crops out along the coast, whereas the *Scaglia Rossa* Formation crops out along the cost but also in the hinterland. Therefore the outcrops of the Scaglia Rossa were divided in two areas: coastline and hinterland due to their different fracture characteristics. The hinterland outcrops are in the gentler dipping layers in the western part of the fold whereas the coastal outcrops are in the steeper layers of the fold in the eastern part. With this separation of areas in the *Scaglia Rossa* it is also possible to study better the relationship between fractures and bedding orientation, and between fractures and the fold axis. In consequence, characterization of the various fracture orientations was made for three areas: *Maiolica* (coastline), *Scaglia Rossa*–hinterland and *Scaglia Rossa*–coastline.

The fracture characterization was based on the following information:

- Mechanical types of fractures (i.e. joints, stylolites, veins, faults and breccias): We studied each type of fracture separately since - how we will explain later - each one has different properties in terms of fluid flow.

- Fracture orientation (dip-angle and dip-direction, Figure 3-7): Studying the orientation of fractures gives us an idea of the orientation of other fractures non-accessible, which is especially important in studies of fractured aquifers.

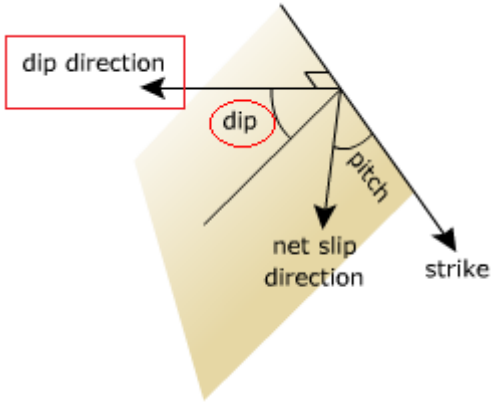

Figure 3-7: Dip-direction and Dip-angle in a plane

- Relative orientation to bedding
- Geometry of fractures (e.g. length, spacing, opening, offset, shearing)
- Fracture crosscutting and abutting relationships
- Evolution of fractures (e.g. from veins to tail-cracks)

This information was collected on outcrops and on maps made from photo-mosaics of the outcrops. A study of thin sections added information at the micro scale.

3.3 Fracture Characterization in Outcrops

Five different fracture types have been observed on the outcrops of *Monte Conero*: veins, stylolites, joints, faults and breccias (as pockets and elongated areas). These fractures appear both arranged in systematic sets and as non-systematic structures. The recognition of fracture sets is important in order to identify the geological stages involved in the deformation of the *Conero* anticline. Each set and each mechanical type of fracture give us an estimation of the field stress under which fractures were formed.

Generally the fractures sets in the outcrops along the coast are easily recognized and well defined. In the Scaglia *Rossa*–hinterland the fracture density decreases considerably in relation to the other zones and fractures are typically confined within stratigraphic layers. In some outcrops of the *Scaglia Rossa*-coast but especially in the hinterland, a systematic arrangement of all fracture types was not possible to identify during the fieldworks. However, the data analysis with stereoplots shows that fractures that are non-systematic when measured individually on different outcrops, show up as groups of the same orientation on the stereoplot. For these groups of fractures only their orientation is given but it was not possible to identify their relationship with other sets. These groups of fractures – in this study – are referred as ‘non-systematic sets’ (in the tables of fracture sets the word ‘set’ is cancelled to indicate these ‘non-systematic sets’).

3.3.1 Veins

Veins occur in different geometries and feature, such as open, cemented with calcite and partially cemented (Figure 3-8). There is not a pattern of orientation but open and semi-open veins are usually located in the coastline. Open veins show evidences - residues of calcite - that they were filled veins before. Veins are present in all outcrops but with a different density level, the grater density is found in the *Scaglia Rossa* Fm. In the hinterland, veins are thinner and shorter than along the coast and they are always filled. Veins are present systematically but they are well-organized only along the coast.

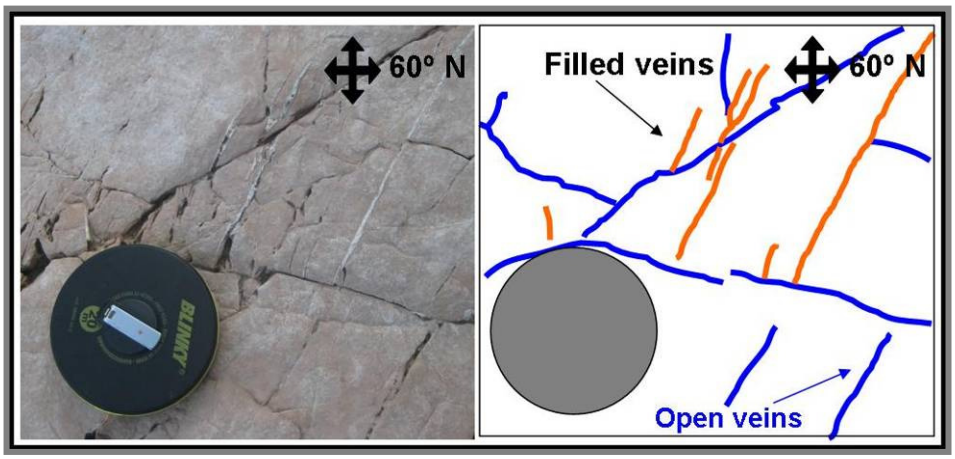

Figure 3-8: Open and filled veins in an outcrop of the *Scaglia Rossa* coastline

In the *Maiolica* Fm. five sets of veins were observed (Table 3-1, Figure 3-9). M-Set I considers open and filled vein which have an average orientation of 154/56º, a vein length which varies from 15 [cm] to 3 [m], a vein opening from 2 to 10 [mm] and a spacing from 2-10 [cm]. Veins of M-Set II are open and have a mean orientation of 293/56º, with 7 to 60 [cm] length and 3 to 22 [cm] of spacing. M-Set III consider open and filled veins which are oriented in the mean plane 54/33º, its typical fracture density is 6 veins per metre, and

veins vary from 5 to 30 [cm] in length and from 2 to 4 [cm] in wide. M-Set IV is composed by open veins which have a mean orientation of 325/88º and fractures length of its veins vary from 20 to 150 [cm], the opening from 5 to 30 [mm] and the spacing from 4 to 30 [cm]. Filled veins in M-Set V are typically oriented at 203/44º, have length from 6 to 15 [cm], openings from 0.5 to 1.5 [mm] and their spacing vary from 4.5 to 17 [cm]. In the coastline of the *Scaglia Rossa* Fm. three systematic sets of veins were observed (Figure 3-10). SR-Set I consider semi-open veins which are characterized by an orientation of 333/55º, veins with lengths from 8 to 30 [cm], openings from 0.5 to 1 [mm], and a spacing which varies from 1 to 8 [cm]. SR-Set II has open veins typically oriented in 283/71º and with 7 to 20 [cm] in length, 1.5 to 5 [mm] of opening and a spacing between 1 and 30 [cm]. SR-Set III has filled veins oriented at 162/71º, its veins have length between 3 and 7 [cm], openings greater than 0.5 [mm] and the spacing varies from 3 to 5 [cm]. In the hinterland of the *Scaglia Rossa* Fm. two sets were identified (Figure 3-11). SRh-Set I has filled veins oriented at 345/80º, with lengths from 13 to 24 [cm], openings from 0.5 to 1.5 [mm] and a spacing from 2 to 10 [cm]. SRh-Set II has filled veins with a mean orientation of 249/86º and veins with lengths which vary from 5 to 15 [cm], openings from 0.1 to 1 [mm] and a spacing of 15 [cm]. Most of vein sets are oriented at high angle to bedding (M-Set I, M-Set II, M-Set IV, M-Set V, SR-Set I, SR-Set II, SRh-Set I and SRh-Set II) and at high angle to the fold axis (M-Set I, M-Set II, M-Set IV, M-Set V, SR-Set I, SR-Set II, SR-Set III and SRh-Set I).

Table 3-1: Geometric properties of systematic veins observed in *Monte Conero*

Lithology	Set ID	Orientation		Angle to bedding	Angle to the fold axis	Density [nº per metre]	Length [cm]	Opening [mm]	Spacing [cm]
		Dip-dir	Dip-ang						
Maiolica (47/48)[1]	M-Set I open + filled	154	56	78	90	12	15-300	2-10	2-10
	M-Set II open	293	56	83	84	18	7-60	0.5-5	3-22
	M-Set III open+filled	54	33	16	36	6	5-30	2-4	4-30
	M-Set IV open	325	88	83	83	24	20-150	5-30	4-30
	M-Set V filled	203	44	78	72	10	6-15	0.5-1.5	4.5-17
S. Rossa coastline (151/18)[1]	SR-Set I semiopen	333	55	73	66	12	8-30	0.5-1	1-8
	SR-Set II open	283	71	84	68	21	7-20	1.5-5	1-30
	SR-Set III filled	162	71	53	77	7	3-7	<0.5	3-5
	SR- IV	354	5	22	23	N/A	N/A	N/A	N/A
	SR- V	97	80	70	48	N/A	N/A	N/A	N/A
S. Rossa hinterland (179/8)[1]	SRh-Set I filled	341	80	89	65	5	13-24	0.5-1.5	20-25
	SRh-Set II filled	249	86	83	33	7	5-15	0.1-1	15
	SRh- III	95	55	55	42	N/A	N/A	N/A	N/A
	SRh- IV	175	40	32	86	N/A	N/A	N/A	N/A

N/A: not applicable; M: prefix for the Maiolica's sets; SR: prefix for the Scaglia Rossa coastline's sets and SRh: prefix for the Scaglia Rossa hinterland's sets

[1] The mean orientation of bedding in the geological formation

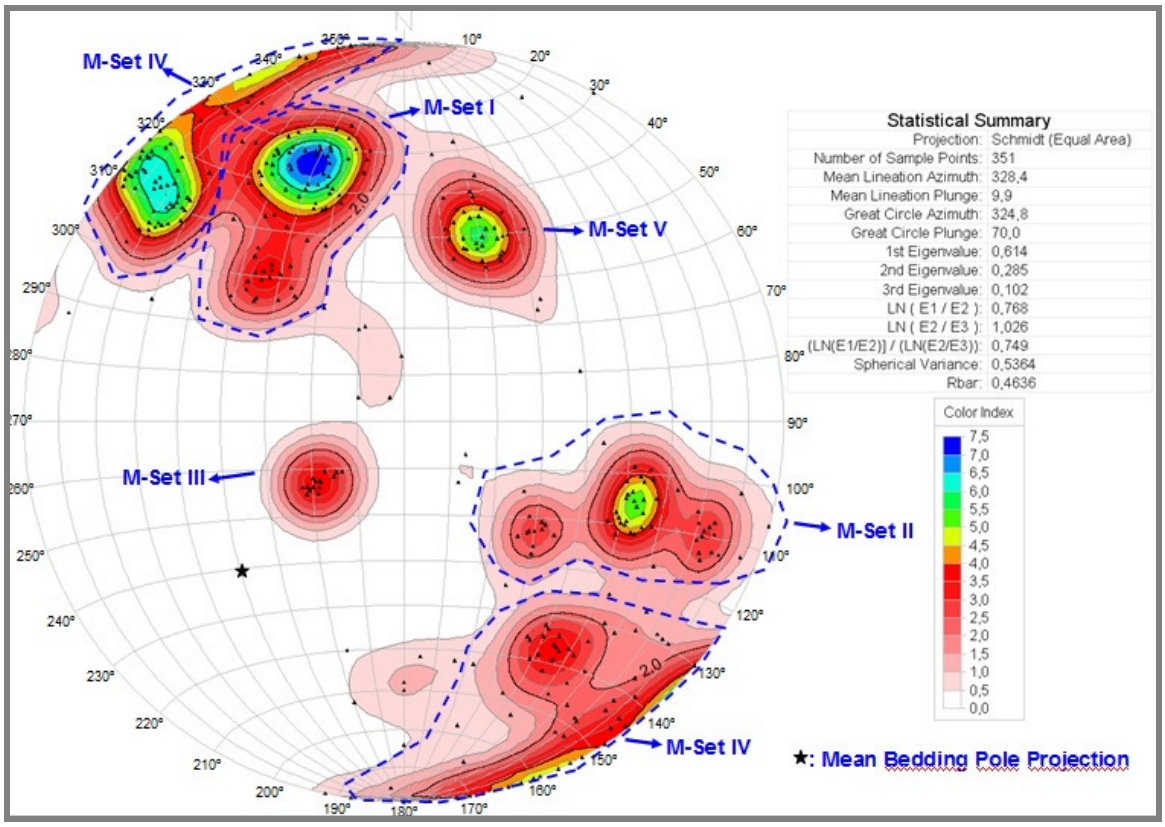

Figure 3-9: Stereoplot of vein sets in *Maiolica*

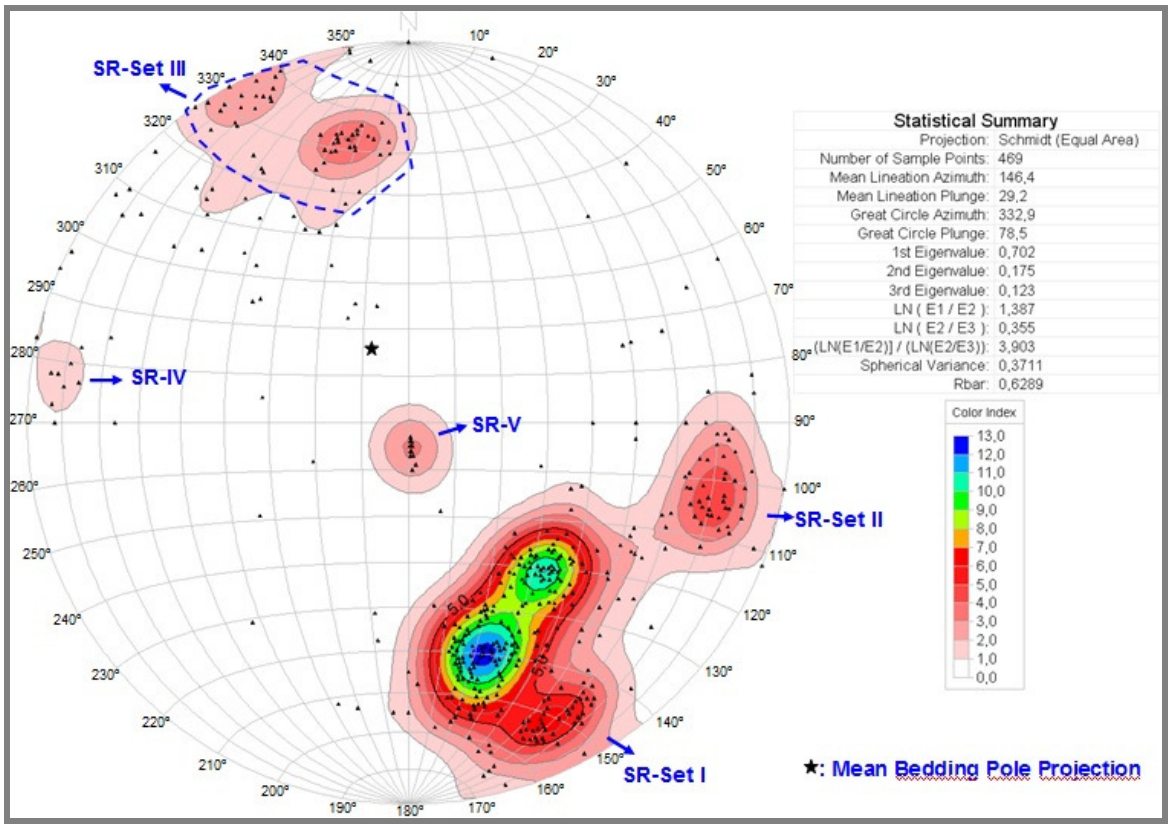

Figure 3-10: Stereoplot of vein sets in *Scaglia Rossa* coastline

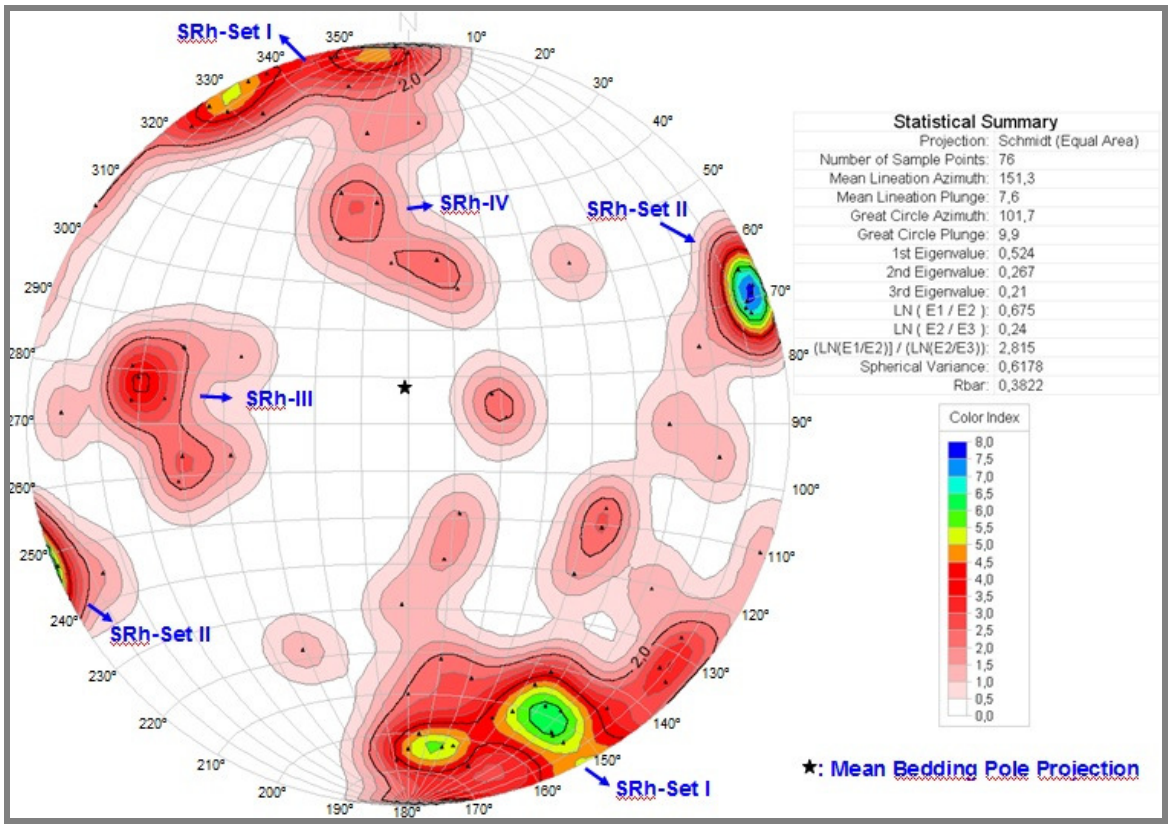

Figure 3-11: Stereoplot of vein sets in *Scaglia Rossa* hinterland

3.3.2 Stylolites

Stylolites are present in all outcrops studied (Figure 3-12) but with different properties like density, roughness, length as well as there are differences in the height and undulation of amplitude of their tooth like columns. Stylolites have different geometries and relation to the bedding. They are predominant in the coastal outcrops showing iron oxide residues. Some single stylolites appear with and intermittent length, that is, small lineal segments of stylolites following the same plane. In networks of stylolites the apparent displacement in crosscutting relationships is also variable while the orientation may have variations.

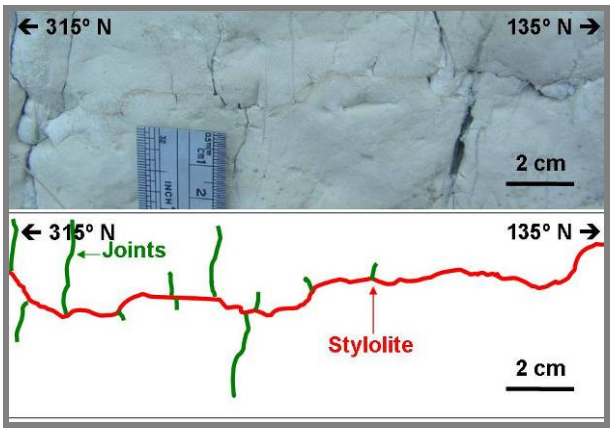

Figure 3-12: Stylolite in the *Maiolica* Fm. with joints associated

In the *Maiolica* Fm. three sets of stylolites were observed (Table 3-2; Figure 3-13). M-Set I is parallel to bedding with an average orientation of 44/47 and fracture density of 15 stylolites per metre. Stylolites of M-Set II have a mean orientation of 342/19, with 150 [m] length and 30 [cm] in spacing. M-Set III is oriented in the mean plane 268/64, with mean stylolites length of 2.5 [m] and 20 [cm] of spacing. In the coastline of the *Scaglia Rossa* Fm. three systematic sets of stylolites were observed (Figure 3-14). SR-Set I is parallel to bedding with an orientation of 87/10 and stylolites spaced in 25 [cm]. SR-Set II has stylolites typically oriented at 59/63 and with 1.2 [m] in length and 15 [cm] in spacing. SR-Set III is oriented at 326/57 with a mean of 1 stylolite per metre and a length of 50 [cm]. This is the only stylolites set with an opening (0.2 [mm]). In the *Scaglia* Rossa-hinterland (Figure 3-15), SRh-Set I is characterized by a mean orientation of 62/68, stylolites with 50 [cm] of length and a spacing of 1.1 [m]. Stylolites in SRh-Set II are typically oriented at 219/46, have lengths of 35 [cm] and are spaced among them by 40 [cm]. SRh-Set III involves stylolites oriented at 111/54º, with length of 80 [cm] and spacing of 50 [cm]. Stylolites sets M-Set III, SR-Set II, SR-Set III, SRh-Set I and SRh-Set II are oriented at high angle to bedding (about 72º). M-Set II, M-Set III, SR-Set I, SR-Set III and SRh-Set II are oriented at high angle to the fold axis (about 67º).

At this scale, all stylolites observed are 'aggregate stylolites', that is, the height of the amplitude is greater than the width (Park & Schot, 1968). According to the geometric classification of Park & Schot (1968), in our study area we found stylolites seams of type 'simple wave-like', 'sutured', 'up-peak', 'rectangular' and 'down-peak' (see Section **¡Error! No se encuentra el origen de la referencia.**). Generally, the height of the amplitude ranges from a micrometric scale to 5 millimetres, while the width ranges from micrometric scale to 3 cm. With respect to the dimensions of length, they vary between 2 cm and the full extension of the layers.

Table 3-2: Geometric properties of systematic stylolites observed in *Monte Conero*

Lithology	Set ID	Orientation		Angle to bedding	Angle to the fold axis	Density [nº per metre]	Length [cm]	Opening [mm]	Spacing [cm]
		Dip-dir	Dip-ang						
Maiolica (47/48)[1]	M-Set I	44	47	3	22	15	As bedding	0	5-25
	M-Set II	342	19	43	62	3	150	0	30
	M-Set III	268	64	78	62	5	250	0	20
S. Rossa coastline (151/18)[1]	SR-Set I	87	10	16	61	4	As bedding	0	25
	SR-Set II	59	63	65	11	7	120	0	15
	SR-Set III	326	57	75	72	1	50	0.2	120
	SR- IV	140	50	33	78	N/A	N/A	N/A	N/A
	SR- V	247	44	48	71	N/A	N/A	N/A	N/A
S. Rossa hinterland (179/8)[1]	SRh-Set I	62	68	72	13	1	50	0	110
	SRh-Set II	219	46	69	66	3	35	0	40
	SRh-Set III	111	54	51	56	2	80	0	50

N/A: not applicable; M: prefix for the Maiolica's sets and SR: prefix for the Scaglia Rossa coastline's sets

[1] The mean orientation of bedding in the geological formation

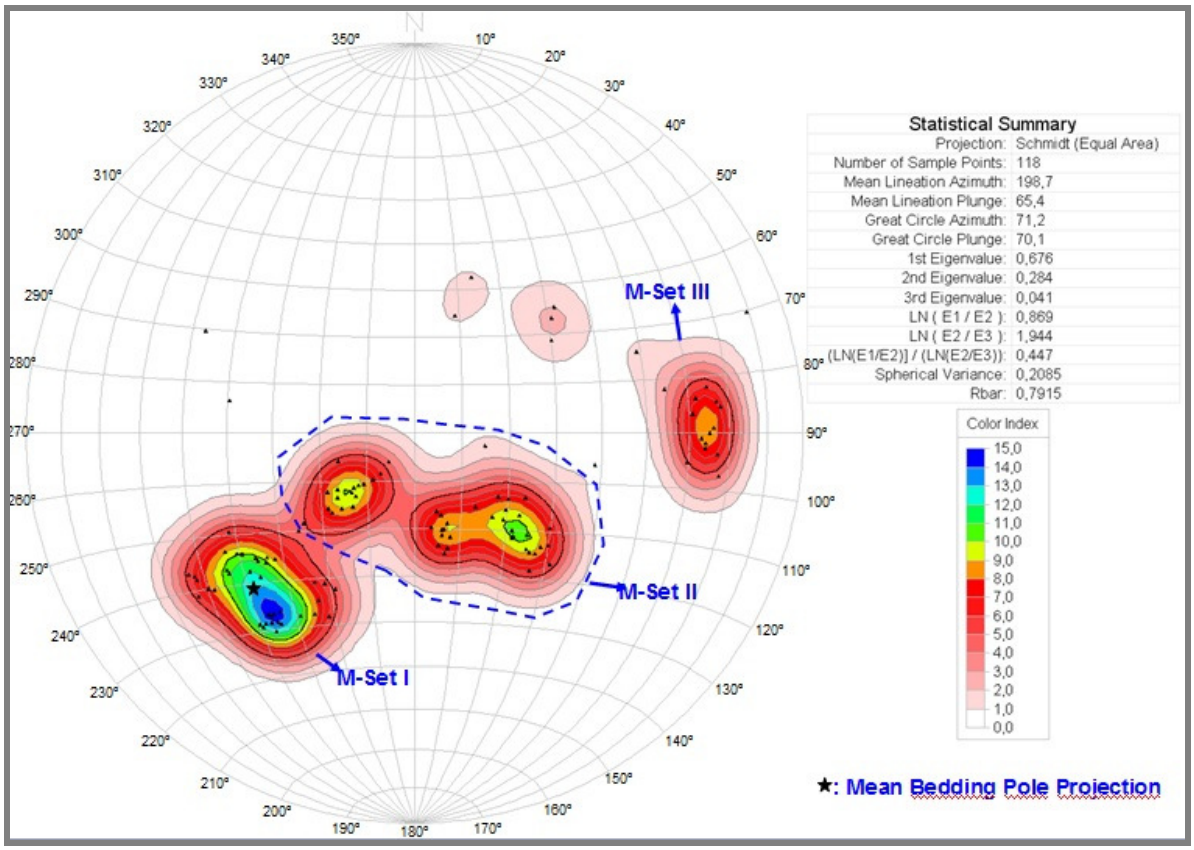

Figure 3-13: Stereoplot of stylolite sets in *Maiolica*

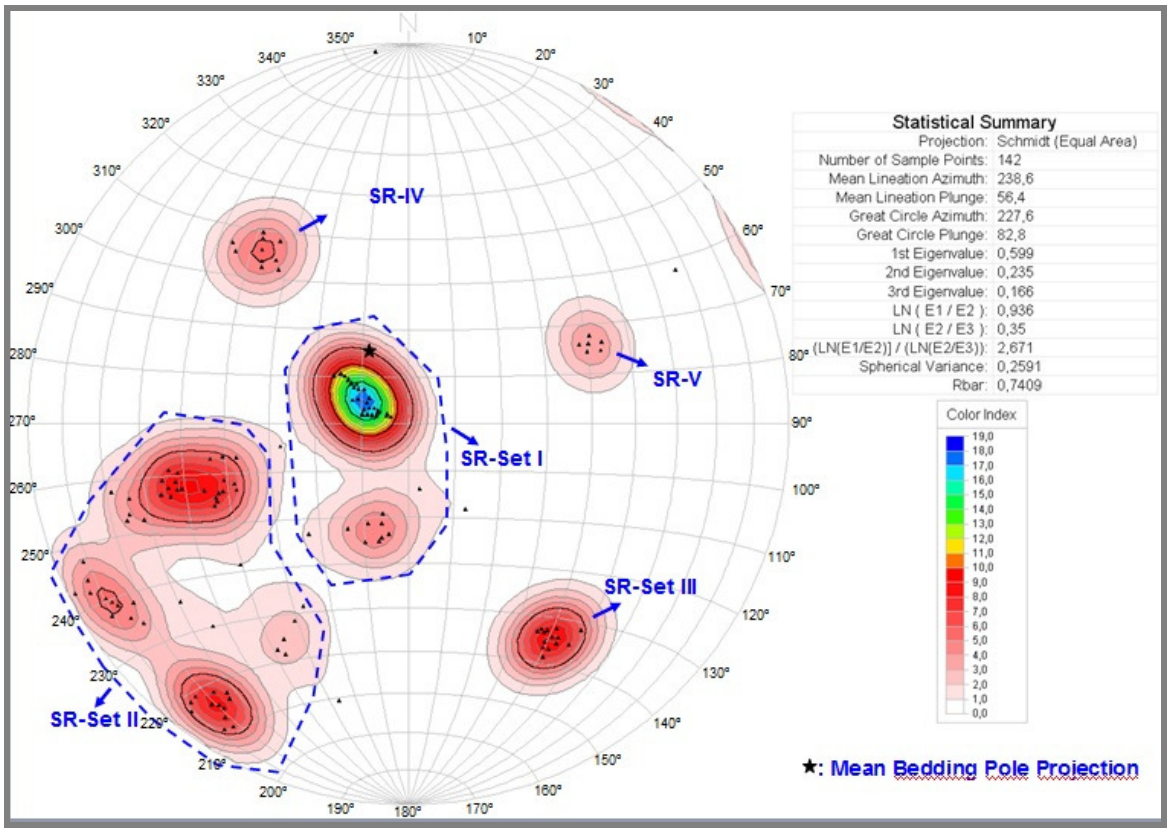

Figure 3-14: Stereoplot of stylolite sets in *Scaglia Rossa* coastline

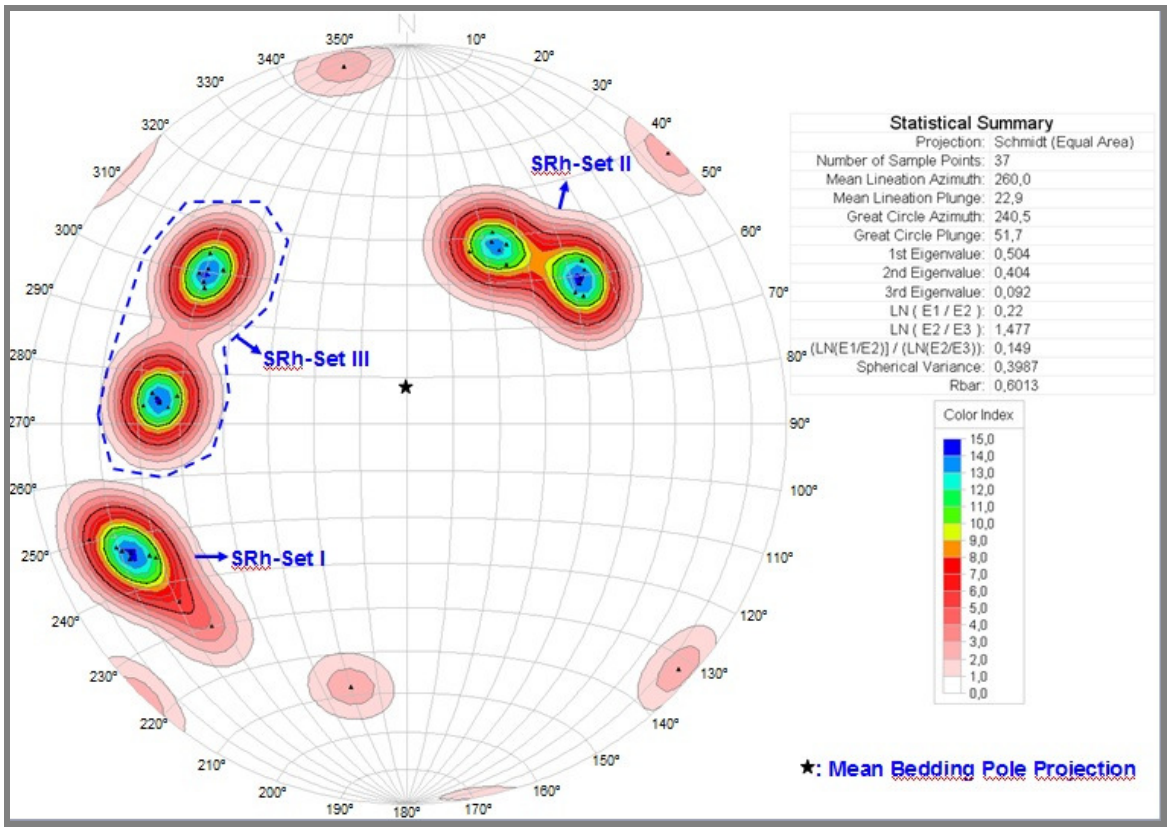

Figure 3-15: Stereoplot of stylolite sets in *Scaglia Rossa* hinterland

3.3.3 Joints

Joints occur in systematic sets only in the *Scaglia Rossa* (Figure 3-16), particularly in the hinterland, where there are three sets recognized in the majority of outcrops (**Table 3-3**). Along the coast only one set was identified in only one outcrop. All sets of joints are confined by layer-boundaries; therefore their lengths are about 15-20 cm.

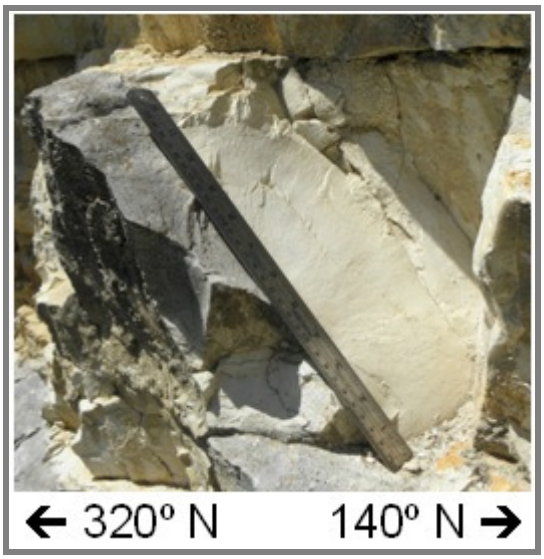

Figure 3-16: Joint observed in the area of *Fonte d'Olio*

SRh-Set I has an average orientation of 182/77º (Figure 3-17), a join opening of 1.5 [mm] and a mean spacing of 30 [cm]. Joints of SRh-Set II have a mean orientation of 278/87º with 1 [mm] of opening. They are distanced among them in about 20 [cm]. SRh-Set III is oriented in the mean plane 65/80º, its typical fracture density is 2 joints per metre, and joints have 1.8 [mm] of opening. All joint sets are oriented at high angle to bedding (about 80º) and are oriented at low angle to fold axis (about 44º).

Table 3-3: Geometric properties of systematic joints observed in *Monte Conero*

Lithology	Set ID	Orientation		Angle to bedding	Angle to the fold axis	Density [nº per metre]	Length [cm]	Opening [mm]	Spacing [cm]
		Dip-dir	Dip-ang						
S. Rossa hinterland (179/8)[1]	SRh-Set I	182	77	69	57	4	15	1.5	30
	SRh-Set II	278	87	88	54	5	15	1	20
	SRh-Set III	65	80	83	20	2	20	1.8	55

SRh: prefix for the Scaglia Rossa hinterland's sets

[1] The mean orientation of bedding in the geological formation

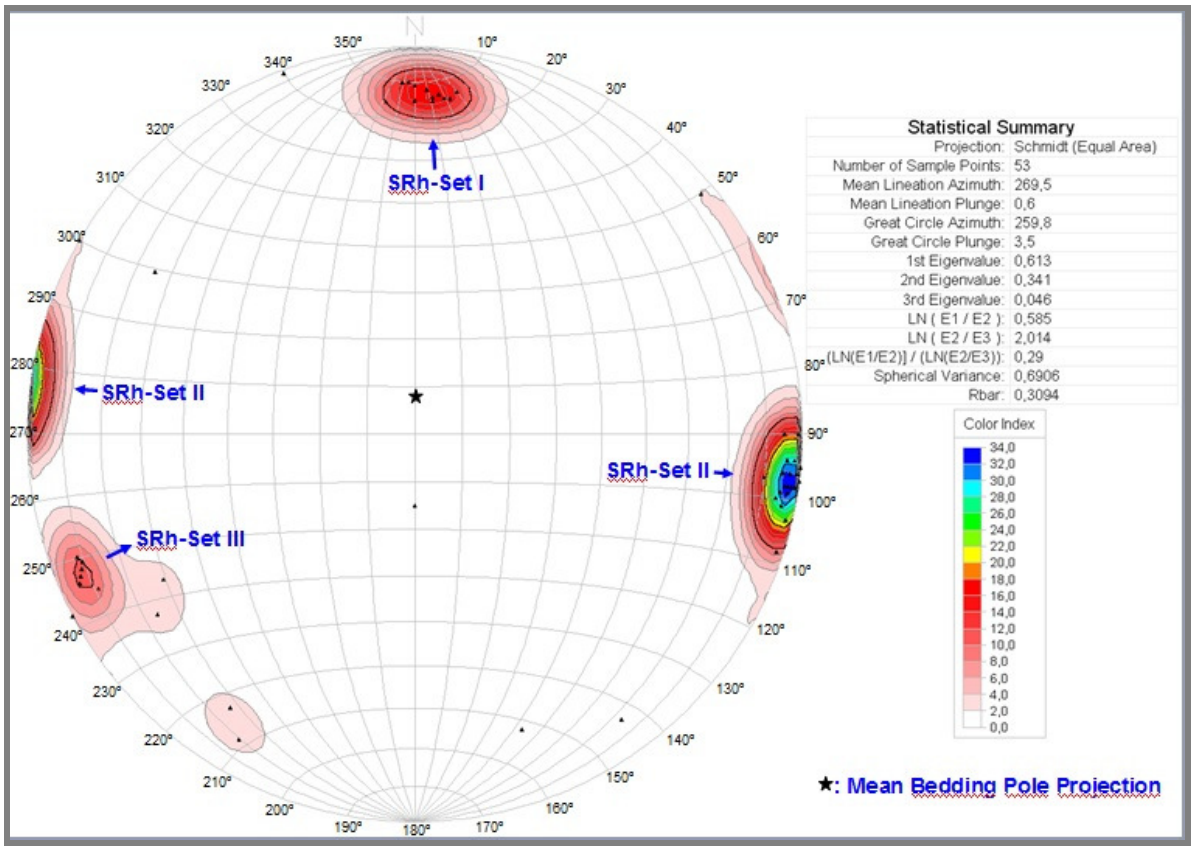

Figure 3-17: Stereoplot of joint sets in *Scaglia Rossa*-hinterland

3.3.4 Faults/Breccias

Faults and breccias have been considered together as 'breccias/faults' because in the majority of cases, faults have a breccia zone (Figure 3-18). But not in all cases was possible to associate a breccia zone to a fault because an offset was not evident. The faults observed in *Monte Conero*'s outcrops are normal or strike-slip. Normal faults are typically in a scale of centimetres while the strike-slip faults are in scale of metres. On the fault surface of the strike-slip faults slickenlines have been observed with an average orientation of 302/42 and their offset across the fault surface ranges from centimetres to 1 metre.

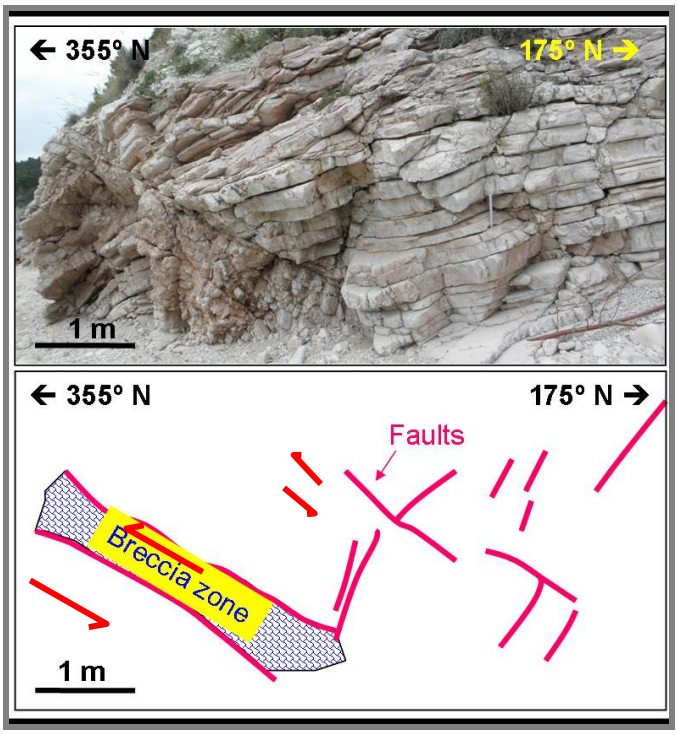

Figure 3-18: Normal faults and normal faults/breccia in the *Scaglia Rossa* Fm.

In the *Maiolica* Fm. three sets of breccias/faults were observed (**Table 3-4**, Figure 3-20). M-Set I has an average orientation of 117/52º, a normal offset that varies between 30 [cm] and 50 [cm], a typical fault length of 3 [m], a fault wide of 50 [cm] and a mean spacing of 40 [cm]. Faults/breccias of M-Set II have a mean orientation of 162/89º, with 2.8 [m] length and 20 [cm] wide. They are distanced among them in about 80 [cm]. M-Set III is oriented in the mean plane 303/66º, its typical fracture density is 2 faults per metre, and faults are 2 [m] length and 30 [cm] wide. In the coastline of the *Scaglia Rossa* Fm. two systematic sets of faults were observed (Figure 3-21). SR-Set I is characterized by an orientation of 9/36º, faults with 1 [m] length and 10 [cm] wide, and spacing of 60 [cm]. Offsets are in the order of 5 [cm]. SR-Set II has fractures typically oriented in 159/56º and with 1.3 [m] in length and 15 [mm] opening, spaced among them by 1.5 [m]. Fault sets M-Set II and M-Set II are oriented at high angle to bedding (about 78º). M-Set III and SR-Set II are the only sets oriented at high angle to the fold axis (about 86º).

Faults wider than 30 [cm] typically have zones of breccias in the centre (Figure 3-19). The length of these breccias zones is typically 2 [m]. The thickness of brecciated area varies from 10 to 50 [cm]. The rock fragments inside the breccias are 3 by 3 [cm], and have a parallelepiped shape. The matrix in between the rock fragment consists of limestone with grain size in millimetre scale.

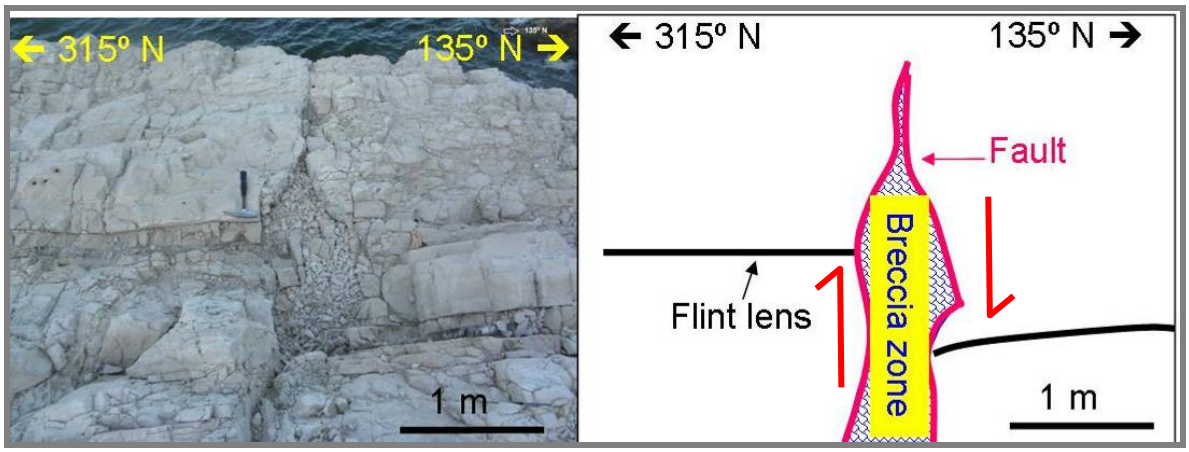

Figure 3-19: Breccia zone in a strike-slipe fault, *Maiolica* Fm.

Table 3-4: Geometric properties of systematic breccias/faults observed in *Monte Conero*

Lithology	Set ID	Orientation		Angle to bedding	Angle to the fold axis	Density [nº per metre]	Length [cm]	Wide [cm]	Spacing [cm]
		Dip-dir	Dip-ang						
Maiolica (47/48)[1]	M-Set I	117	52	53	60	4	300	50	40
	M-Set II	162	89	72	68	3	280	20	80
	M-Set III	303	66	84	87	2	200	30	50
S. Rossa coastline (151/18)[1]	SR-Set I	9	36	52	44	2	100	10	60
	SR-Set II	159	56	38	86	1	130	15	150
	SR- III	116	82	67	66	N/A	N/A	N/A	N/A
	SR- IV	206	65	56	52	N/A	N/A	N/A	N/A

N/A: not applicable; M: prefix for the Maiolica's sets and SR: prefix for the Scaglia Rossa coastline's

[1] The mean orientation of bedding in the geological formation

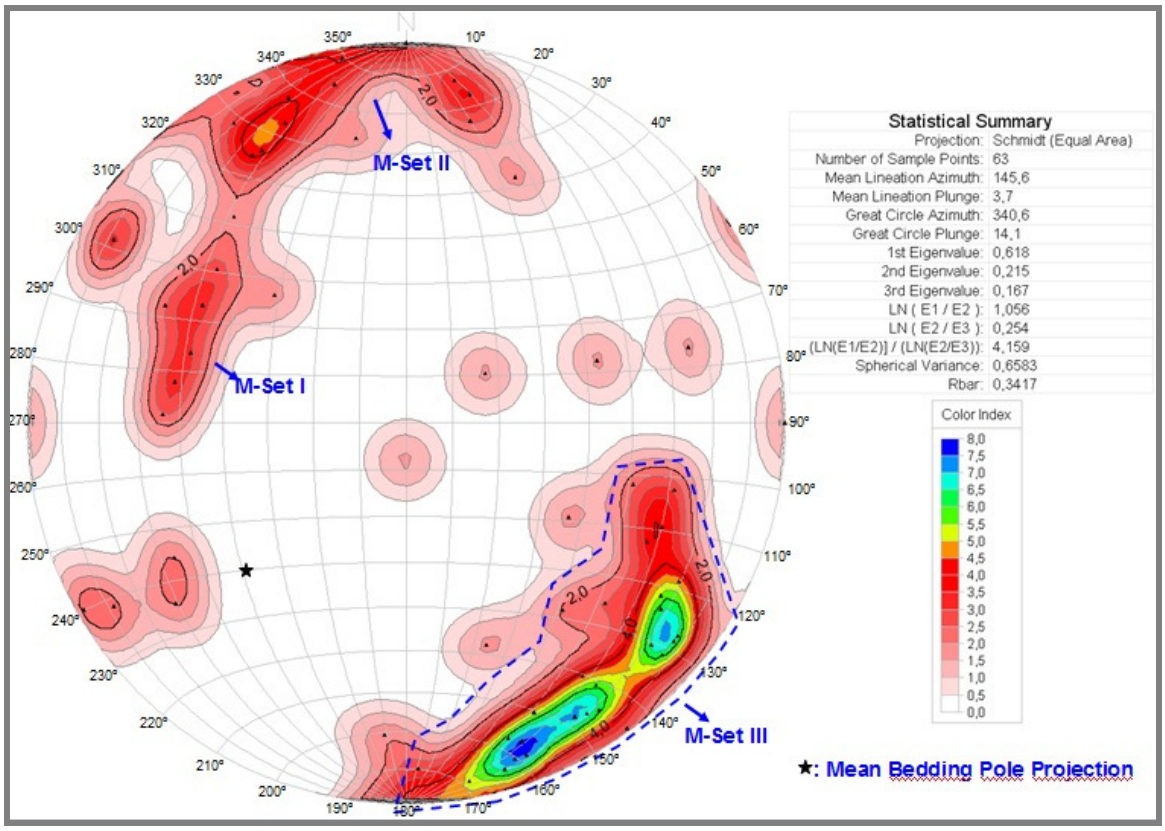

Figure 3-20: Stereoplot of fault sets in the *Maiolica*

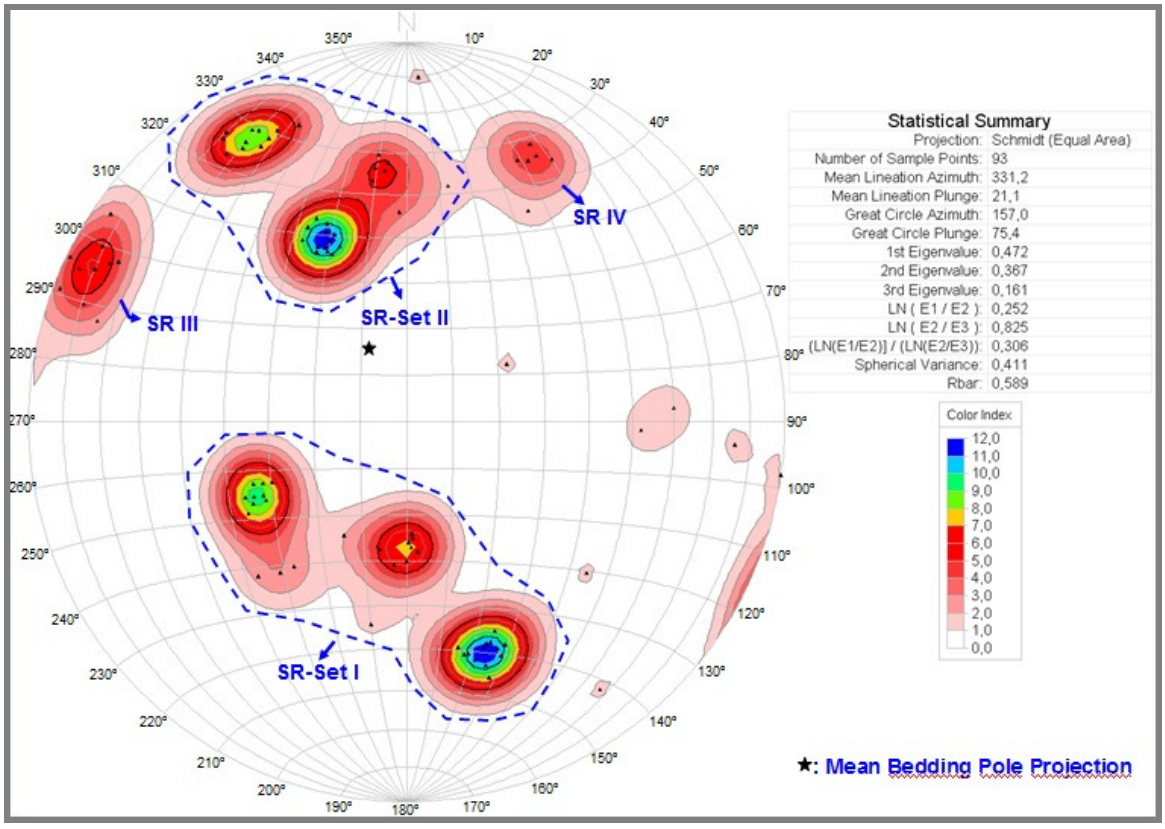

Figure 3-21: Stereoplot of fault sets in the *Scaglia Rossa* coastline

Pockets of breccia (Figure 3-22) are a variation of breccia, in *Monte Conero* they are present without an apparent systematization. The only pattern found for this discontinuity is that in all examples studied they have at least one stylolite and one vein involved in their structure. Also, the pockets of breccia typically occur at the tip of smaller faults in between tail-cracks related to one particular fault and in areas where two faults over lap. They are more frequent in the *Maiolica* Fm. and typically they have an oval shape while in the *Scaglia Rossa* Fm. they follow an elongated shape.

The size of the pockets is between 1 and 10 cm long and between 1 and 10 cm wide. Typically from the stylolites that cross the pockets, joints are formed, which tend to define the size of rock blocks inside of pockets. The dimensions of the blocks range from 3x3 mm to 2x2 cm.

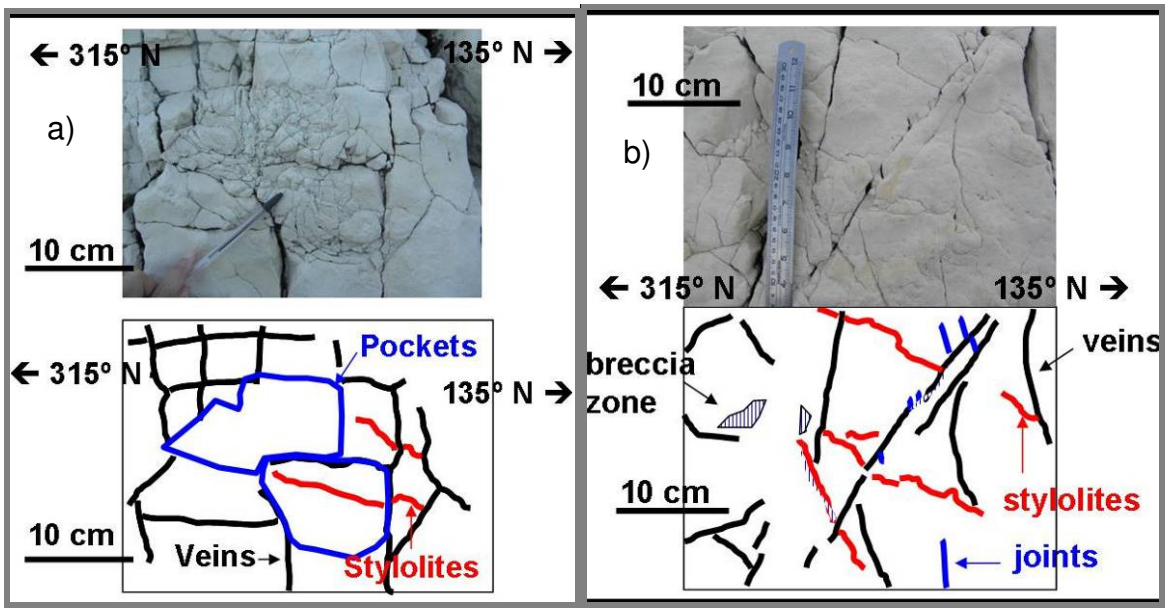

Figure 3-22: Examples of pockets of breccia in the *Maiolica* Fm. a) is an example of a circular pocket and b) an example of an elongated pocket.

3.3.5 Structural Map

Figure 3-23 shows the structure map elaborated on the basis of field data and using the base-map from Coccioni *et al.* (1997). The sets here were disaggregated according outcrop to appreciate the spatial distribution of fractures. In the *Maiolica*'s outcrops there are at least two sets of systematic veins that are intersected by their dips and all they have a trend normal to fold axis and parallel to big faults. In contrast, on the *Sirolo*'s coastline, the sets of veins have no a regular strike and are crossed between them in various directions. In general stylolites have a trend parallel to fold axis and normal to veins. The majority of breccias have a same trend of veins but some of them tend to be orientated parallel to fold axis.

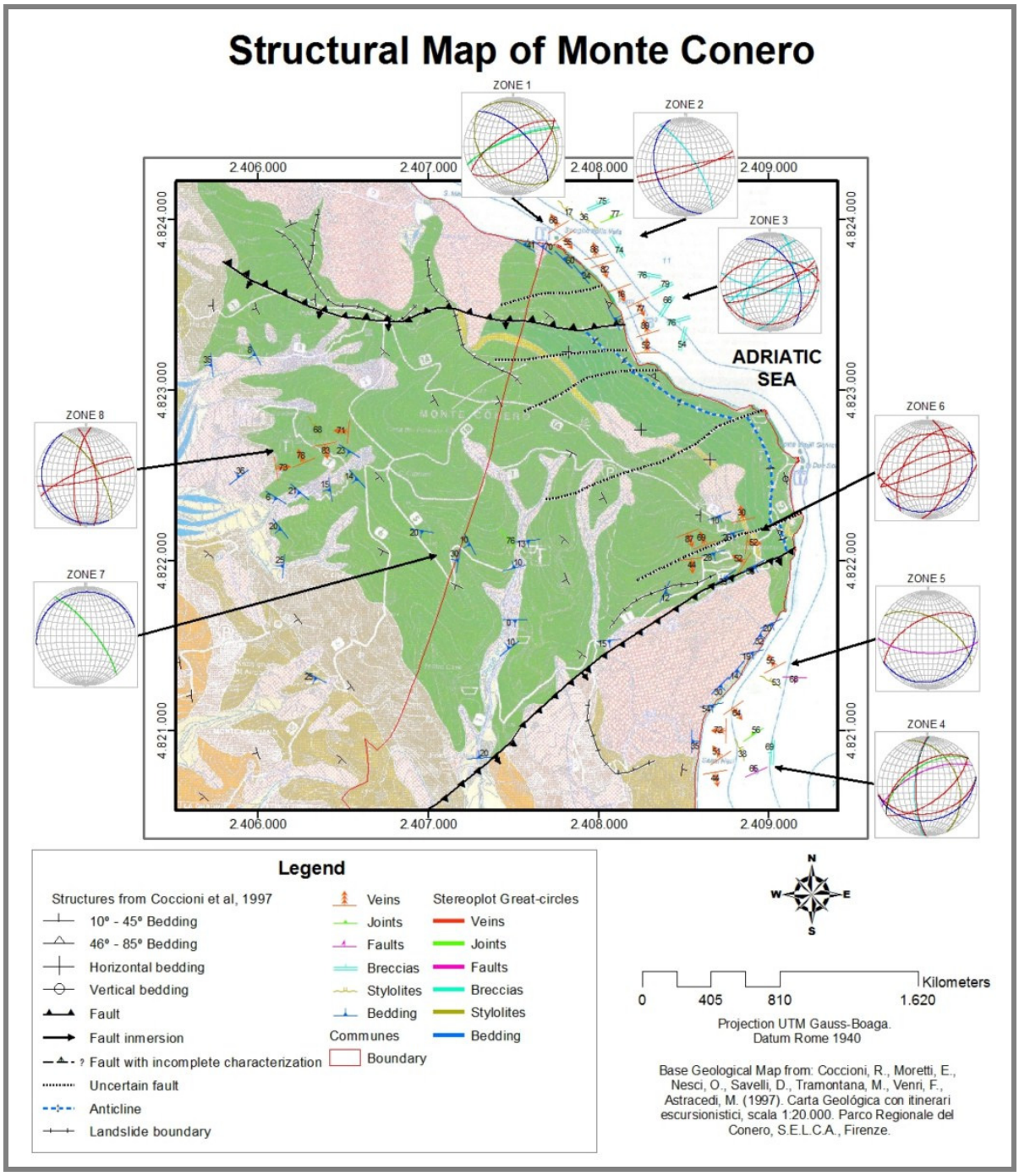

Figure 3-23: Structural Map of *Monte Conero*

3.4 Fracture Characterization in Microstructures

3.4.1 Introduction

In order to compare the internal structure of rocks and the characteristics of fractures at micro-scale with the observations made at meso-scale, in this section is described the analysis of microstructures, where matrix, micro-fractures and breccia porosity of the *Conero* rocks have been studied.

Carbonates have been characterized by different authors according their matrix composition, for example Folk classification (1959, 1962) and Dunham classification (1962). In this study the classification of Dunham (1962) has been adopted to characterize the matrix of the rocks.

In terms of the assessment of the porosity of the breccia zone at micro-scale in *Monte Conero*, in this study the following composition of a breccia is considered:

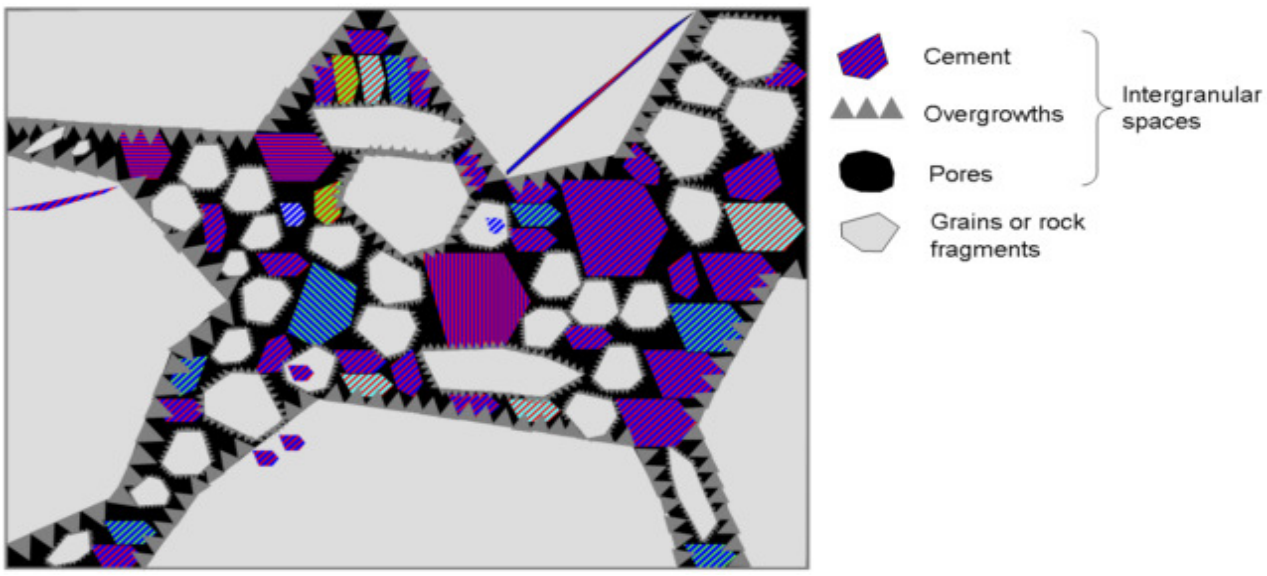

Figure 3-24: Schematic diagram showing the composition of a breccia, which involves the following elements: cement as calcite crystals, overgrowths, pores and grains or rock fragments

Considering these elements, a breccia is divided in:

1. Grains, and
2. Inter-granular spaces, which are composed by: pores, overgrowths and cement

We refer to ‘Grains’ as the rock fragments from the original matrix and of detrital origin. ‘Pores’ are considered as void spaces. ‘Cement’ as the spaces filled with calcite crystals, which may be formed either in the vadose zone or in the saturated zone. And ‘Overgrowths’ as crystals that grew around the original grains.

Therefore, in this study the term ‘porosity’ is referred to the spaces occupied by only pores, whereas ‘inter-granular porosity’ is referred to the spaces occupied by pores, cement and overgrowths. In both cases, we are referring to an areal porosity since this has been measurement in a bi-dimensional plane.

3.4.2 Methods

The microstructures of the rocks exposed in Monte Conero were studied in thin sections made from the rock samples taken during fieldwork. Fourteen thin sections were analyzed with the microscope. Two of these thin sections are from a breccia zone and the remaining thin sections show different microstructures. For a best identification of microstructures was used parallel filter and Cross Nicols.

For the calculating of porosity and inter-granular porosity of the breccia zone, two methods were used:

Method 1: Point Counting

Using this method, grains, pores, cement and overgrowths were quantified on the breccia thin sections. Large calcite crystals and overgrowths were counted and the diameter of pores and grains was measured. These elements were identified in a random sample of 301 points for the two breccia thin sections. With the results of this method was possible calculate the porosity and inter-granular porosity of the samples.

Method 2: Binary Image

The accuracy of binary image method only allows calculating the inter-granular porosity of the breccia. The binary images were obtained from the processing of scanned images at high resolution (1200 ppp) of the rock samples where the thin sections were originally cut. The raw tiff images were processed in the software Image J, first they were converted to an 8 bit image, then they were adjusted by threshold and finally they were transformed into binary images. Both sides of the rock for each sample were scanned and processed obtaining two inter-granular porosity values for the two samples (Figure 3-35). These values were averaged to obtain a global inter-granular porosity for each sample.

The porosity and inter-granular porosity obtained with the two methods above described, were used in the equations reported in Aydin (2000), which consider the approximations of Kumar, Zimmerman and Bodvarsson and the Kozeny-Carman model. These equations were used to calculate the permeability (K_f) of the breccia zone and they are detailed bellow.

$$K_f = \frac{\phi^3 \cdot a^2}{45 \cdot (1-\phi)^2 \cdot \left[1 - \frac{\tanh(C \cdot R)}{C \cdot R}\right]}$$ Equation 3-1

Where,

ϕ : porosity

t : breccia thickness

a : radio of spherical particles

C : function of porosity $C = 3.4 \cdot \left(\frac{1}{\sqrt{\phi}} - \sqrt{\phi}\right)$ Equation 3-2

R : ratio of the thickness to the radius of the spherical particles $R = \frac{t}{a}$ Equation 3-3

3.4.3 Characterization

According to the carbonate rock classification made by Dunham (1962), the *Conero* rocks have a mud-supported matrix. These grains in the mud matrix are of skeletal origin, both fossil and bioclast. In the *Maiolica* Fm., the matrix contains more than 10% of these kinds of grains, and has a wackestone texture. The matrix of the *Scaglia Rossa* Fm. has less than 10% of grains and consequently corresponds to a mudstone.

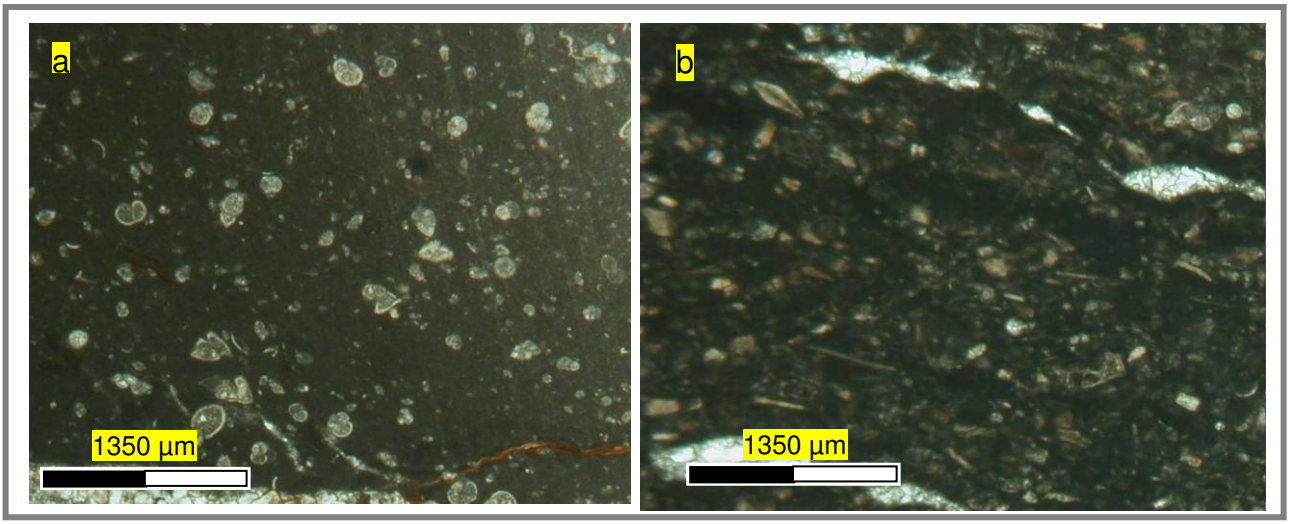

Figure 3-25: a) Microscopical view of *Scaglia Rossa* matrix. b) Microscopical view of *Maiolica* matrix. Both images were taken with parallel filter

The thin sections analyzed show as predominant fractures veins and stylolites (Figure 3-26: to Figure 3-32), whereas joints were not observed and some faults were identified.

Veins

Most of the veins are filled with calcite crystals of areal dimensions of about 0.035 x 0.02 [cm^2] but some cemented veins have besides calcite crystals also matrix fragments, similar to breccia. Furthermore, there are a few open veins and partially open veins. The pores of these veins appear isolated between calcite crystals.

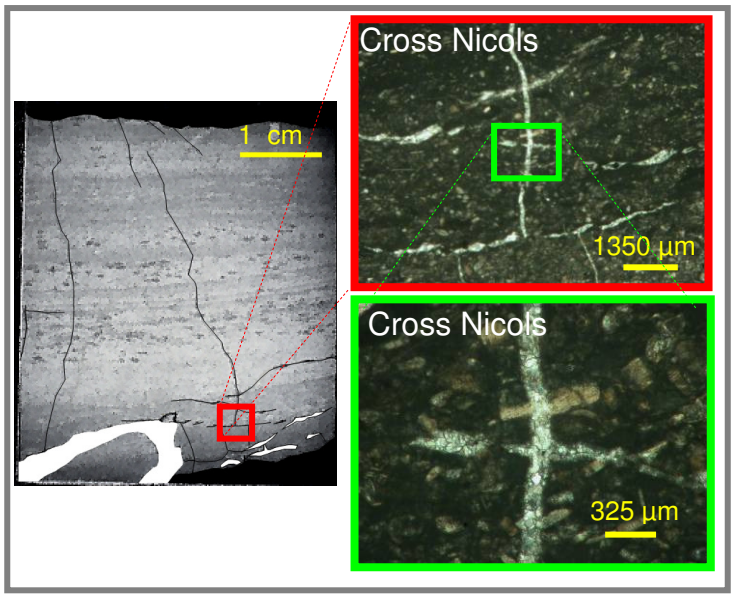

Figure 3-26:

On the left a thin section from the *Maiolica* Fm. showing two sets of cemented veins (grey lines) at high angle.

The Figures on the right are a close up of the cross cut veins. The crystals in the veins reveal that these sets of veins belong to two different generations. Both images were taken with Cross Nicols.

Others veins have an en-échelon pattern, which is developed at different orientations.

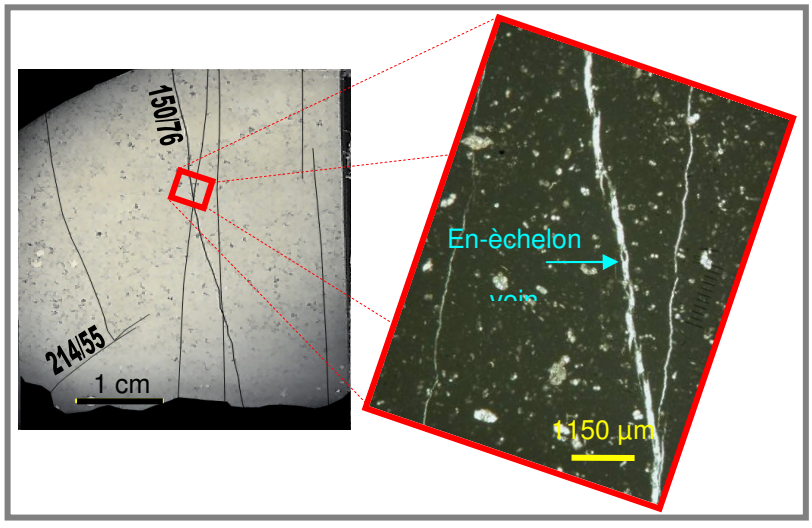

Figure 3-27:

On the left a thin section from the *Maiolica* Fm. showing two sets of cemented veins (black lines).

The image on the right is a microscope image with parallel filter, showing the en-èchelon structure of the veins.

Stylolites:

The stylolites contain residues of iron oxides and show different degrees of dissolution, both in the fossils and in the. The stylolites cut across the veins and are generally at high angle to these veins.

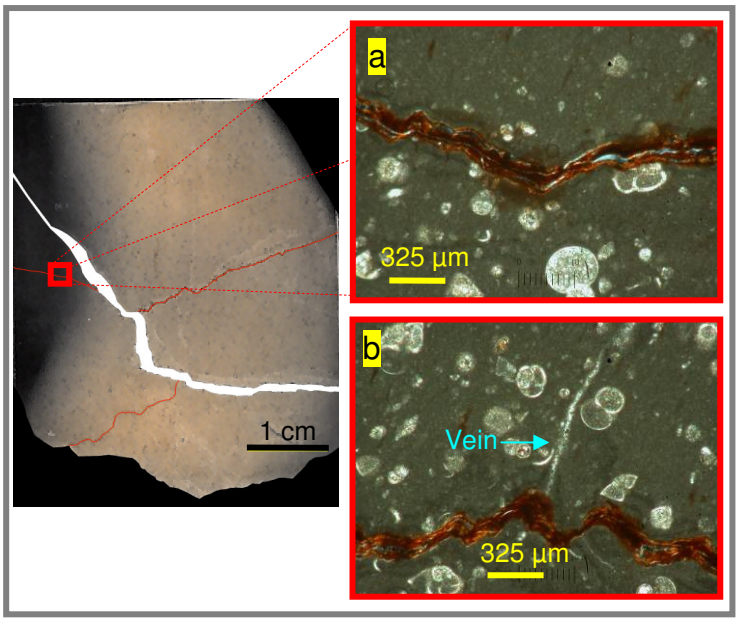

Figure 3-28:

On the left a thin section from the *Scaglia Rossa* Fm. showing a filled vein (white line) which cross cut one stylolite (orange line).

On the right Figure a) shows an open stylolite and Figure b) other segment of this stylolite from where a vein is developed at high angle to the stylolite. Both images were taken with Cross Nicols.

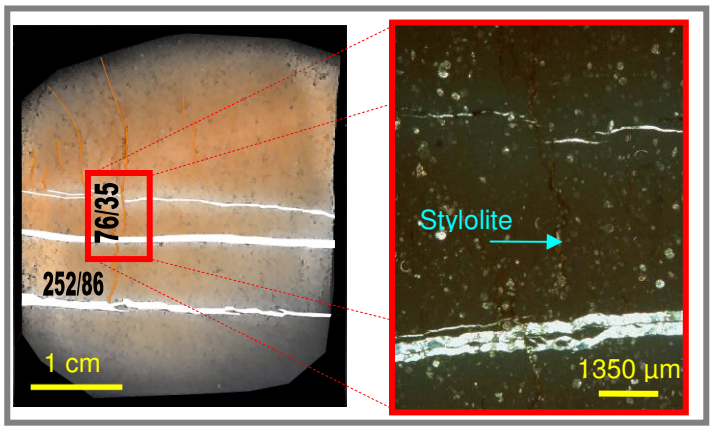

Figure 3-29:

On the left a thin section from the *Scaglia Rossa* Fm. showing filled veins (white lines), which cut cross a stylolites (orange line).

The Figure on the right was taken with Cross Nicols and shows the relationship at high angle between the stylolites and veins.

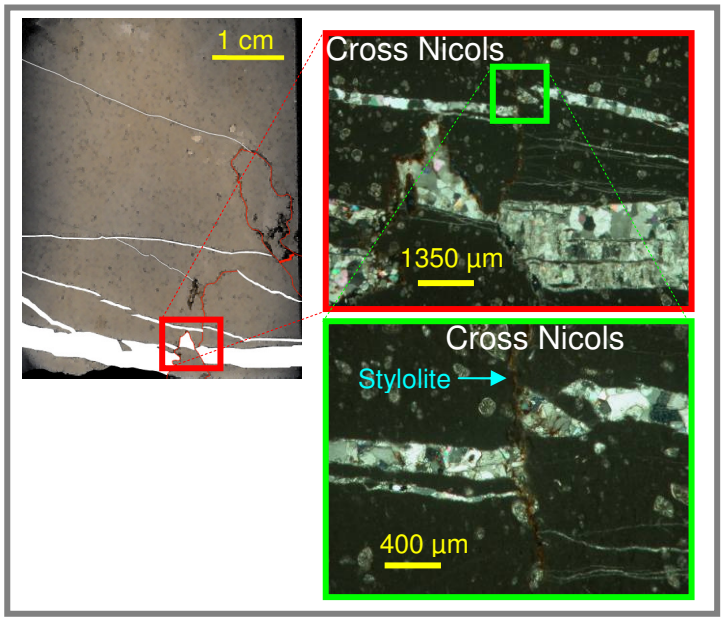

Figure 3-30:

These images from the *Scaglia Rossa* Fm. show veins cut by stylolites with apparent offsets of these veins.

Faults:

Normal faults were observed as consequence of the reactivation of veins.

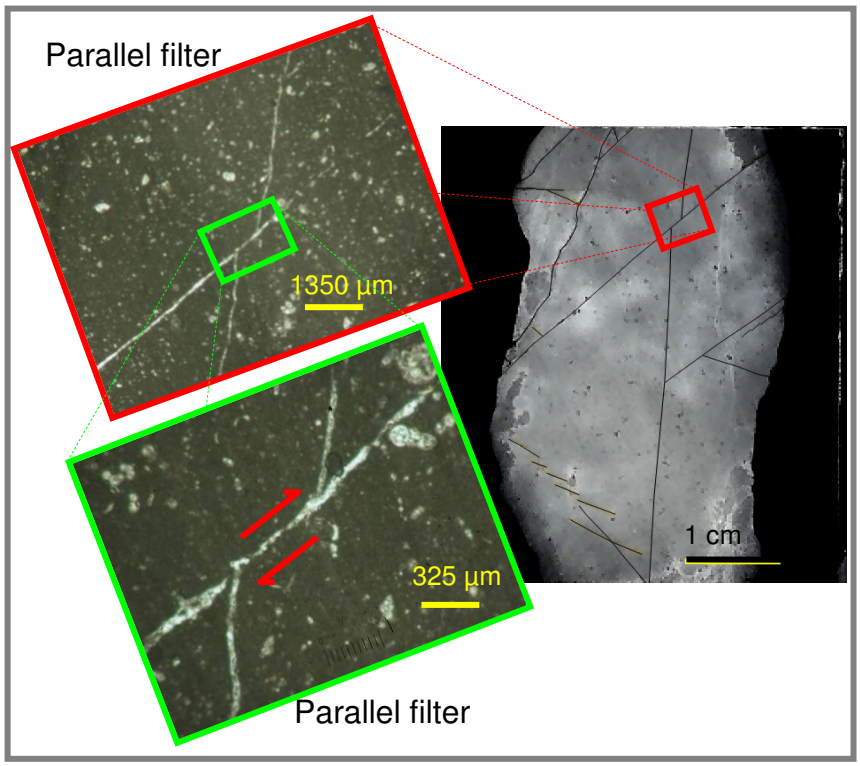

Figure 3-31:

These images show the reactivation of a vein as a right lateral fault, in the *Maiolica* Fm.

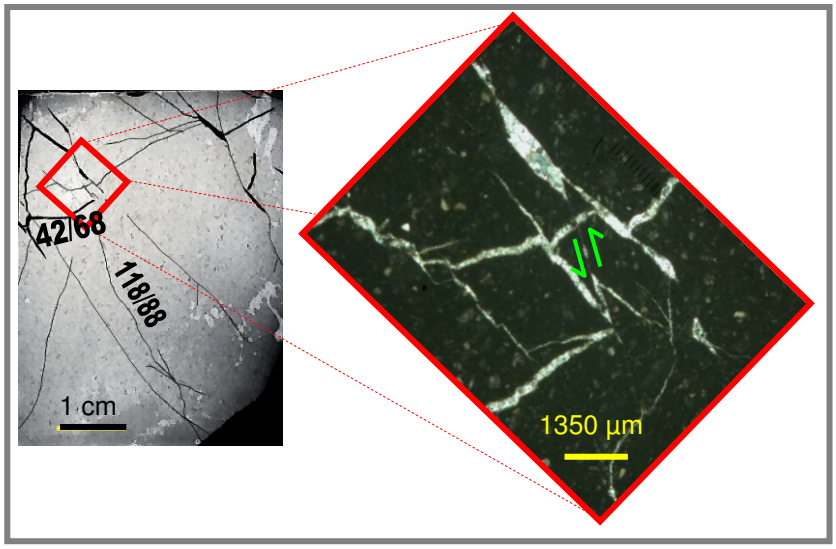

Figure 3-32:

This is another example of a vein reactivated as a left lateral fault in the *Maiolica* Fm. The image on the right was taken with Cross Nicols.

3.4.4 Breccia-zone porosity

The breccia observed in the thin sections of the *Maiolica* Fm. (Figure 3-33 and Figure 3-34) is composed of rock fragments which are rectangular in shape with sides ranging from 0.02 x 0.02 [mm] to 1.3 x 1.0 [cm] with an average radius of 1.7. Pores have a diameter ranging from 0.01 [mm] to 4.5 [mm]. Many of the pores are not interconnected.

The following figures show the thin sections studied with a close up to identify the components mentioned in the Section 3.4.1 and a histogram of the distribution of the radios of the grain size.

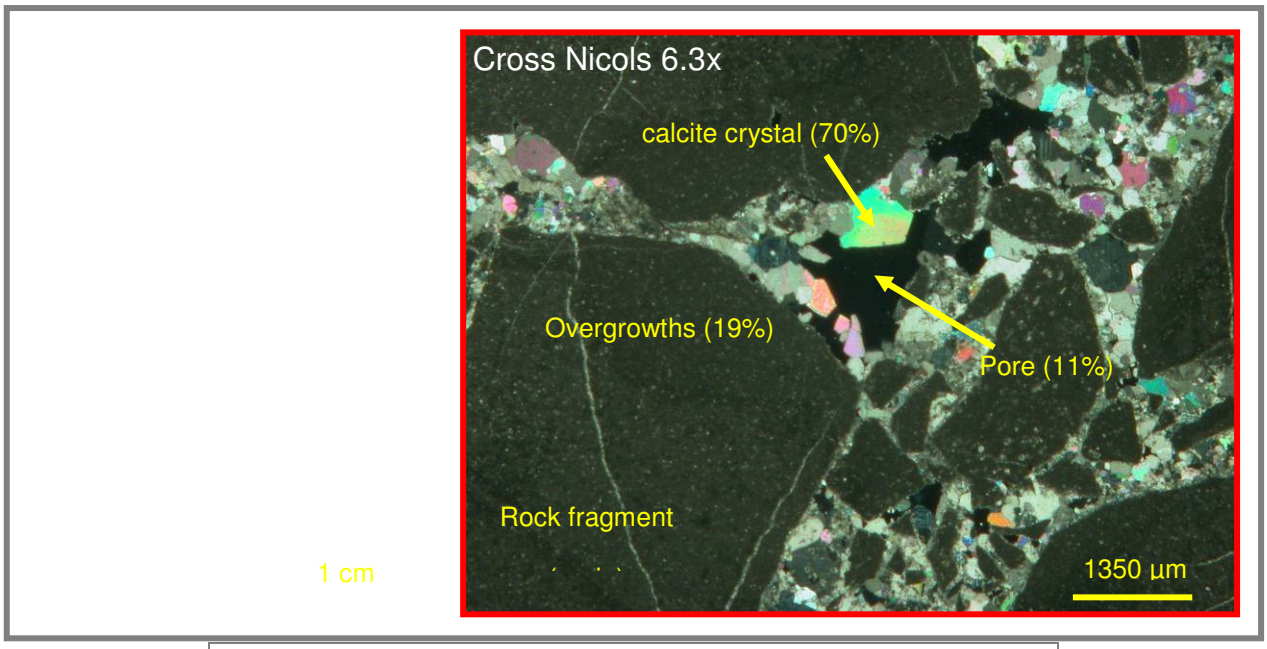

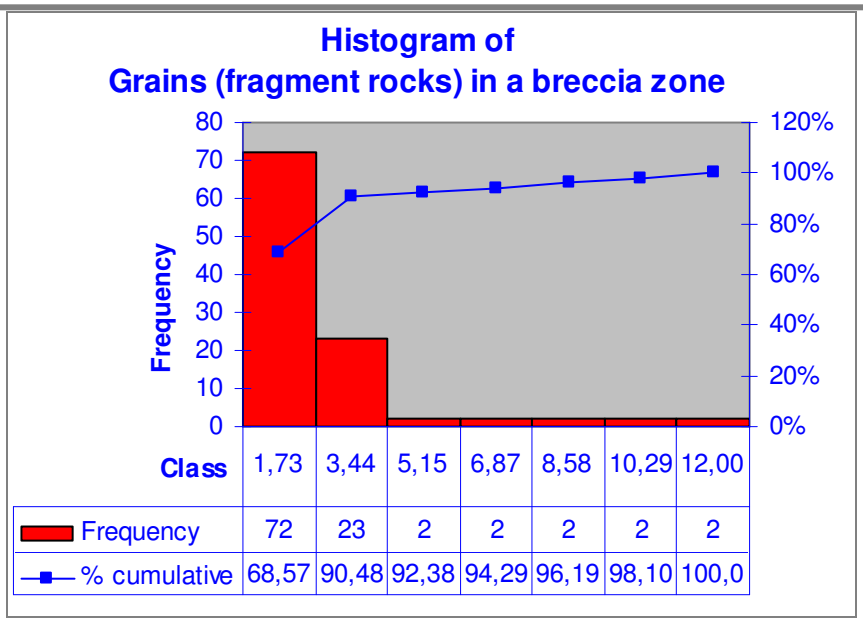

Figure 3-33: Breccia sample 1. The intergranular space of this thin section is composed of 11% of void spaces, 19% of crystal overgrowths and 70% of calcite crystals.

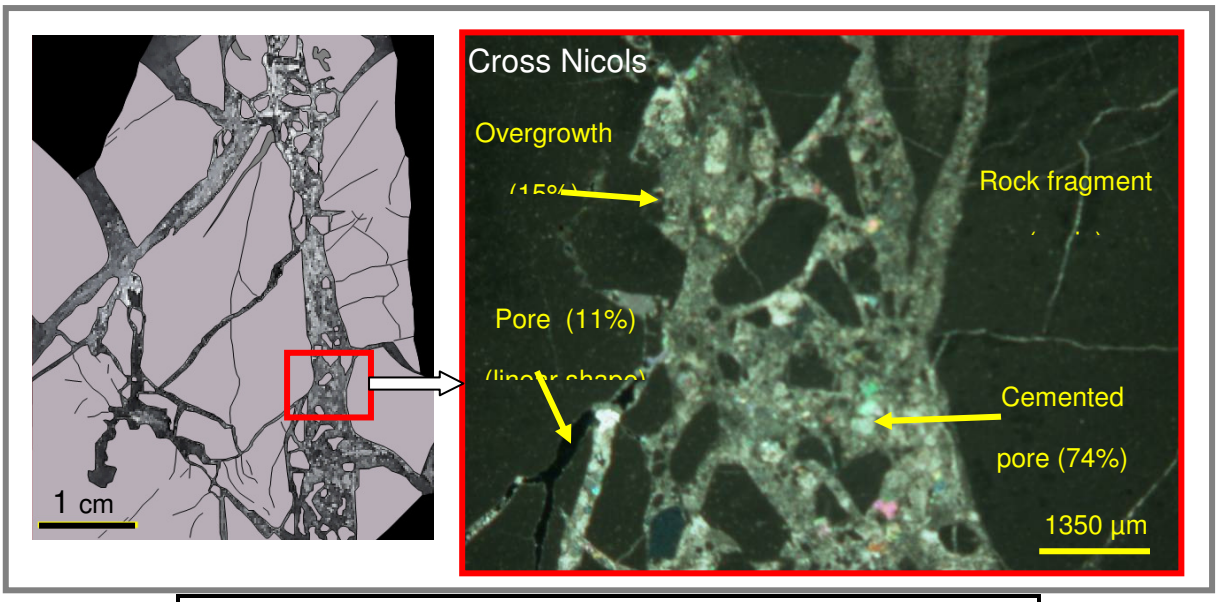

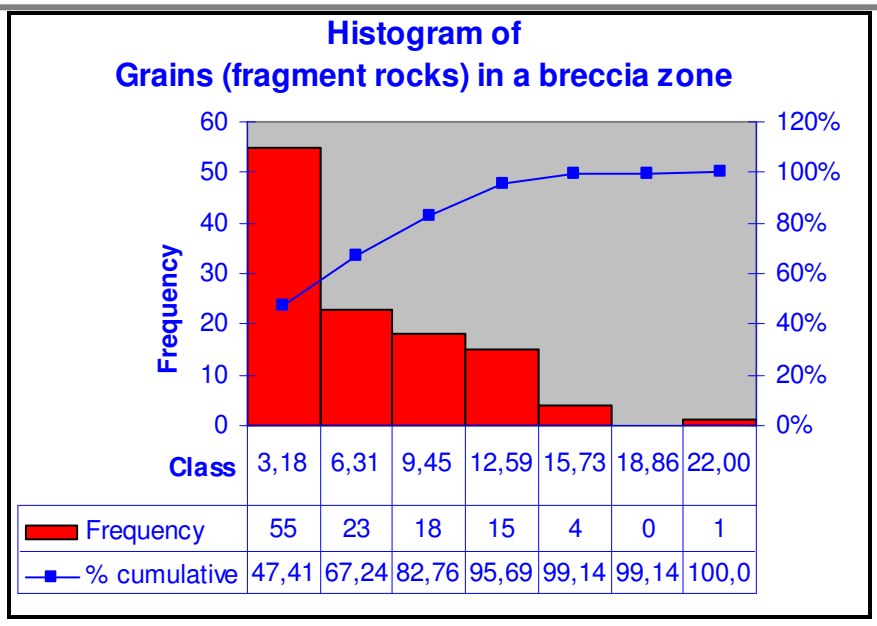

Figure 3-34: Breccia sample 2. The intergranular space of this thin section is composed of 11% of void spaces, 15% of crystal overgrowths and 74% of calcite crystals.

These thin sections are from two different samples belonging to the same breccia zone; and show similar grain diameter size distributions and shapes of grains. In both cases, diameters of grains are concentrated in the lowest values, 1.73 [mm] for the sample 1 and 3.18 [mm] for the sample 2. The grain diameter size distribution in sample 2 is more homogeneous than the grain size distribution of sample 1, despite the fact that it has higher maximum values (22 [mm]). In the close-up, it is possible to distinguish this

difference, where in the sample 1 the components of the breccia are well-defined whereas in sample 2 they are diffuse and difficult to identify. The portion of breccia shown in sample 1 has a fracturing which forms euhedral fragments while in the sample 2, fracturing is controlled principally by the shape of the veins. As a consequence the respective pores have these shapes.

The following Figure shows the images used to calculate the porosity by the ‘binary image’ method.

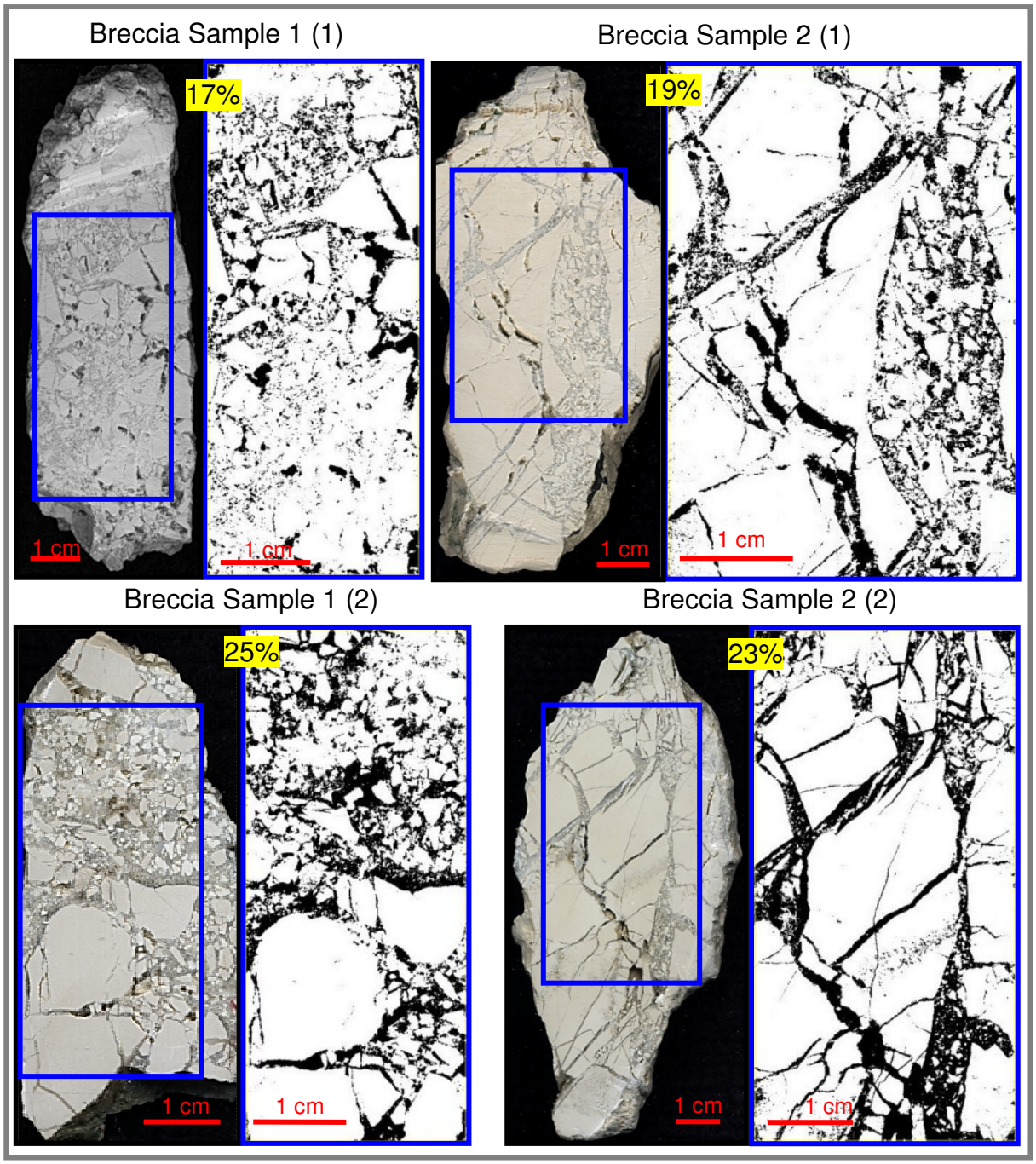

Figure 3-35: Binary images of the breccia samples used to calculate its intergranular space. On the left, the scanned images at high resolution are shown. On the right, are the binary images processed with the software Image J are shown: white colour is for rock fragments and black colour is for pores (void spaces, overgrowths and cemented pores). The values in yellow indicate the porosity measurement on the respective binary image.

The application of the method of 'Point Counting' gave the following percents in the components of the breccia:

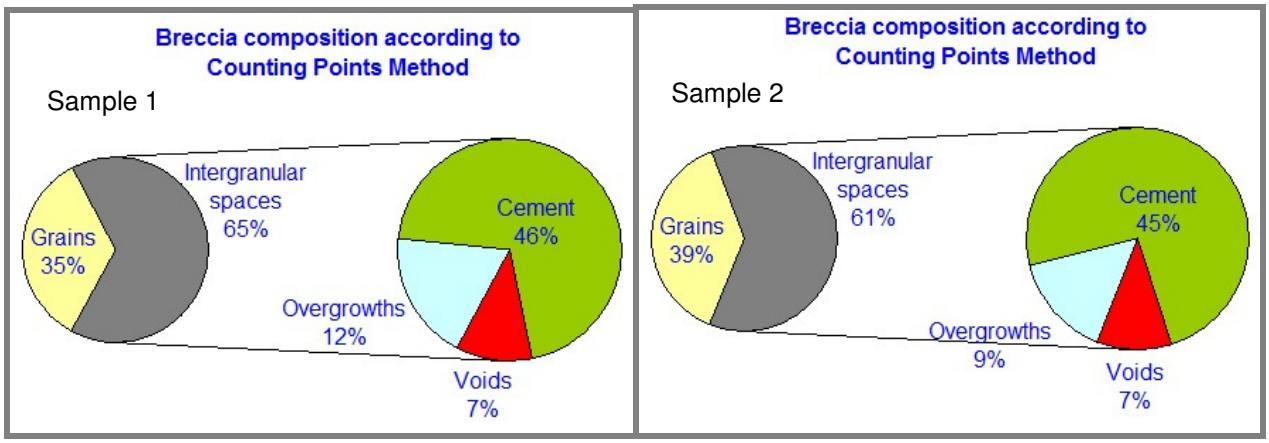

Figure 3-36: Composition of the breccia according to the 'Counting Points' method

From these compositions the portions for the intergranular space can be determined:

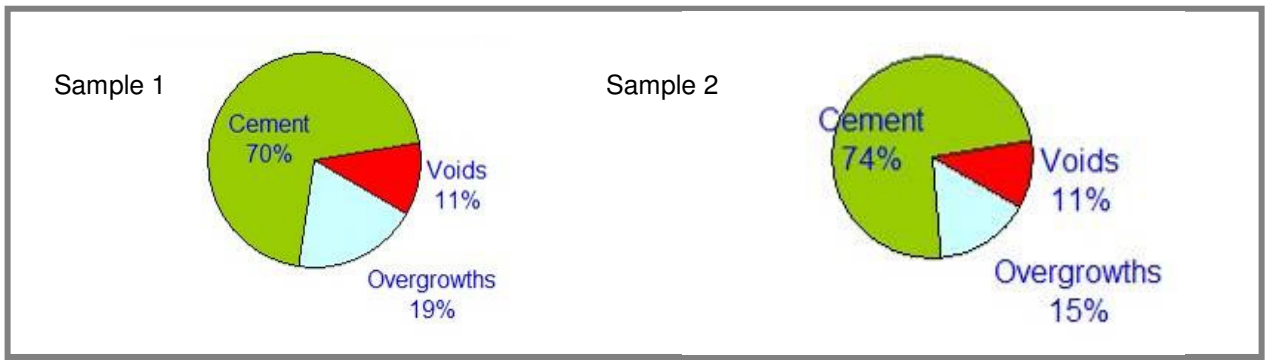

Figure 3-37: Portion of the intergranular space calculated from the 'point counting' method

With these portions, we estimated the composition of the breccia zona for the results of the method 'binary image'. The results obtained were the following:

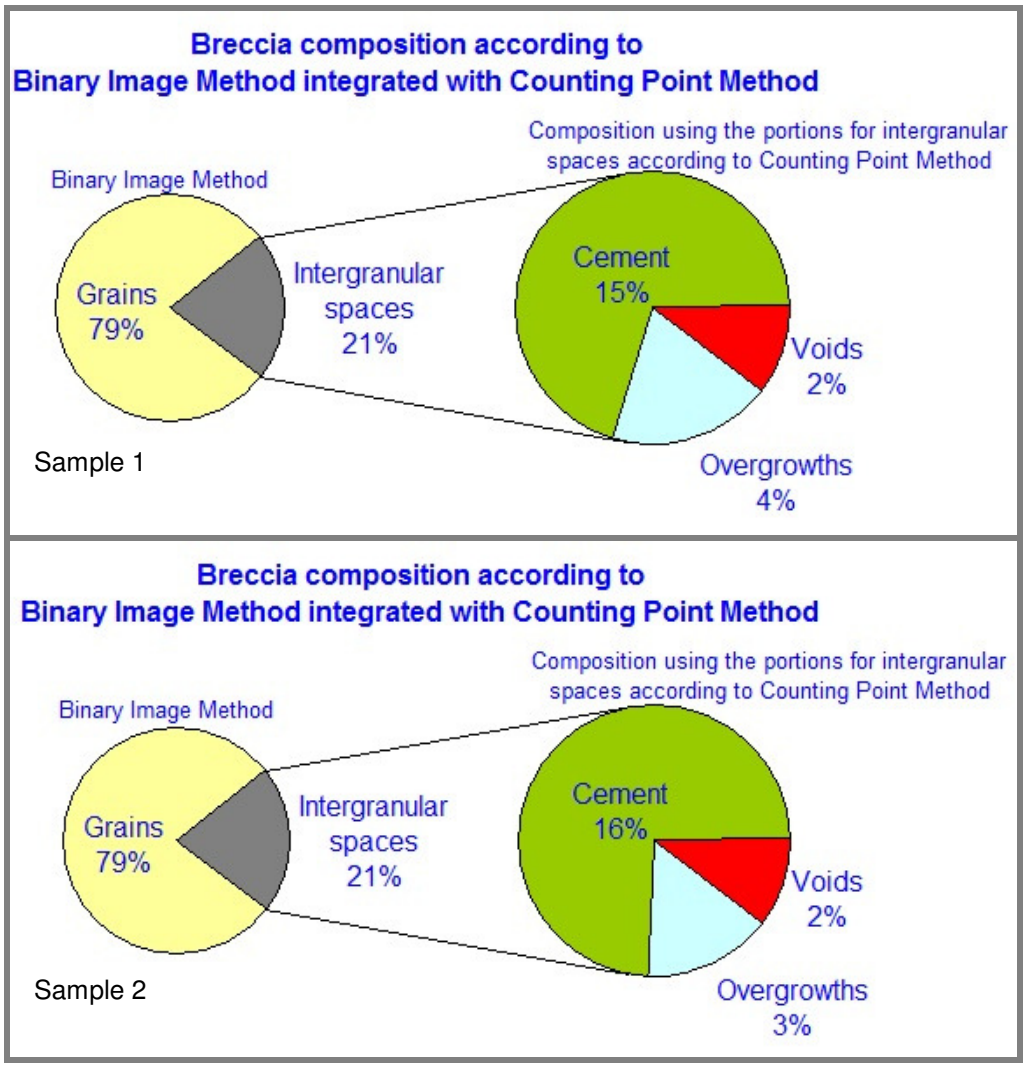

Figure 3-38: Composition of the breccia according to the 'binary image' method integrated with the ' point counting' portions.

Finally, we applied the composition of obtained for both methods and estimated the permeability with the application of the Equation 3-1. The results are resumed in the following table.

Table 3-5: Porosity and permeability of a breccia zone

		Point Counting Method		Binary Image Method with Point Counting Portions	
	Breccia zone (50 cm thickness)	**Voids**	**Voids + cement**	**Voids**	**Voids + cement**
Sample 1	**Porosity [fraction]**	0.0698	-	0.0227	-
	Intergranular spaces [fraction]	-	0.5282	-	0.1719
	Permeability [mD]	231	389,091	7	4,353
Sample 2	**Porosity [fraction]**	0.0664	-	0.0227	-
	Intergranular spaces [fraction]	-	0.5216	-	0.1782
	Permeability [mD]	231	1,654,430	33	22,360

The integration of both methods gives better and most realistic results of the permeability. As definitive value, we will considerer the permeability as 7 [mD].

3.4.5 Discussion and Conclusions

The results of the thin sections analysis indicate that the types of fractures observed at the micro-scale are similar to the types of fractures observed in outcrops, except for joints which were not observed under the microscope. In the thin sections analyzed the predominant fractures are veins and stylolites as in the outcrops.

The pores of these veins do not appear to contribute to effective porosity because the open spaces are isolated.

The images above and the analysis made on other thin sections allow an interpretation of the age-relationship among these microstructures. This analysis,

considering the cross-cutting relationships among the micro-fractures, indicates the following sequence of events:

- a first set of veins, afterwards
- a set of stylolites formed at high angle to veins and
- later these stylolites were opened and reactivated as veins
- A second set of thinner veins was developed since they intersect the first set of veins it is clear that are younger than the first set of veins. But because there are not cross cutting relationship with the stylolites in the thin sections it is not clear the age relationship between the stylolites and the second sets of veins.
- Some veins were reactivated as faults, generating an offset in other fractures and fossils.

Therefore, at this scale of analysis it is possible to infer that there have been at least three phases of deformation in *Monte Conero*. The following diagram shows the schematic sequence described above.

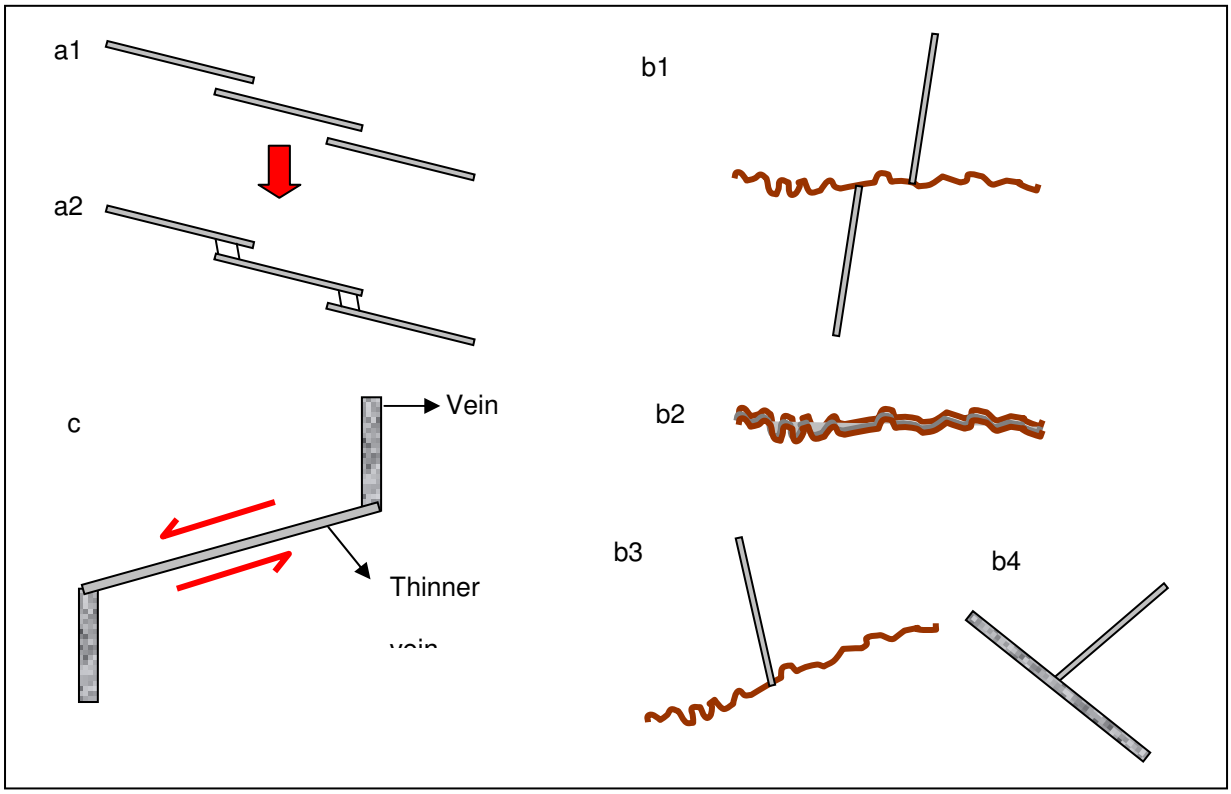

Figure 3-39: Sketches of microstructures observed both in the *Maiolica* and in the *Scaglia Rossa* Fms. a1) Cemented en-échelon veins. a2) Some en-échelon veins are connected. b) Veins oriented at high angle are cut by stylolites. b2) Stylolites are opened and become veins. They are partially or completely filled by calcite. b3) and b4) A second generation of thinner cemented veins abut against the older stylolites and veins. The younger veins are oriented at a different angle with respect the older structures. c) Some thin veins are re-activated as faults.

Considering the results of the table above it is possible to say that the presence of fractures in a low porosity mud carbonate matrix, like the *Maiolica* Fm., increases the porosity of the rock and, in consequence, its permeability; from 0% to 2% the porosity and 0 [mD] to 231 [mD], respectively. Despite the fact that overgrowths occupy almost twice as much space as the (open) pores, they are believed to play a very small role in fluid flow.

The fault/breccia development is closely linked to the concentration of veins and stylolites with their associated joints (see Section about fault development). The majority of these veins are filled with calcite but afterwards they are reactivated as faults forming a breccia zones. Thus, these veins and joints would be responsible for the observed

increase of porosity in a 15% considering cemented pores reaching values greater than 17%. The previous conclusion is based on the analysis of the crystal shape in the breccia zone and veins. Figure 3-40 shows some examples of the distribution and shape of the crystals inside different veins and in the breccia. In the majority of the cases the crystals have a euhedral shape with well-defined boundaries but crystals with irregular shapes are also observed.

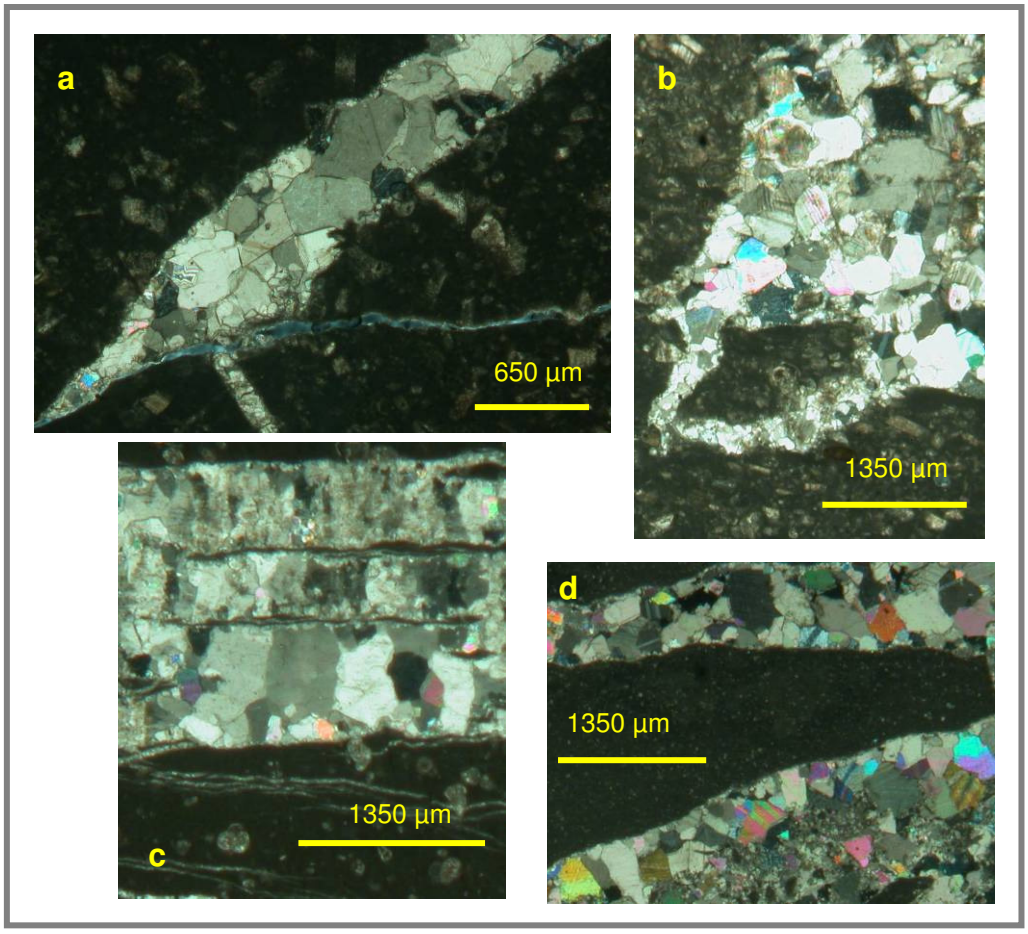

Figure 3-40: Images of crystals in veins and breccia zone. a) Vein in the *Maiolica* Fm. with crystals having a euhedral shape. b) Vein in the *Maiolica* Fm. with crystals having a shape with tendency to euhedral but also with crystals having irregular shapes. c) Three parallel veins in the *Scaglia Rossa* Fm., the first one has crystals with irregular shape whereas the last one has a well-defined euhedral shape. d) Breccia in the *Maiolica* Fm. with crystal shapes with well-defined boundaries.

The shape of the crystals is an indication that there were two processes of diagenesis in the *Monte Conero*. The predominant was generated after that the rock was uplifted above the water table, in the vadose zone, and then likely crystals were precipitated by rainwater; therefore, this was a cementation occurred after the deformation of the layers forming crystals with a euhedral shape. The overgrowth cement around the grains would have been formed under saturated conditions or when the rocks were still below the water table; therefore, probably crystals were formed during or just after the fault formation obtaining an irregular shape. In this way, the first type of cementation is the responsible of the high cemented porosity

Therefore, it is possible to say that before present time, the porosity and permeability due to fracturing and breccias formation in the *Monte Conero* would have been larger than today (e.g. 17% v/s 2% of porosity, in breccia zones). The subsequent diagenetic processes resulted in cemented veins and the development of overgrowths, which reduced the hydraulic properties of the rocks. However, its fracture geometry and fractures spatial distribution make of *Monte Conero* a good model for analogue studies.

Despite the previous observations, it is important to note that the actual contribution of the veins and stylolites to permeability for fluid flow is small since most of them are partial or fully cemented and have a low and non-effective porosity, that is, their pores are unconnected. Although the porosity in breccias in many cases is also non-effective, they are the only structures with a significant importance in quantitative terms of porosity. Considering the similarity of the microstructure geometry with the field observations, in the next phases of the research including Discrete Fracture Network modelling and calculation of fluid flow properties two cases will be included:

- Case 1: Current state of *Monte Conero*. It will consider only the distribution of the sets of breccias and joints. Joints will be included because they are open fractures and contribute to fluid flow.
- Case 2: State of the *Monte Conero* fractures before cementation of the fractures. To the breccias and joints described in Case 1, the sets of veins assuming they are non-cemented and thus open for fluid flow will be added. In other words, this is the case of *Monte Conero* as an analogue model.

3.5 Discussion of the Chapter

The characterization of the fractures on *Monte Conero* has allowed us to distinguish several systematic sets of veins, stylolites and faults of various sizes as well as their relative age. The study so far shows that the veins have been a key factor to *Monte Conero* deformation because from them small fractures were developed. Both in the *Maiolica* and the *Scaglia Rossa* Fm. these small fractures formed discontinuities along which at a later stage faults could localize.

3.5.1 Age Relationships between Fractures and Tectonic Phases

We intend to establish the relative age of the fractures by studying the cross-cutting relationships between different types and sets of fractures. To see whether some of the fracture sets were formed before the formation of the anticline in the *Conero*, we performed rotations of the orientation of the bedding and fracture sets.

Age relationships between different fractures typically result in one fracture offsetting another fracture. If a younger vein cuts across a stylolite, then the plane of the stylolite will be interrupted and vice versa (Figure 3-41). Not all cross cutting relationships between all sets of fractures are exposed in one or more outcrops so the final chronological order of fracture sets formation is an interpretation of observations made on many outcrops.

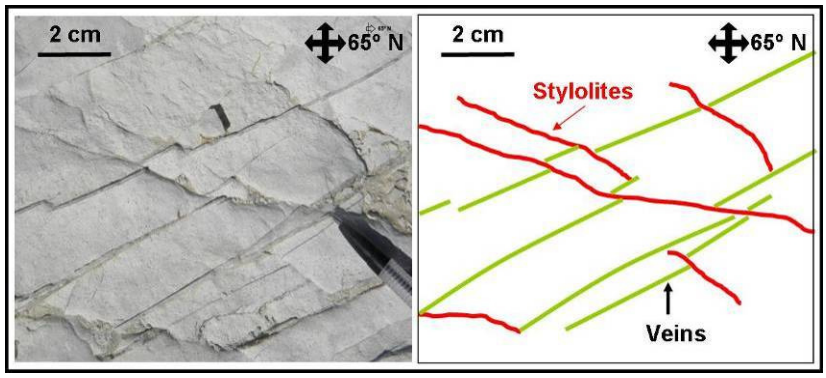

Figure 3-41: A sets of stylolites cuts across a set of veins.

Since there are no single outcrops in the *Monte Conero* where all the sets of different fractures are present or because the spacing of the different types of fractures varies from set to set, not all crosscutting relationships and age relationships could be observed. However it was possible to establish the age and cross-cutting between sets of veins and stylolites and some sets of breccias/faults along the coast. The following sequence of events is derived from the cross cutting relationships:

1. The formation of one set of stylolites (Set I) parallel to bedding
2. The formation of two sets of veins oriented at high angle to bedding which cross-cutting Set I of stylolites. The relationship between these two sets of veins is ambiguous because they are cross cutting mutually

3. The formation of another set of stylolites (Set II) oriented at high angle to bedding (about 65º) which cross-cuts both sets of veins
4. Some stylolites of Set II are reactivated like veins (only in the *Scaglia Rossa* Fm.)
5. Some veins of one of the sets of veins of the point 2 (referred as Set I) are reactivated like normal faults and cross-cutting the set II of stylolites

The observations on the outcrops did not allow confirming the relationship between the two sets of veins since they appear cross cutting mutually, that is, veins of Set I are seen to cut across veins of Set II and vice versa. However, assuming that Set I is younger than Set II; the faulting could be responsible of the mutual cross-cutting. Not all field observations agree with this hypothesis because some veins of Set I that are not reactivated like normal faults are observed to cross-cut veins of Set II.

The following image is an examples of the relationships mentioned above:

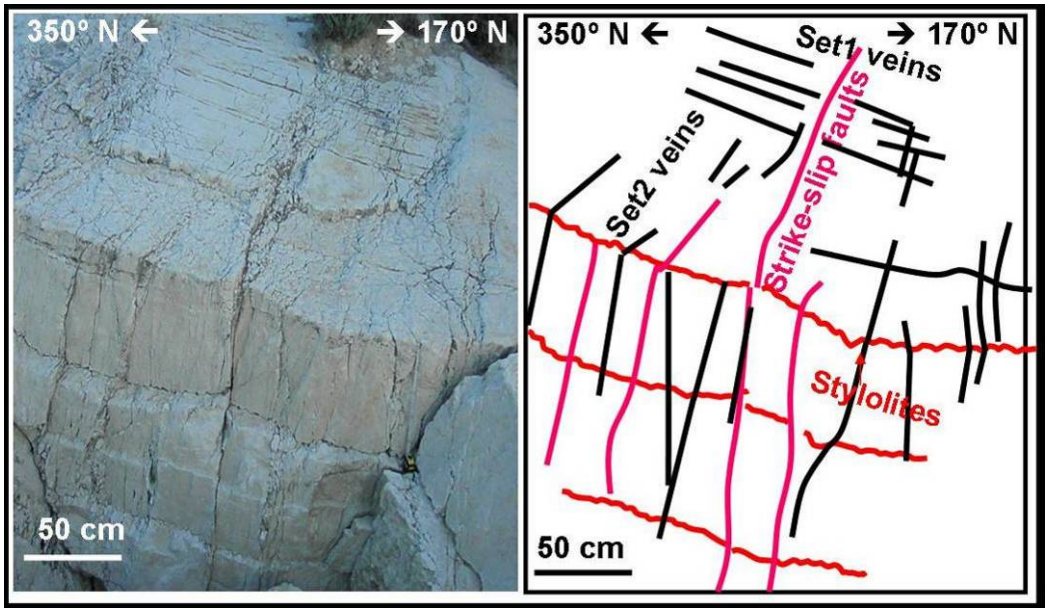

Figure 3-42: Example of outcrop showing the age-relationships among fracture sets. 1. Stylolites parallel to bedding, 2. 1st set of veins at high angle to bedding, 3. 2nd set of veins at high angle to bedding. 4. Strike-slip fault with breccia zone parallel to the 2nd set of veins. 5. Stylolites cutting veins, and 6. Stylolites reactivated like veins.

Finally, the following diagram shows schematically the observed fracture types and sets and their mutual relationship. The north arrow is also indicative, because for the *Maiolica* Fm. this orientation is 302N whereas for the *Scaglia Rossa* Fm. is 65N.

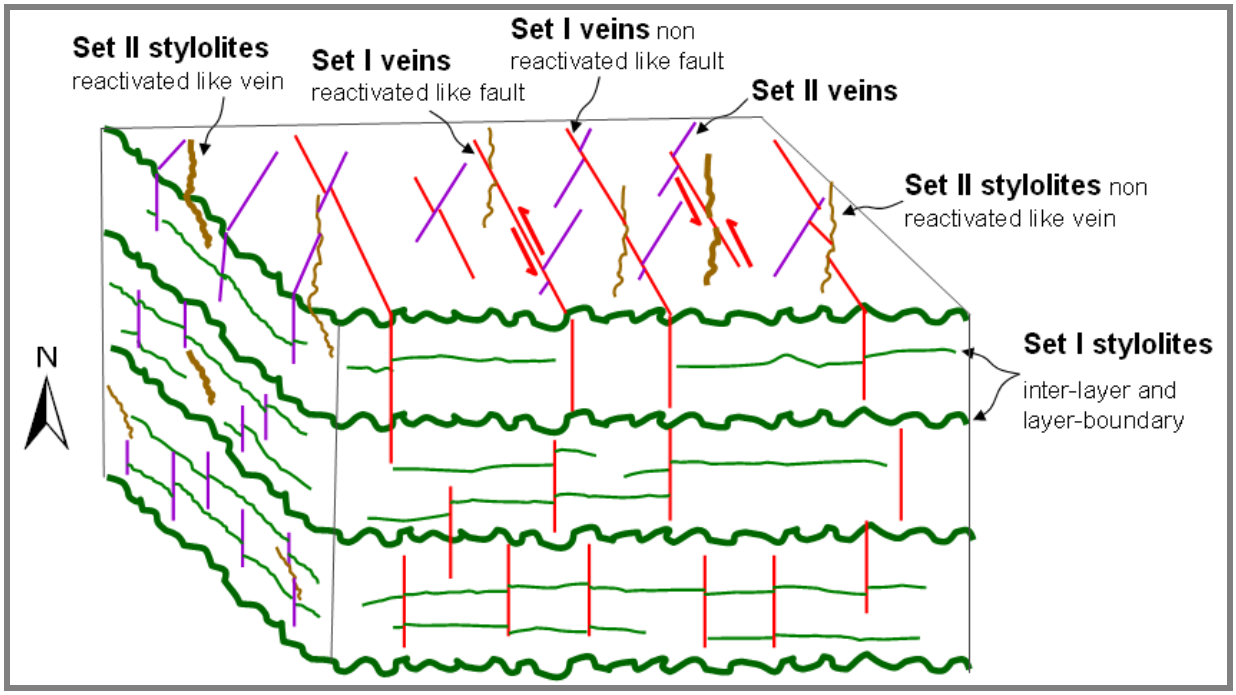

Figure 3-43: Schematic model of the fracture relationships in *Monte Conero*

3.5.2 Conceptual Model of Fault Development

Considering the relationships among fractures described in the previous chapter we are able to define a conceptual model about fault development. Faults are developed in four stages which are common to both geological formations studied. After these phases the fault development in each formation follows a different behaviour resulting in different fracture patterns.

Fault development in both geological formations is characterized by associations of veins, stylolites, joints and faults. These associations may be explained by Linear Elastic fracture mechanics theory. This theory predicts that during slip along the plane of a fault, fields of high local stresses are generated at the tip, which in turn may cause the formation of secondary structures such as veins and stylolites. At each fault tip there is a quadrant where there are high local compressive stresses and a quadrant where there are high local tensile stresses, while the remote principal stresses are oriented at 45º to the fault trace (Figure 3-44). In carbonate rocks stylolites may form in the compressive quadrant and veins or joints in the tensile quadrant (Pollard and Segall, 1987).

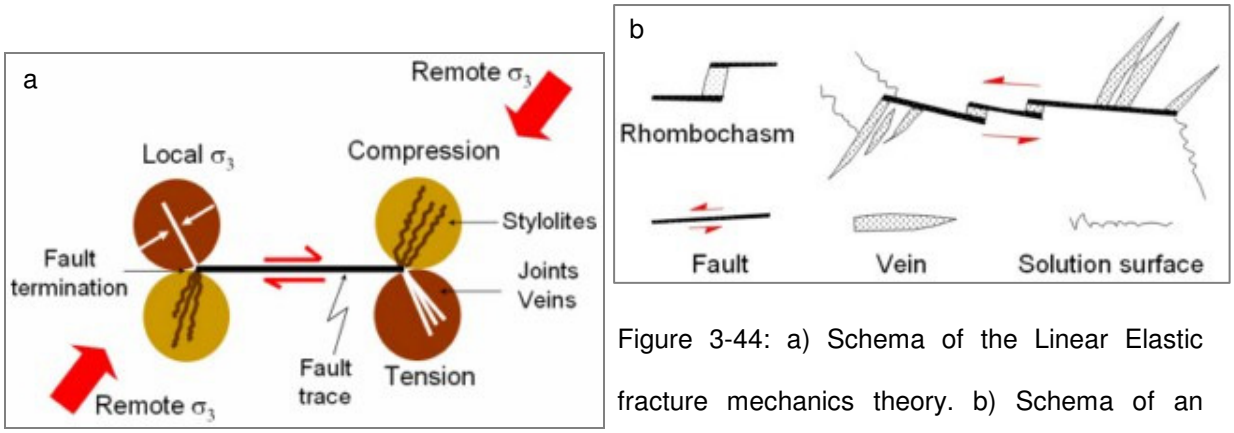

Figure 3-44: a) Schema of the Linear Elastic fracture mechanics theory. b) Schema of an

Figure 3-45 shows the sequence of stages in Monte Conero, when the fault development process starts from pre-existing parallel veins (1), which later are reactivated like faults (2). As we mentioned in the theory above, the displacement generated by the faulting, concentrates the stress at the tip of the faults forming open fractures or veins (3). These open fractures become connected and form a dense fracture network (4).

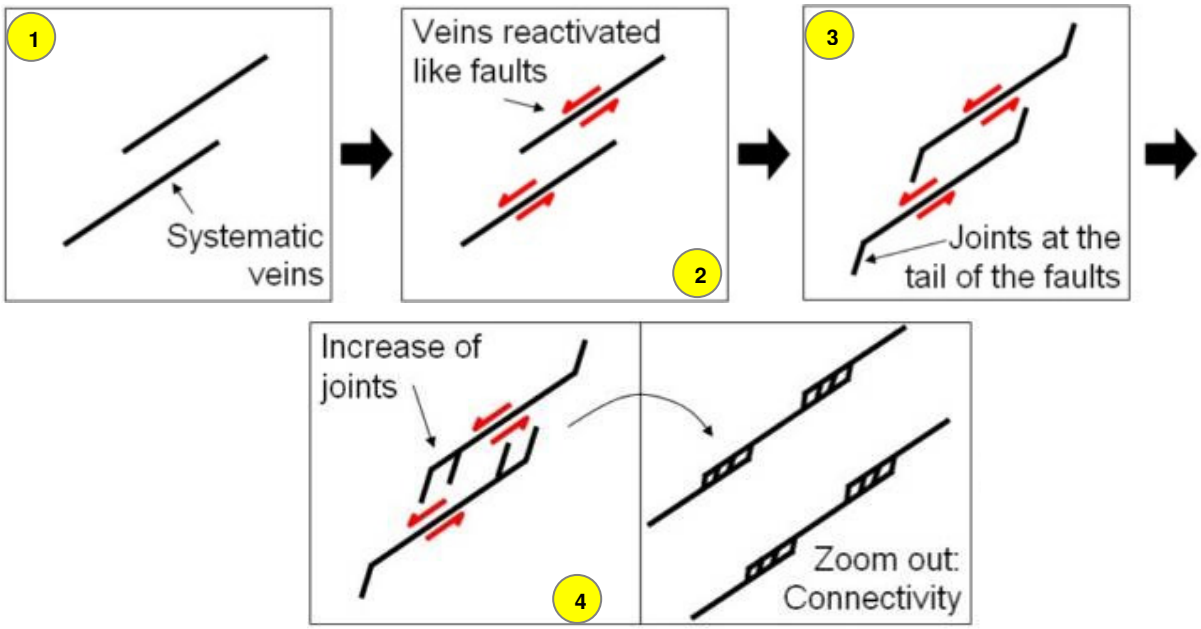

Figure 3-45: Fault-development model: sequence of stages observed both in the *Maiolica* and in the *Scaglia Rossa* Formations.

After phase 4, the fault development process is different depending on the geological formation. In the *Scaglia Rossa* Fm. (Figure 3-46) the development is dominated by cracks at the tail of the small faults formed in the junction of two tensile quadrants (5). From these tail cracks small breccia zones are developed (4) which later are converted in larger breccia zones.

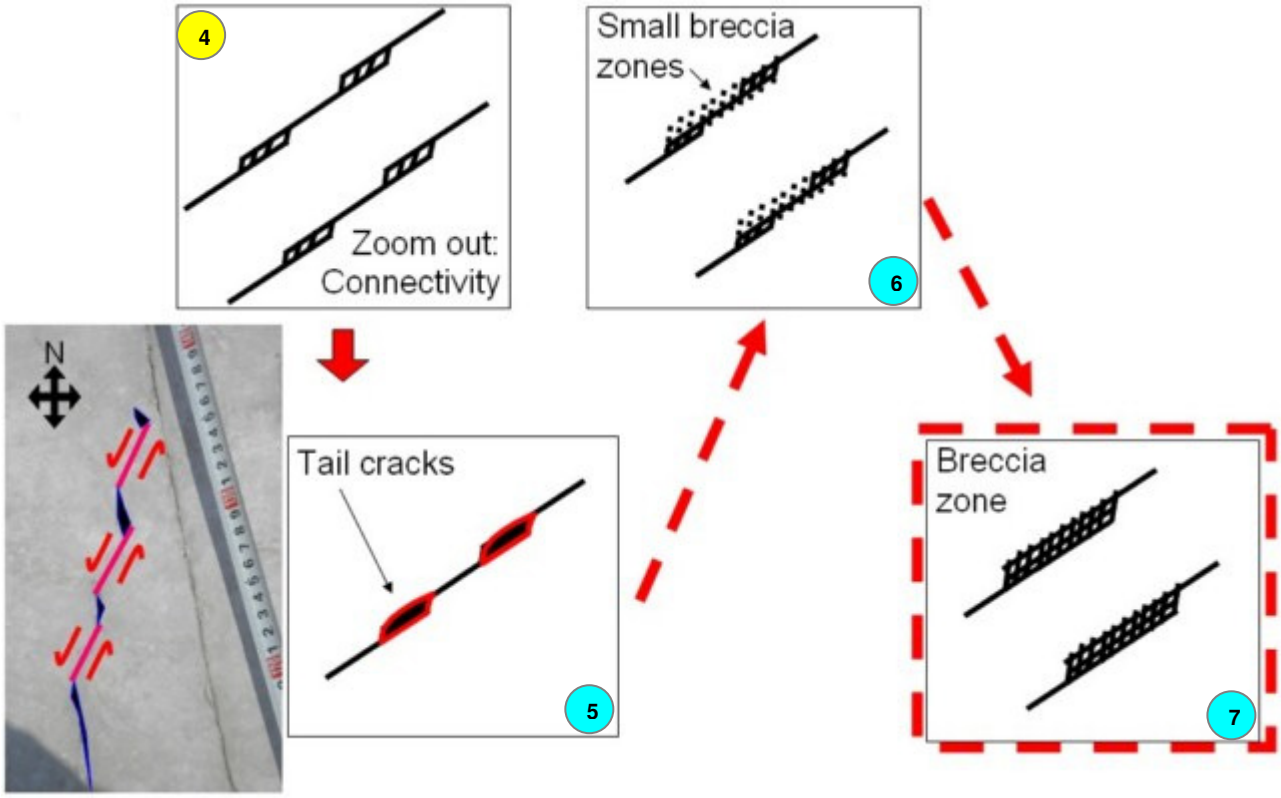

Figure 3-46: Fault-development model: Continuation of the sequence of stages for the *Scaglia Rossa* Fm.

In the *Maiolica* Fm., fault development involves more structures and stages than *Scaglia Rossa* Fm. Small breccia zones are also formed but without the formation of tail cracks (5), and in this case the effect of the compressive stresses are manifested with the generation of stylolites at the tips of the faults (6). Also in these stress zones the development of pockets of breccia was commonly observed and typically a development of joints as consequence of the tensile stress (7). Finally, all these structures are associated and integrated forming fragmented areas and bigger breccia zones (8).

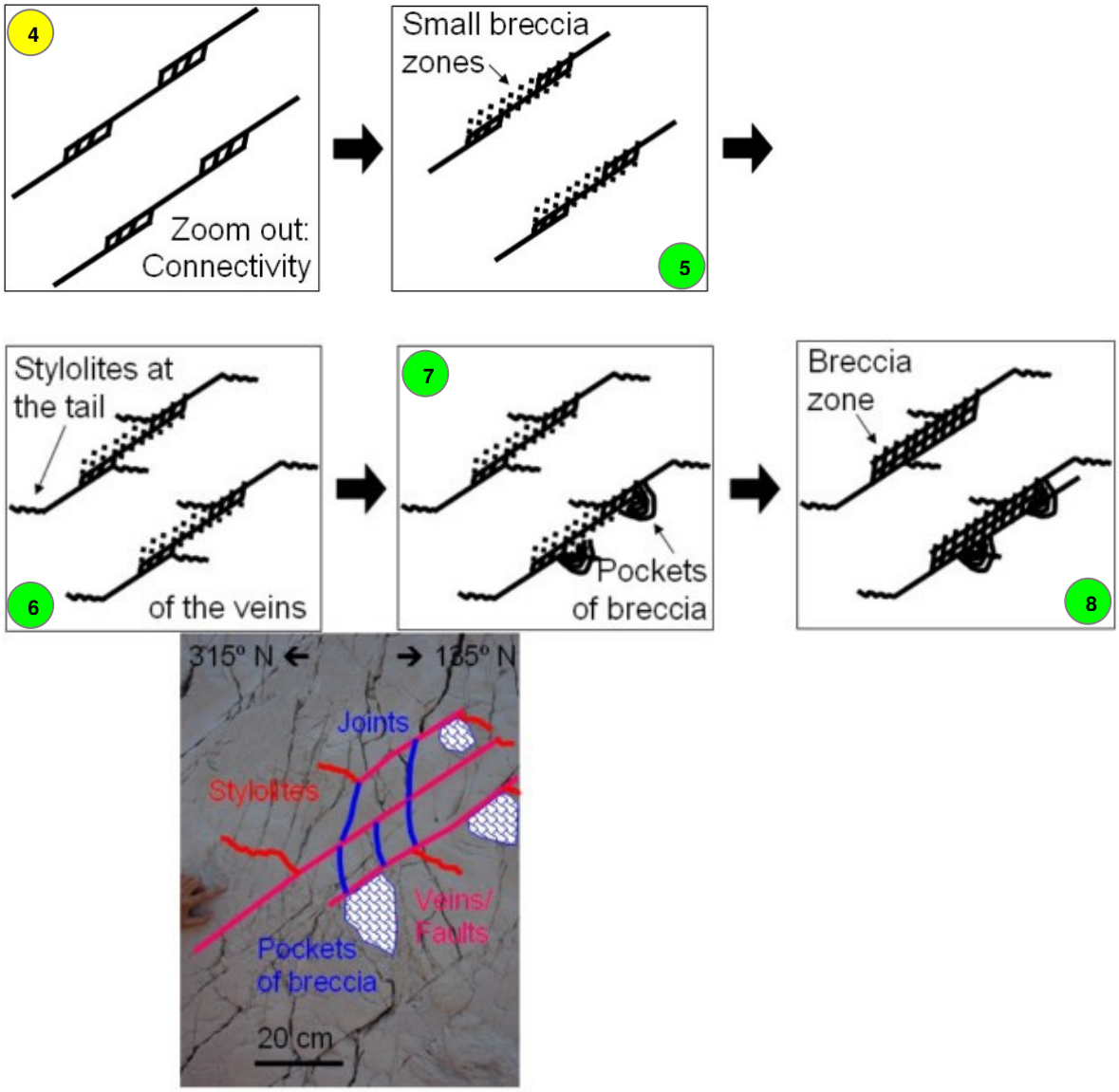

Figure 3-47: Fault-development model: Continuation of the sequence of stages for the *Maiolica* Fm.

In addition, in both geological formations joints at high angle to stylolites were observed (Figure 3-48). In areas where the density of stylolites is important, these joints generate an echelon arrangement of parallel joints. This fracture-development is more visible in the *Maiolica* Fm. due to the stylolites involved in its fault development process.

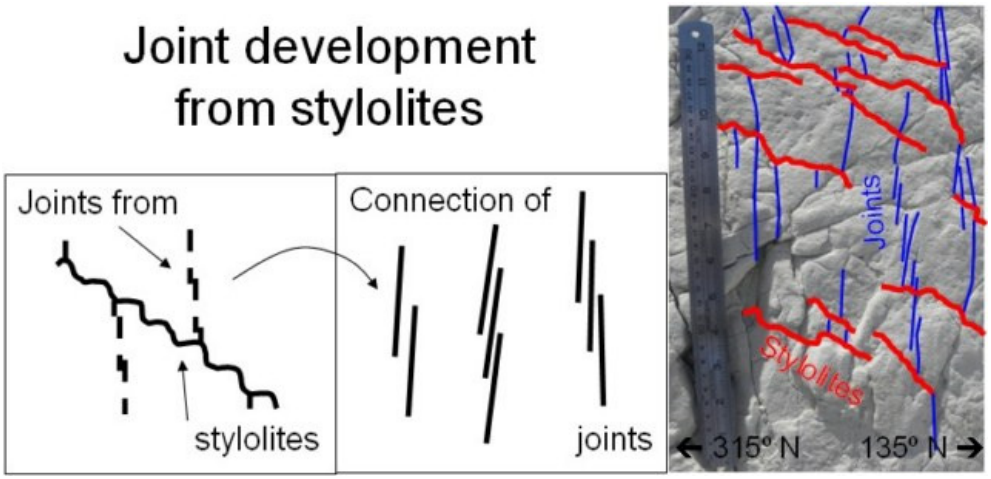

Figure 3-48: Fault-development model: Joint development from stylolites

In conclusion, fault development, both in the *Scaglia Rossa* and the *Maiolica* formations, is controlled by local compressive and tensile stresses caused by small faults and involves other structure in the process. Each mechanical type of fracture contributes in a different way to this process. On the one hand, veins and stylolites are the key structures in the *Conero* area controlling the overall deformation although since they are close/filled fractures they currently do not contribute to the permeability of the rocks. They are part of the initial and fundamental phases of the process which leads to the development of faults, pocket of breccia and breccia zones. These last fracture types are the beginning of the porosity creation. On the other hand, the high density of veins and stylolites, with their associated joints, allows to generate networks of connectivity and potential pathways for fluid flow.

The different fault development in both geological formations explains the difference of density of breccia zones, which is greater in the *Maiolica* Fm. This difference also could have been caused for the high density of stylolites in this formation and their associated joints arranged in echelon.

CHAPTER 4: MODELLING OF THE FRACTURE NETWORK GEOMETRY

4.1 Introduction

We used the code *FracSim3D* (Xu & Dowd, 2010) for the application of the Discrete Fracture Network (DFN) models in *Monte Conero*. This code offers a representation of fractures in two and three dimensions and statistical tools for the analysis of the results. A DFN model is based on the stochastic modelling of data for the generation of more data with the same statistical properties of the input data (Massart *et al.*, 2010; Bradbury & Muldoon, 1994). In the case of FracSim3D, Monte Carlo simulations are used together with fracture properties taken from the field-work data and represented in statistical models (Xu & Dowd, 2010). The fracture generated with DFN models are used for flow modelling and the analysis of petrophysical properties. In general, models as DFNs have several of assumptions to valid their application. In the case of FracSim3D, we have identified the following assumptions:

- The fracture geometry can be represented by lines for 2D fractures and ellipses or circular discs for 3D fractures.
- The fracture properties, such as, length, orientation, size, density and spatial distribution follow a statistical distribution and can be modelled by these.
- The fracture network can be elaborated on the basis of Monte Carlo simulations.
- Fracture length is finite.

Figure 4-1 shows the sequence of the work made by FracSim3D for a simulation of fractures. Field-work geometrical data are the inputs for FracSim3D, that is, fracture

length, fracture orientation and fracture density; although additional properties like spacing, hydraulic conductivity, opening, etc. might be entered. These data can be taken from a fracture map of an outcrop and/or taken directly from measurements made on outcrops. The data are usually entered as sets of fractures defined according to their orientation. The entered data for length and orientation may be processed by a statistical distribution through a parametric model or a non-parametric model. The parametric models vary according to the kind of data to be modelled (Table 4-1). Length may be modelled by the Uniform, Exponential or Lognormal distributions, whereas orientation may be modelled by the Uniform, Wrapped Normal, Von Mises and Fisher distributions. The non-parametric modelling is approached by a histogram generated directly from field-work data. Fracture spatial distribution is approached by point process models which consist of a single point, usually the centre of the fracture, used to represent the location (Xu & Dowd, 2010). The point process models available into FracSim3D are Homogeneous Poisson model, Non-homogeneous point process model, Cluster point process model, Cox process model. If a parametric model is used we need to enter into FracSim3D the value of the parameters of the statistical distribution of our field-work data. If a non-parametric model is used we need load a file with the number of classes and the range of classes of the histogram for our field-work data. For the point process models we need enter the fracture density, that is, the number of fracture (points) within a unit area (2D) or a unit volume (3D). On the basis of the statistical data inputs FracSim3D generates new fractures, with their associated properties, using Monte Carlo simulations. Each single simulation generates different fractures and properties, that is, fractures with different length, orientation, distribution and density, but the results always tend according to the statistical model used. The final outputs of this process is a database with the properties of the generate fractures and a fracture map, this in 2D or 3D. If the process is started in 3D, to obtain a fracture map it is necessary to define a plane which intersects the fractures to be represented in the map.

Finally, databases are associated to the fracture map (2D) independently if the simulation was made in 3D.

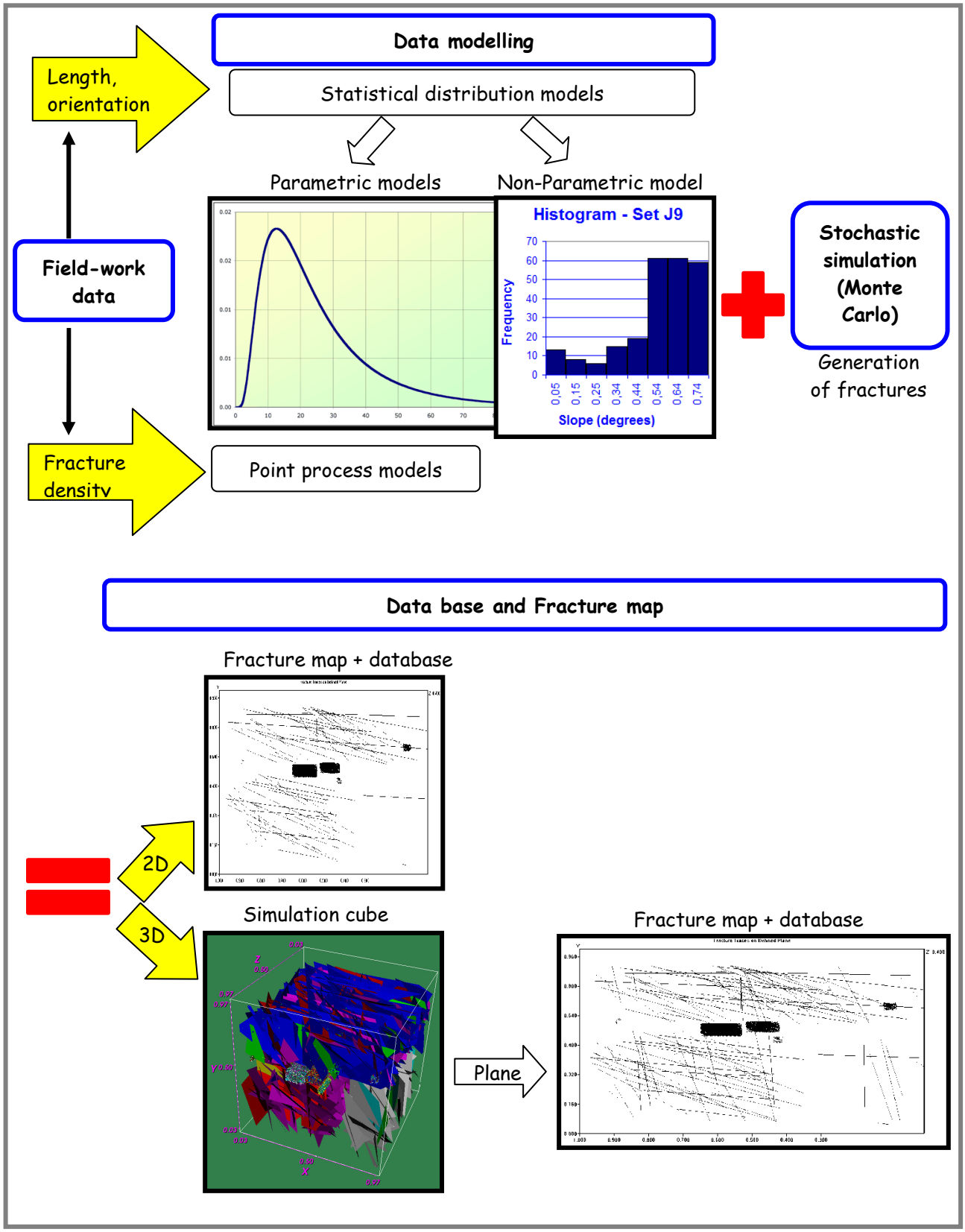

Figure 4-1: Sequence of the simulation process into FracSim3D. The process is based on the field-work data which are modelled by statistical models and are integrated with Monte Carlo simulations. The result is a data base and fracture map of new fractures which follow the parameters of the statistical distributions.

Table 4-1: Statistical Models used on FracSim3D (Xu & Dowd, 2010)

Property of Fractures	Type of model	Statistical Model on FracSim3D
Location	Point process	Homogeneous Poisson model
		Non-homogeneous process
		Cluster process
		Cox process
Length	Statistical parametric	Uniform distribution
		Exponential distribution
		Lognormal distribution
	Statistical non-parametric	Histogram
Orientation	Statistical parametric	Uniform distribution
		Wrapped normal distribution
		Von Mises distribution
	Statistical non-parametric	Histogram
	Statistical parametric (for a mean orientation plane)	Fisher distribution

One of the objectives of this section is to asses and to compare the results of DFN modelling with fracture maps of a carbonate outcrop. This evaluation was made in terms of the geometrical, mechanical and hydraulic properties of fractures, such as, length, connectivity, orientation, position and structural typology, in order to define the accuracy of the model for a fluid flow analysis. The second objective is to apply DFN models to calculate the variation of the hydraulic conductivity of *Monte Conero* according to fractures, for the three scenarios defined in the Microstructure Analysis (Chapter 3).

The use of Geographic Information System (GIS), Excel macro-script, field-work data and fracture maps, was combined to crate the input for FracSim 3D. Fracture properties including orientation, length, opening and fracture type, were measured during field-work on exposures of *Monte Conero*.

4.2 Methods

4.2.1 Data entry Methods for FracSim3D

The methods applied were defined according to the characteristic of fractures in carbonate and the results obtain after each simulation test. We tested four different methods into FracSim3D:

1) Non-parametric models with individual domains of density in 3D
2) Non-parametric models with one global domains of density in 3D
3) Integration method 1 and 2
4) Parametric models in 2D

We refer to density domain as the area o volume of simulation in which the dispersion and density of fractures is relatively homogeneous. We use this domain to represent the differences of fracture density in an outcrop.

Method 1: Non-parametric models with individual domains of density in 3D

A methodology for the creation of a three-dimensional DFN from a map of fractures was established. This methodology was created, initially, according to the characteristics of the input geometrical data used, which were taken from a fracture map (Figure **4-2**) of the Dolomites area in Northern Italy (Mollema & Antonellini, 1999).

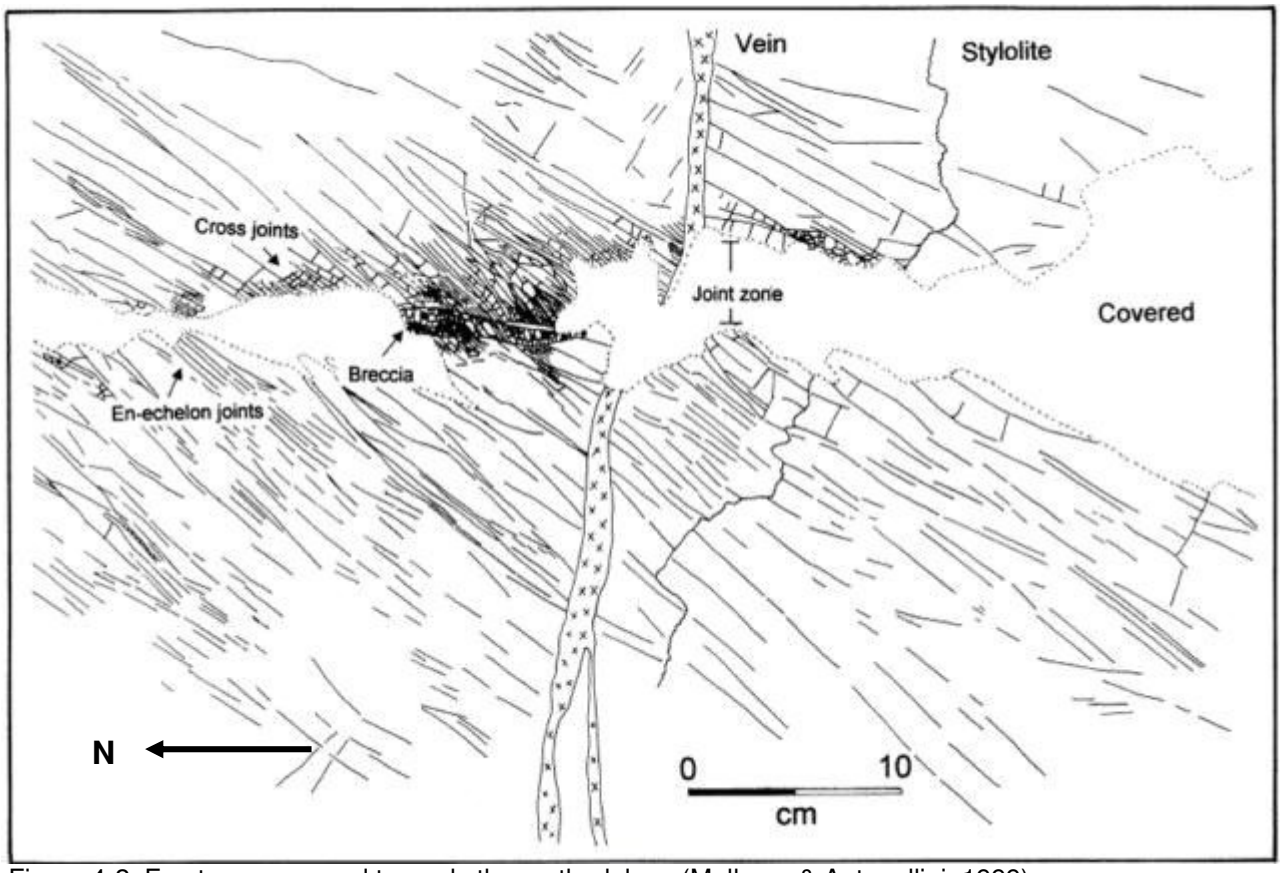

Figure 4-2: Fracture map used to apply the methodology (Mollema & Antonellini, 1999)

The methodology is summarized in the following steps:

- Step 1: Digitalization of a fracture map and calculation of spatial properties

A shapefile of lines was created in a GIS system in which each single trace in the fracture map in study was manually digitizing. Spatial properties such as coordinates X, Y (initial, middle and end point), length and angle of the dip direction (it is calculated using trigonometry) were automatically obtain using the GIS tools. This information and the type of fracture that each line represents (fault, vein, stylolites, joint or breccia) were joined to the table of attributes of the shapefile of lines generated.

- Step 2: Definition of fracture sets for the simulation

  The sets were defined under different criteria:

  - 1st criterion: Each trace in the digitalized map is classified according to the type of fracture which they represent. Under this criterion only the type of fracture with a density greater than 4 fractures per metre can be considered, since FracSim3D is unable to simulate sets with a lower density.
  - 2nd criterion: It classifies fractures according to length and neighbourhood. This criterion allows distinguish a same type of fracture which, due to their arranged in groups, may represent another type of structure. For example, small joints grouped may represent a breccia zone.
  - 3rd criterion: This criterion classifies fractures according to their spatial distribution. Fractures which are close among them may form clusters with a homogeneous dispersion. Clusters are identified representing the central point of each single trace of fracture in a graphic.
  - 4th criterion: It criterion classifies each fracture of the sets identified above according to their orientation. The orientation was divided in four intervals, each pi/2 radians.

- Step 3: Statistical modelling of fractures properties for each fracture sets

The fracture properties - lengths and orientations - are prepared as input for FracSim3D through a non-parametric model (a histogram for FracSim3D). Histogram is one of the models available into FracSim3D which allow enter directly the fieldwork data without approximations through the parameters of a statistical distribution. To automate the collection of statistics with the structure of a histogram a script was programmed where

the number of classes of the histogram is defined according to the rule of Sturges (Hyndman, 1995). The script also meets others two functions. On the one hand, using the z-score method, it normalizes the coordinates of the centroids of fractures to represent the fractures within a unit cubic and thus avoid conflict with the graphic design of FracSim3D. On the other hand, the script gives the extreme coordinates that define the rectangular area of simulation for each set. The histograms of each set and properties of fractures were stored in various text files with the format required by FracSim3D. For the fracture map used in this methodology, as there is no field data, the dip-angle was held constant in the histograms with the value of pi/2 radians, while rotation as 0, and finally fractures were modelled as circular planes.

- Step 4: Statistical representation of fracture distribution

The previous definition of cluster with homogeneous dispersion facilitates this step of simulation. It allows assuming a uniform spatial distribution (Poisson distribution) of fractures within each simulation domain. This distribution requires the parameter lambda, which is a constant which represents the fracture density. Lambda was calculated from the one-dimensional fracture density measured in fieldwork. In this case, the calculating for three-dimensions considers the parameter lambda as the density times the length of the simulation domain, as is indicated by Wang & Ghassemi (2011). The three-dimensional simulation was made considering the XY area covered by the centres of the fractures and a depth of 1 in the Z axis.

- Step 5: Simulation of each set of fracture type

The data of the outcrop are entered in the software following. First, the parameters of fracture distribution are assigned and then, points are displayed in the simulation cube.

Second, fractures are generated from these points and, the non-parametric models are loaded for each fracture propriety. The process is repeated for each fracture set. As result, fracture sets are displayed into the cube.

- Step 6: Definition of a virtual plane

A virtual plane that intercepts the 3D unitary cube is defined, in the same position of the original fracture map. From this plane the fracture traces are generated and compared with the original fracture map.

Method 2: Non-parametric models with one global domains of density in 3D

This method follows the same structure of the Method 1, except for the Step 2. New fracture sets are not defined in this method. Fracture sets here are the same sets observed in fieldwork. As consequence of this, we have only one density domain which is equivalent to the whole outcrop.

Method 3: Integration method 1 and 2

This method is a combination of the method 1 and 2, in which both individual and global domains of density are considered. The individual domains of density are spatially separated and are used to represent concentrations of fractures uniformly distributed in an outcrop. The global domain of density considers the complete area of the outcrop, and includes the individual domains of density within it.

Method 4: Parametric models in 2D

This method considers the definition both individual and global domains of density if it is necessary. However, the main difference with the above three methods is that considers parametric models and the simulation is made in two dimensions. Fracture proprieties are defined in such a way that ensures the homogeneous distribution of them into an individual domain of density. Thus, each one of the fracture propriety (length, orientation, size and distribution) can be modelled by the Uniform distribution. The probability distribution function for the Uniform distribution is defined by the following equation:

$$f(x) = \begin{cases} \dfrac{1}{b-a}, \_ a \le x \le b \\ 0, \_ otherwise \end{cases}$$ Equation 4-1

Where, 'a' and 'b' are the parameters of the distribution and represent the minimum and maximum value that 'x' can takes. 'x', in our case, represents the fracture propriety to be modelled.

4.2.2 Method of Estimation of Hydraulic Conductivity from DFNs

The Discrete Fracture Network model generates with the Method 4, was used as input data to estimate the Hydraulic Conductivity of *Monte Conero*. The fracture sets proprieties of the DFN were entered in the Oda's Model (1985, 1986), which was applied as is explained in Harstad *et al*. (1996) to estimate the permeability tensor (k_x, k_y) in two dimensions. The hydraulic conductivity tensor (K_{Dx}, K_{Dy}) was calculated using the Darcy's Law (1855, 1856).

The Oda's method defines the permeability tensor (k_x, k_y) with the following equation:

Component X: $k_x = \frac{1}{2}(k_{11} + K_{22}) + \sqrt{k_{12}{}^2 + \frac{1}{4}(k_{11} - k_{22})^2}$ Equation 4-2

Component Y: $k_y = \frac{1}{2}(k_{11} + K_{22}) - \sqrt{k_{22}{}^2 + \frac{1}{4}(k_{11} - k_{22})^2}$ Equation 4-3

Where,

$k_{ij}{}^{(f+m)} = \lambda \cdot (\overline{P}_{kk} \cdot \delta_{ij}) + k^{(m)} \cdot \delta_{ij}$, is the bulk permeability tensor Equation 4-4

$P_{ij} = \frac{\sum_{k=1}^{N} t^3 \cdot L_k \times n_i \cdot n_j}{A}$ is the two dimensional P-tensor Equation 4-5

$F_0 = F_1 + F_2$ is the two dimensional fabric tensor related to the crack geometry

Equation 4-6

The principle values of the fabric tensor are:

$F_1 = \frac{1}{2} \cdot (F_{11} + F_{22}) + \sqrt{F_{12}{}^2 + \frac{1}{4} \cdot (F_{11} - F_{22})^2}$ Equation 4-7

$F_2 = \frac{1}{2} \cdot (F_{11} + F_{22}) - \sqrt{F_{12}{}^2 + \frac{1}{4} \cdot (F_{11} - F_{22})^2}$ Equation 4-8

$F_{ij} = \frac{\sum_{k=1}^{N} L_k{}^2 \cdot n_i \cdot n_j}{A}$ Equation 4-9

$\lambda = 0.0210 + 0.0017 \cdot F_0$ is a constant based on regression of lambda vs. F_0

Equation 4-10

$A^{(F)} = \frac{F_1 - F_2}{F_1 + F_2}$ is the anisotropy index Equation 4-11

$A^{(F)}$=1 for isotropic fracture system, 1> $A^{(F)}$ >0 for anisotropic fracture system

The direction cosines of the fracture pole to the fracture trace

$n_i = -\sin(\omega)$ Equation 4-12

$n_j = \cos(\omega)$ Equation 4-13

$\omega = \theta \cdot \frac{\pi}{180}$ is the simulated fracture orientation expressed in radians Equation 4-14

$\phi^{(f)} = \frac{V^{(f)}}{A} \cdot 100\%$ is the fracture porosity Equation 4-15

$V^{(f)} = \sum_{k=1}^{N} t \cdot L_k$ is the fracture volume Equation 4-16

θ : is the measured fracture orientation (in our case the simulated fracture orientation)

L : is the measured fracture length (in our case the simulated fracture length)

A : is the measured area of the plan view rock face

k_m : is the matrix permeability

$t = t_0$: is the constant aperture width

The assumptions of the Oda's Mehod are (Harstad *et al.*, 1996):

- Non-steady interaction between the double porosities can be neglected.
- Each crack can be replaced by parallel planar plates.
- No head loss at intersection between joints.
- Fractures extend the full thickness of the reservoir bed, vertical continuity (2-D)
- Constant fracture aperture (2-D) along individual fractures and for each fracture.

The Darcy's lay defines the hydraulic conductivity tensor (K_x, K_y) from the permeability tensor (k_x, k_y) as follows:

$$K_i = k_i \cdot \frac{\rho \cdot g}{\mu}$$ Equation 4-17

Where,

k_i is the i component of the permeability tensor expressed in [m^2]

ρ is the water density, considered as 999.7 [kg/m^3]

μ is the water viscosity, considered as 0.001307 [Ns/m^2] at 10º C

g is the gravitational acceleration, considered as 9.81 [m/s]

Finally, to determine a constant fracture aperture for the Oda's method, the arithmetic mean of the typical aperture of each fracture set was computed. To consider the aperture of the breccia zones, their effective aperture (b) was calculated using the Cubic law.

$$K_f = \frac{b^2}{12 \cdot \mu}$$ Equation 4-18

$$\Rightarrow b = \sqrt{K_f \cdot 12 \cdot \mu}$$ Equation 4-19

Where,

μ is the water viscosity, considered as 0.001307 [Ns/m^2] at 10º C

K_f is the hydraulic conductivity of the breccia, expressed in [m/s]

4.3 Fracture maps generated from DFN models

The result of applying the four criteria of Method 4 for the definition of fracture sets, resulted in a total of 40 sets, 12 joint sets and 18 breccia sets (Graphic 4-1). The fracture density of the sets varies from 4 to 242 fractures, 6 joint sets have a density less than 30 (which would be considered statistically unrepresentative.) The 78% of the breccia sets have less than 30 fractures; however, as explained above ultimately this value should not be considered.

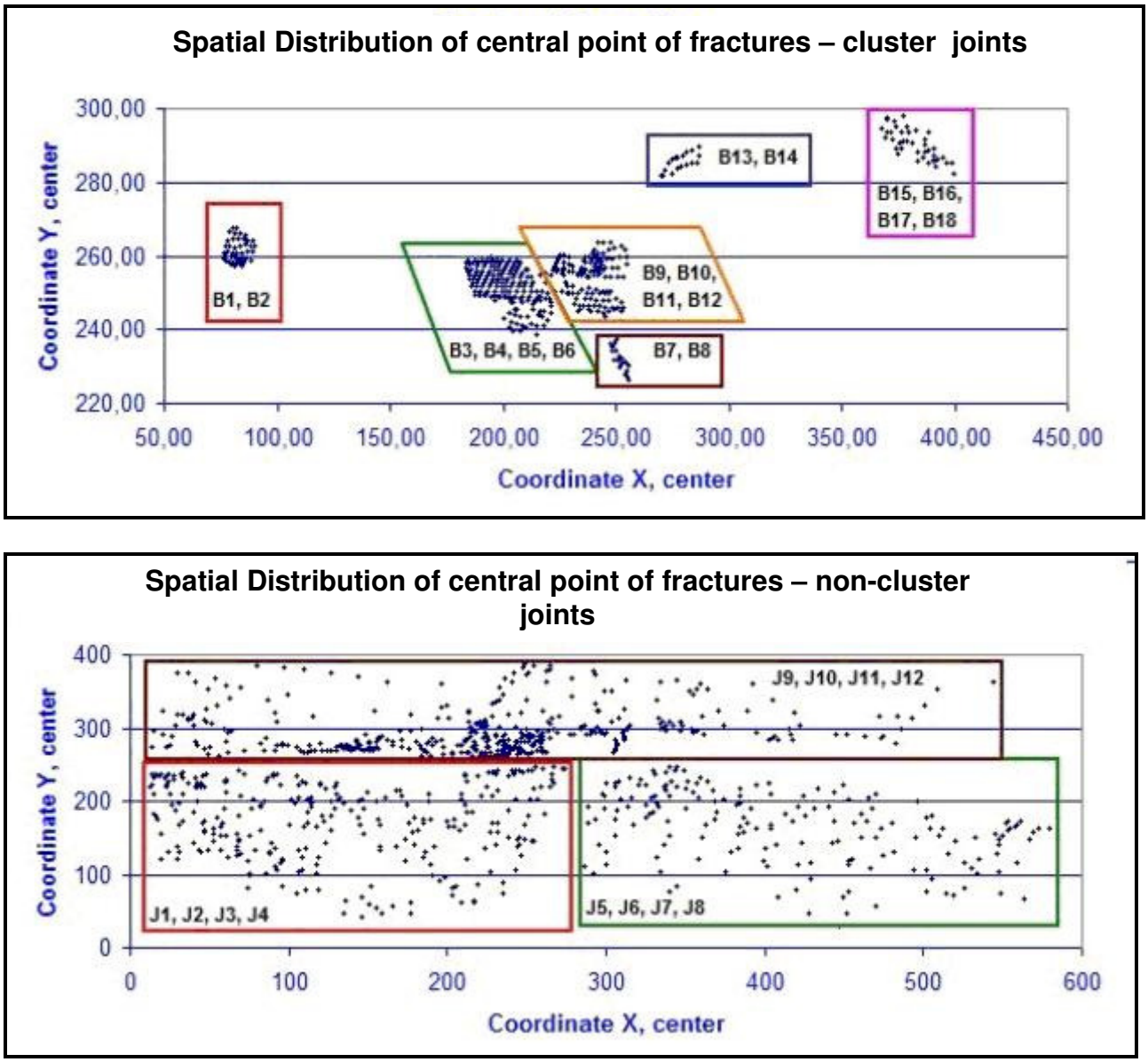

Graphic 4-1: Classification sets. a) Classification of breccias. b) Classification of joints. The coloured polygons indicate the sets of breccias/joints classified according to the third criterion of location by cluster. The alphanumeric characters within each polygon indicate the final subdivisions of the sets according the orientation criterion. Coordinates are relative and not georeferenced.

Figure 4-3 shows the results of the simulations of individual domains of density in three phases.

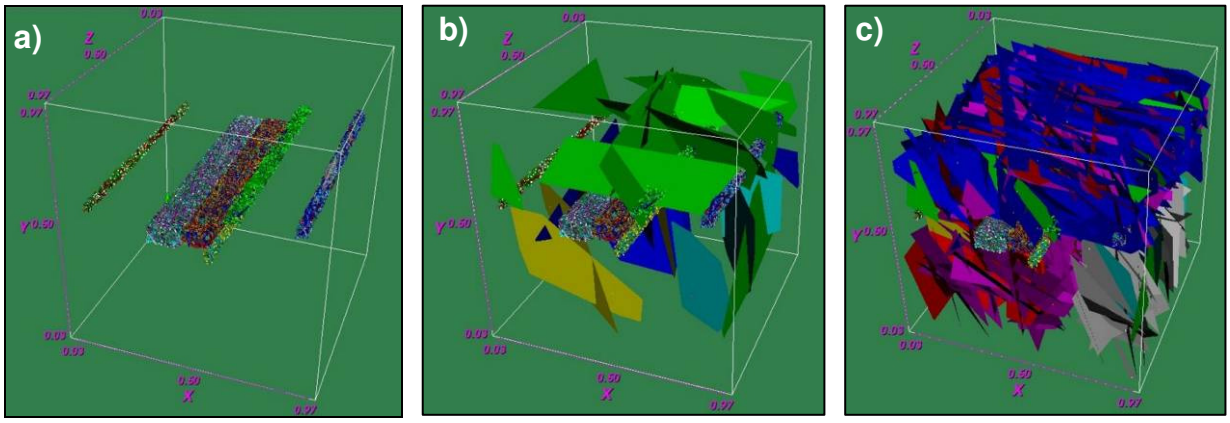

Figure 4-3: Stochastic simulation individual domains of density. a) Breccia simulation. b) Simulation of joints with density less than 30 fractures. c) Final simulation, 12 joint sets and 18 breccia sets.

The fractures intersected with the plane defined in X=0, Y=0 and Z=0.4 and dip angle = 0º, are showed in

Figure **4-4**. The total density of the plane is 2007 fractures. The red arrows indicate the similarities in the breccias zones with respect the original fracture map, and the blue arrows indicate the similarities in the joint sets.

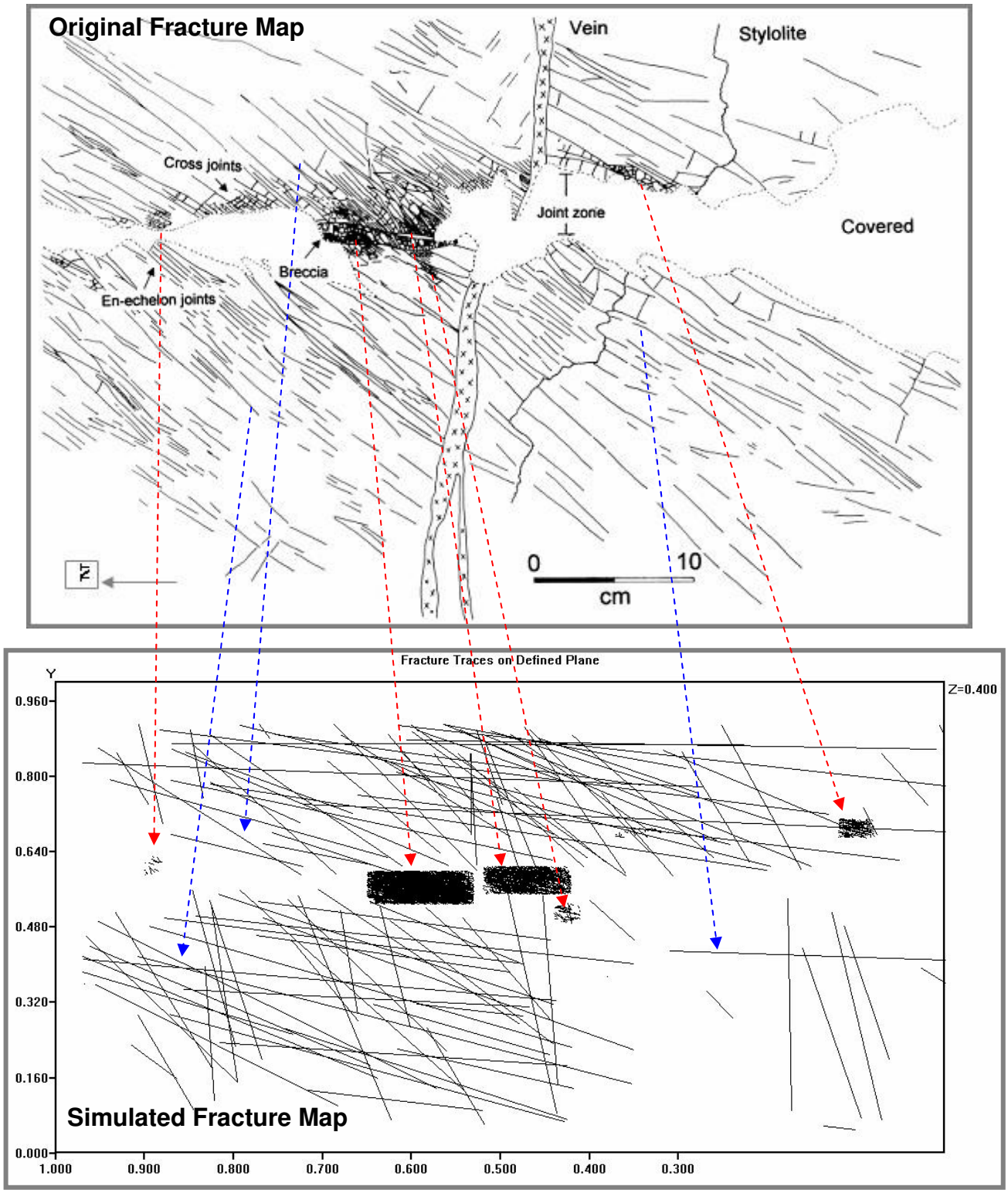

Figure 4-4: Simulated fracture map versus original fracture map The X axis values are reversed because FracSim3D generates an inverted image on this axis, but the value of 1 represents 0 and increases to the right.

In the application of the Method 2 an outcrop of the *Monte Conero* was used. Figure 4-5 shows the sequential results obtained. Fracture map was derived from a photo of the

outcrop. The simulated cube was obtained from the fieldwork data and the fracture map. Finally, from the fracture simulation is derived the fracture map, whose results differs considerably from the original fracture map.

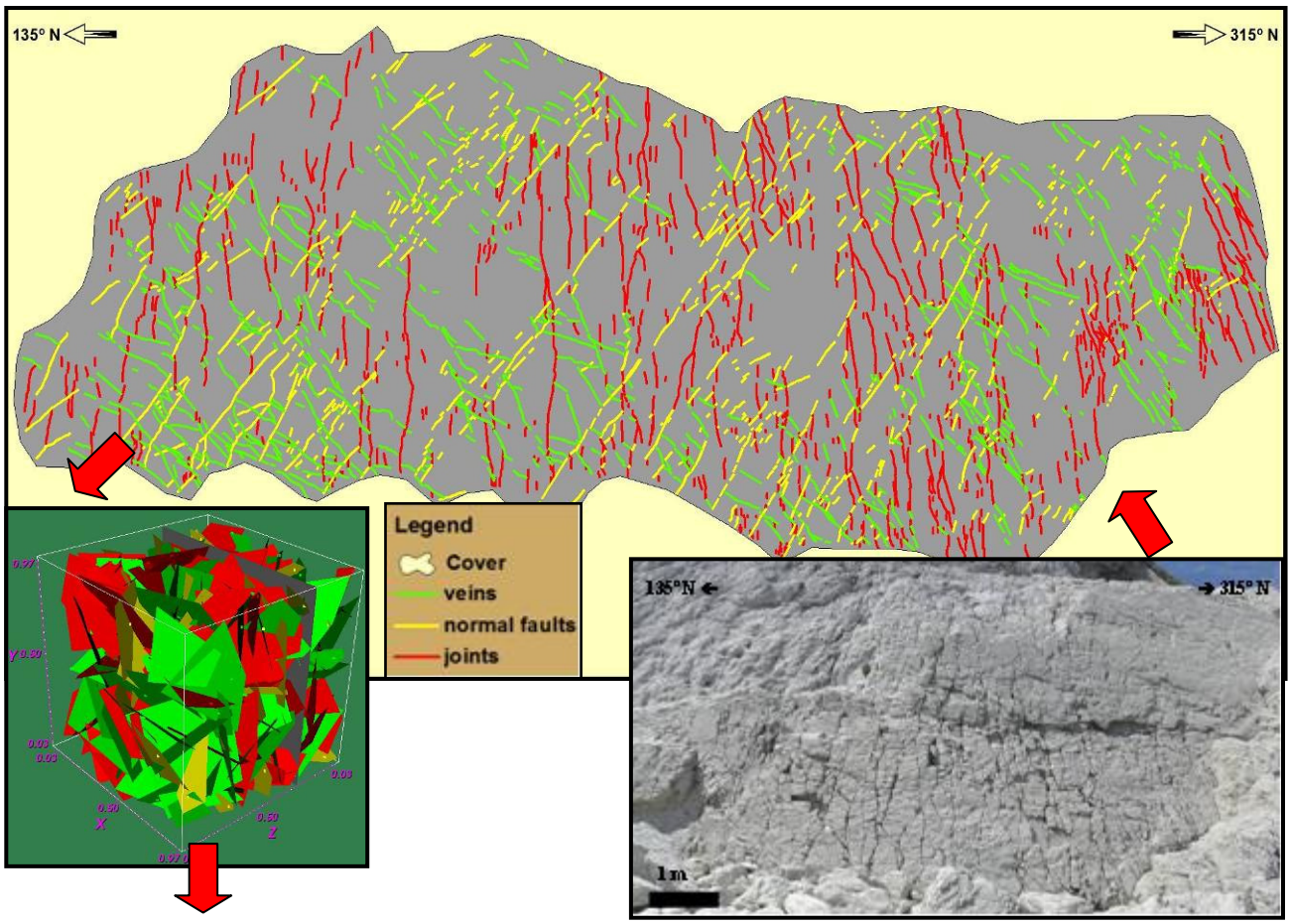

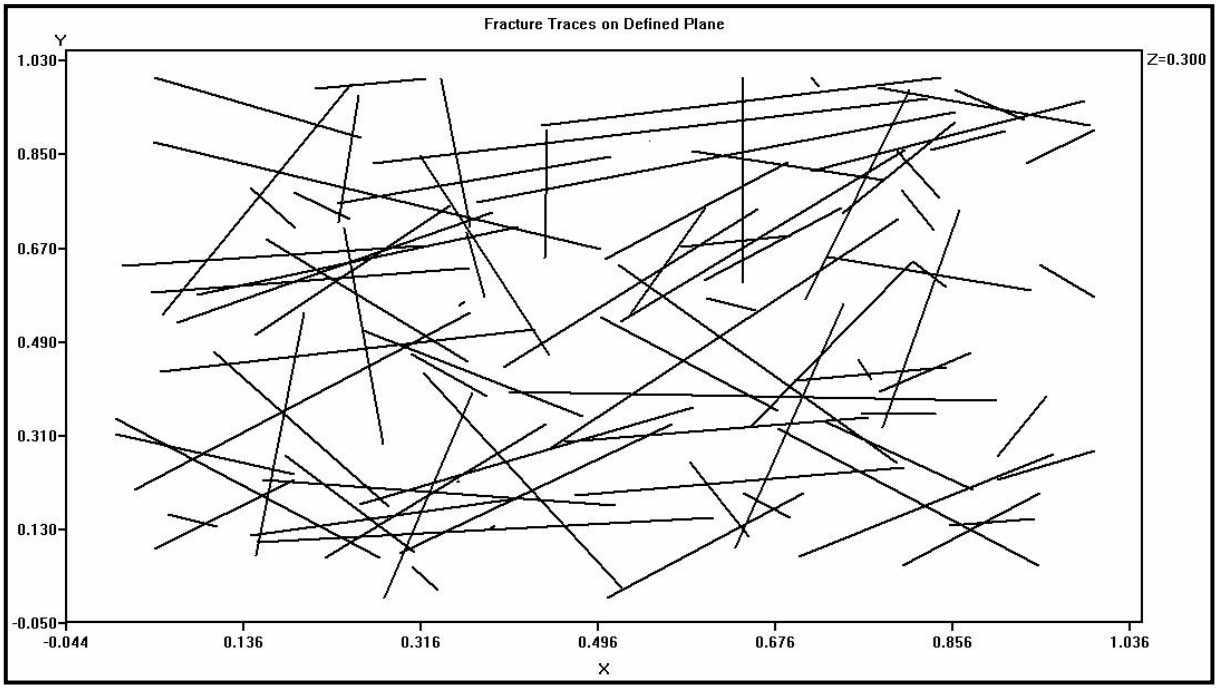

Figure 4-5: Sequential results for the application of Method 2

In the Method 3 the fracture map of a previous study of Mollema and Antonellini was used. The area is located in the Navajo Sandstone, Buckskin Gulch in Utah (USA), and the fractures represented are deformation bands. Figure 4-6 shows the sequential results of the application of the method 3. The sequence goes from the original fracture map, to the digitalization of the original fracture map with the identification of the individual domains of density and the global domain of density. The data of this map are simulated and the cubic simulation is obtained. The final simulated fracture map is presented with the identification of the density domains for a best contrast with the original map.

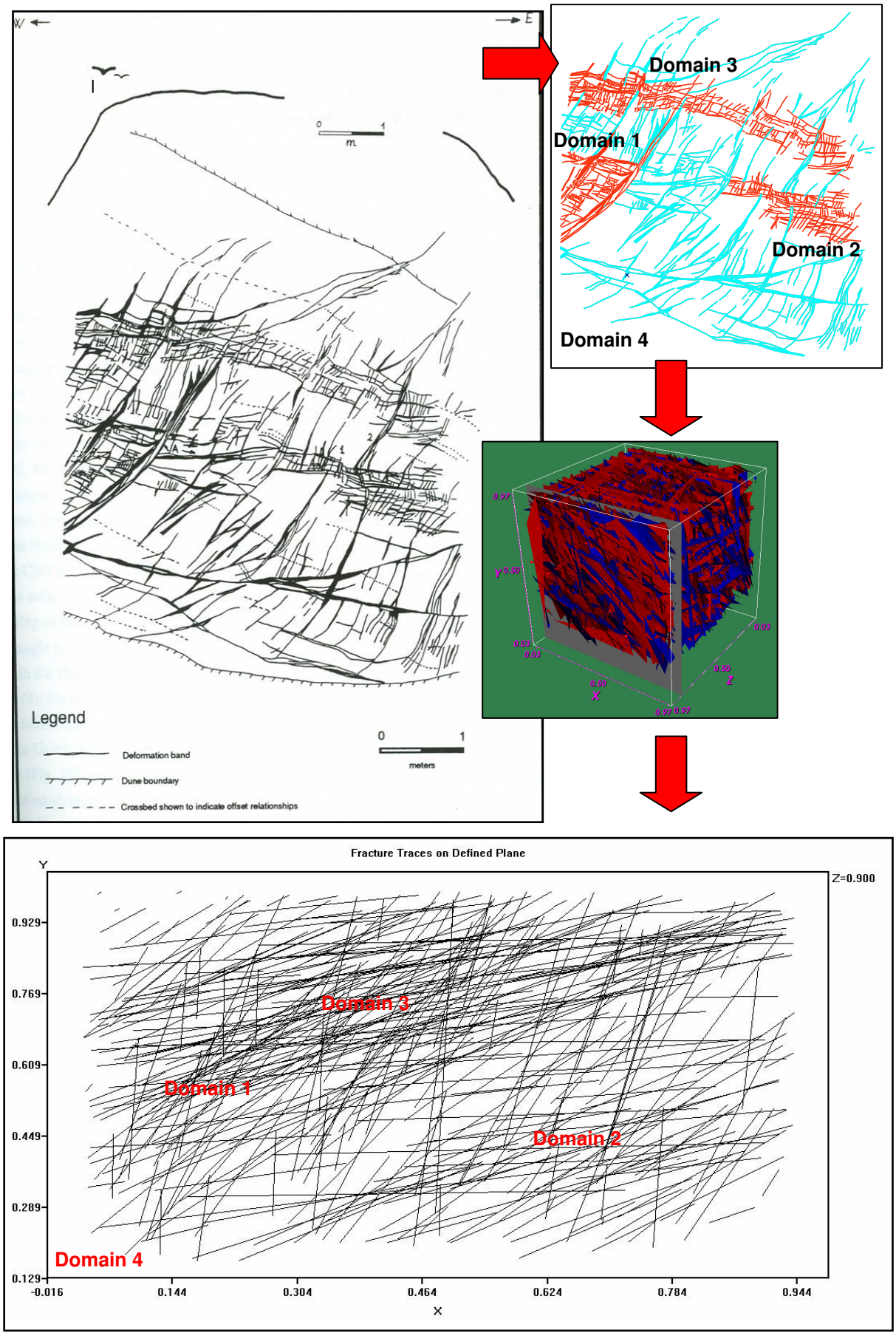

Figure 4-6: Sequential results for the application of Method 3

The results of the Method 4 are presented in Figure 4-7. This figure confronts the bi-dimensional simulations for Scenarios versus the areas in which *Monte Conero* was divided.

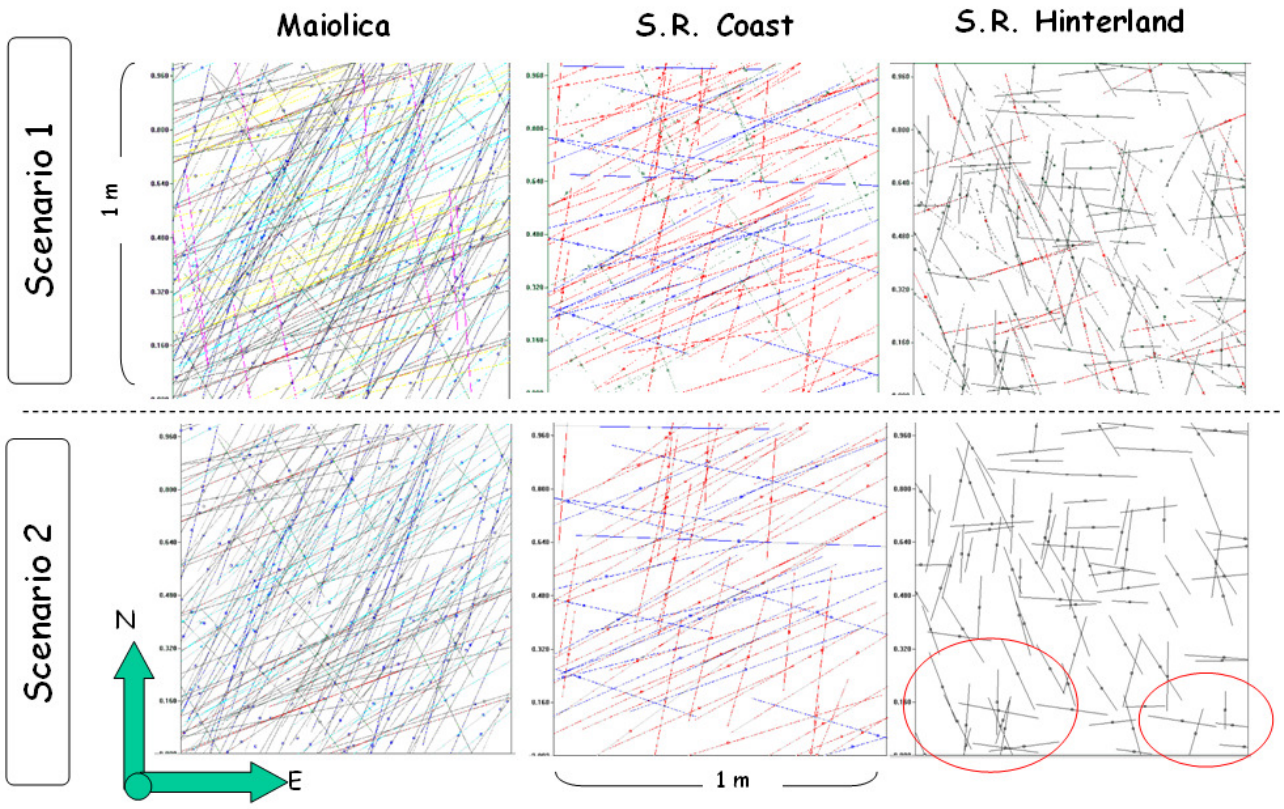

Figure 4-7: Bi-dimensional fracture maps generated with the Method 4

4.4 Estimation of Hydraulic Conductivity using DFNs models

Table 4-2 shows the results obtained with the application of the Oda's method and the Darcy's law. The columns 2 to 5 list the number and type of sets considered for each Scenario of simulation and each zone in the *Monte Conero*. The next columns list: the total number of simulated fractures obtained in the unit cube, the zones of *Monte Conero*, the area of each zone expressed in m^2, the mean aperture calculated expressed in m^2, the

secondary porosity and permeability tensor estimated with the Oda's method, and the hydraulic conductivity estimated with the Darcy's law.

For the application of the Oda's method the hydraulic conductivity of the matrix was considered as 7.8 x 10^{-8} [m/s], this is the value indicates by Davis (1969) as value for K in limestone rocks. We have preferred this value instead of the value observed with the microstructure analysis (0 [m/s]). The estimation of the effective aperture for the breccia zone resulted of 0.8 [mm]

The *Maiolica* area, along the coastline, present 4 sets of veins (V), 2 sets of stylolites (S) and 3 sets of breccia/faults (B/F), which totalizes 231 simulated fractures. In Scenario 2, the total number or fractures is reduced to 193 units (without the consideration of the sets of stylolites). In the *Scaglia Rossa* coast zone is obtained the lowest number of simulated fractures (135 in Scenario 1 and 76 in Scenario 2). In the *Scaglia Rossa* hinterland the quantity of fractures is dominated principally for joints (101 of 176 fractures). The *Scaglia Rossa* coastal zone is the smallest and for this reason reaches values of hydraulic conductivity in the range of the other zones. Aperture in the three zones and for the two scenarios is of the order of 10^{-3}. The secondary porosity is considerably low in the *Scaglia Rossa* hinterland (in the order of 10^{-4}) this because of the small length of the fractures in this zone, Lastly, hydraulic conductivity tensor tends to be more anisotropic in Scenario 1 than in Scenario 2.

Table 4-2: Estimation of Permeability and Hydraulic Conductivity tensors for Scenario 1 and Scenario2

Scenario	Total of Sistematic Sets considered				#frac simulated in a 'REA'=1x1	Zone	Area zone	Aperture	Secundary Porosity	Permeability Tensor k		Hydraulic Conductivity Tensor KD	
							[m2]	[m]	[fraction]	X[m2]	Y[m]	X[m]	Y[m]
	V	S	J	B/F	*FracSim*		*GoogleEarth*		*Oda's Model (1985,1986) – **2D***			*Darcy's Law(1855,1856)*	
1	4	2	-	3	231	**Maiolica**	1.250.000	2,60E-03	0,02	1,15E-10	2,15E-11	8,59E-04	1,61E-04
	3	2	-	2	135	**S. Rossa Coast**	322.000	1,70E-03	0,01	1,04E-11	2,61E-12	7,77E-05	1,96E-05
	2	3	3	-	176	**S. Rossa Hinterland**	8.750.000	1,00E-03	6,61E-04	1,15E-13	7,05E-14	8,66E-07	5,29E-07
2	4	0	-	3	193	**Maiolica**	1.250.000	2,10E-03	0,02	4,62E-11	7,09E-12	3,46E-04	5,32E-05
	2	1	-	2	76	**S. Rossa Coast**	322.000	1,60E-03	0,01	6,15E-12	1,11E-12	4,61E-05	8,34E-06
	0	0	3	-	101	**S. Rossa Hinterland**	8.750.000	1,30E-03	8,29E-04	1,07E-13	7,19E-14	8,03E-07	5,40E-07
V: veins, S: stylolites, J: joints, B/F: breccias/faults. REA: Representative Elementary Area													
Hydraulic Conductivity Matrix= 7,8x10e-8 [m/s] (Davis, 1969), BUT Hydraulic Conductivity Matrix= 0 [m/s] (microstructures observation)													

4.5 Discussion of the Chapter

In the first part of this chapter we evaluated three methodologies for data elaboration and entering the input data into the DFN, FracSim3D. The resulting images obtained from the FracSim3D simulations showed some similarities and many differences in relation to the original fracture map. The model changes, increasing or decreasing, the hydraulic properties of the fractures depending on the method to introduce the data input. For example, the software generates fractures planes that are infinitely long. These long fractures are much better connected than the fractures observed in the outcrops. Therefore the hydraulic conductivity of the simulated fracture network is much higher than the hydraulic conductivity of the fractured outcrop. These results also depend of the characteristics of the simulation code used and the tools offers to simulate. For example, the DFN Modeler (Pashin *et al.*, 2008) offers the generation of compartments and the connection between them that would be the equivalent to our domains which are discussed bellow.

In the first methodology separated and individual domains defined by fracture density and type of mechanical fracture were simulated. In the results, only the location of the breccia and the orientation of joint sets were similar to those of the original outcrop map. However the location of the breccia was conditioned by the definition of the domains. The differences between the simulated and original fracture maps are:

- The internal structure of the breccias: In the original fracture map, the internal structure of the breccias is well organized, following the lineaments of the sets of

joints, whereas in the simulated fracture map this characteristic is not kept and the fracture density is considerably higher.

- Covered areas: The areas which are covered with vegetation or landslides are represented as a discontinuity of the fracture zone in the simulated fracture map. This situation is unreal since under the coverage material fractures should be connected and related to the rest of the fractured area. Situations like this are important for our study since we have assumed that the distribution of superficial fractures represent the fracturing in the aquifer.
- Increase in fracture length: Most simulated fractures have a greater length than the original fractures.
- Fracture connectivity: The increase of fracture lengths generates an increase in the fracture connectivity; since if a fracture length is high, it is most probably that a fracture is crossed by another.
- Fracture density: This property is increased in relation to the original density. This occurs into the all domains used for the simulation.
- Discontinuity between different density domains: This due to the fact that the boundaries of each domain were defined according to the position of the centre of fractures.

In the second methodology, in which a global domain is used to define different fracture densities and types of mechanical fractures, the fracture properties and hydraulic parameters are altered with respect to outcrop. In the simulation, fractures tend to be longer and the discontinuity of the fracture traces, that is typical for the outcrop, is not represented in the model. Pockets of breccia could not be represented by the model. The simulated increase in fracture length also increases connectivity. However, the decrease in

the fracture density shown in the simulated map is a factor that reduces the connectivity between the fractures and, therefore, the probability of circulation of a fluid.

In the third methodology, in which an integration of the first and second methodology is used for one particular type of fracture (deformation bands in sandstone), the results are similar to the previous cases: length, connectivity and density of fractures have all increased in the simulation, whereas fracture orientation is correctly represented. Domains are not clearly identifiable due to the high fracture density. In this case, due to the type of rock with a porous matrix, pathways for fluid flow are reduced. Long fractures at high dip-angle are clearly visible.

We can recommend the following possible solutions to reduce the differences between the original and simulated fracture maps. These solutions refer to the difficulty of representing correctly fracture location, fracture density and fracture geometry.

- In general, the model has some difficulties to represent accurately small or very large areas, like pockets of breccia or the original dimensions of an outcrop. For this reason it is better to use a unitary cube for the simulations.
- The main factor which controls the similarity between the original and simulated map is the location of the fractures, i.e. classification of the sets with the location criterion. This approach allowed to control the spatial location of different types of fractures, because if this criterion is not considered the fractures would be localized randomly within the entire unit cube. The disadvantage of this criterion is that it creates areas of discontinuity (and consequently disconnection between fractures) nonexistent in reality, which can be significant when using the DFN for the flow modelling. Therefore

it is necessary to increase the extension of simulation areas for to ensure connection between all them.

- The sets with low densities do not generate simulations that are representative in terms of the number of points from which fractures are generated. This alters the final result because densities must be increased in ten or more times their original value to get a representation in the simulation. For this reason, there are a large proportion of fractures oriented in directions almost nonexistent in the original maps. It could be resolved by considering only the fractures sets with the most significant densities. Or alternatively, by generating subsets, according to orientation criterion, which are subdivided each pi radians instead of each pi/2 radians.
- Fracture density is a property that should be studied in detail. The software has limitations for simulating low-density sets in small areas/volumes, and as a result it could locate points outside this area/volume. Points which are located outside of the simulation area/volume are not considered for the fracture generation. This problem can be resolved generating fractures from the smallest areas/volumes to the largest. Thus, we can control manually the stochastic generation of fracture by repeating the process until the points are generated within the volume in which we are simulating.
- Each fracture density was quantified on a two-dimensional map and then this value was applied for a three-dimensional simulation. Therefore, to make the simulations more similar to the original map, it is necessary to reduce the depth Z of the simulation volume, making it more similar to a two dimensional area. Another solution is to make the conversion of properties from 2D to 3D by calculations and statistical analysis before starting the simulation, as it is suggested by Xu and Dowd (2010).
- The problems associated with changes in fracture density can be resolved creating as many simulation domains as is necessary to represent the different levels of concentration of fractures, as was proved with the case 3. However, this method does

not guarantee the connectivity between the simulation domains and can generate conditional results.

- The actual geometry of the various types of mechanical fractures can not be accurately simulated by DFNs. This is particularly important in breccias which in our case of the carbonates of the *Monte Conero*, generate porosity in a non-porosity matrix. To represent the breccia effectively, one needs to significantly increasing the value of lambda (the parameter of the Poisson distribution which represents the fracture density). This increasing in lambda can cause unrealistic results or too saturated fracture zones. For this reason, quantification of the fracture density within the breccia is not important to generate the required effect in FracSim3D, but it is necessary to define an optimal value for lambda. However, spatial location remains as the most important factor for the breccias simulation.
- The real irregular shape of breccias pockets can not be represented currently in the DFN and are idealized as parallelepipeds. A more realistic shape of breccias pockets can be created by joining of multiple continuous parallelepipeds.

Finally, we should consider that the above observations have a qualitative character. A statistically significant comparison of the two maps would be achieved with the comparison between the average of minimum 30 simulations and the original values. However, in the study carried out by Voeckler & Allen (2012) the arithmetic mean of 5 simulations has been considered as representative.

We considered that a combination of both individual and global domains of fracture density, as in case 3, is the best method to introduce de data input. Despite the errors mentioned above, the result of the case 3 is the most realistic model.

In other studies, comparisons are based on the result contrast of one or more properties, calculated with DFN simulations and with the in situ measurements. For example, Dershowitz & Doe (1997) consider that hydraulic connectivity and heterogeneity are represented appropriately by DFN models. Voeckler & Allen (2012) found satisfactory results when comparing the simulated and measured hydraulic conductivity and specific storage.

In the last part of this chapter, fracture network models were used to estimate the hydraulic conductivity tensor, using the Oda's model, Darcy's law and cubic law. A fourth and different method to those analyzed above was used to enter the input data to generate the DFNs. The simulation was made in two dimensions, because the Oda's model used is in two dimensions. In addition, the data are referred to the whole *Monte Conero* and not only to an outcrop. This method, which considers the Uniform distribution for the modelling data, gave best result in terms of the fracture orientation. The results of this method keep the original orientation of a set and each simulated fracture varies its orientation in the range of values specified. These results are optimistic in contrast with those obtained in the previous methods, in which fracture properties were entered through non-parametric models (histograms). The use of histograms generated fracture orientations in many directions in a same set. That was the reason why we decided to use the Uniform distribution. To be able to evaluate the anisotropy of the conductivity one needs to consider the orientation.

In general, this method does not generate problems in other fracture proprieties, unlike the first three methods analyzed. The fracture density is not affected by the use of two dimensional data because a conversion into three dimensions is not necessary. Length is also modelled by the Uniform distribution and the values simulated are in

concordance with the original values. This situation is easer to appreciate in the models with less fracture sets, for example, 'Scenario 2' for the Scaglia Rosa coastline and Scaglia Rossa hinterland. The simulation of fracture location is not well represented. The uniform distribution is not respected, generating clusters of fractures nonexistent in reality. The majority of the properties are well represented in two dimensions, but disconnection between the clusters affects to the fluid circulation in the network. However, this disconnection occurs only when one fracture type is modelled, for example, only joints (Scenario 2, S. Rossa Hinterland).

Values of hydraulic conductivity obtained from the fracture network models are into the typical ranges for fractured limestone. For the first scenario, where all fractures are included, the hydraulic conductivity tensor has its major component in the X-direction and this values varies from 8.66×10^{-7} to 8.59×10^{-4} [m/s] in comparison with 3.3×10^{-4} [m/s] indicated by Rabinowitz and Gross (1972) for fractured limestone. In scenario 2, where only open fractures are considered, the hydraulic conductivity tensor tends to be isotropic with a low predominance in the X-direction. In this case values vary from 8.03×10^{-7} and 3.46×10^{-4}. Orders of magnitude of hydraulic conductivity of $10^{-8} – 10^{-7}$ are in agree with others studies made on fractured aquifers (Voeckler & Allen, 2012).

Despite the agreements with the calculated hydraulic conductivity and values from literature, there are possible errors which could affect the results:

- Simulations of DFN in 2D are not representative of the real fracture properties, but they are necessary for the Oda's method. Some information, like fracture orientation, is lost when it is simulated in two dimensions and, thus, fractures are represented as bi-dimensional lineaments instead of planes.

- The definition of the Representative Elementary Area (REA), used to take the fracture set data, may not be appropriate to represent the whole *Monte Conero* (the concept of REA is discussed in Fan and Bras, 1995). All fracture sets do not occur in all outcrops or may not be visible. This may lead to an apparent higher hydraulic conductivity.
- The only fractures with significant contribution to permeability, breccias, can not be used with their real aperture in the Oda's method. Oda's method uses a constant aperture for all fractures considered. To be able to consider breccias in the model together with other fractures, it is necessary to calculate the intrinsic permeability using the cubic law.
- Disconnected fractures have also been included in the calculation of the conductivity. FracSim3D is unable to delete the fractures which do not contribute to fluid flow, such as isolated fractures. Some DFN modellers have incorporated the tool for calculating the hydraulic conductivity, deleting automatically the non-connected fractures, for example FracMan (Dershowitz *et al.*, 2004). In the case of FracSim3D this tool is unavailable and it is impossible to identify what fractures are connected and what not. Thus, the calculation of the hydraulic conductivity should be made on the basis of the complete fracture network model. This situation increases the permeability of the network because of the assumptions of the Oda's method. The Oda's method assumes the connectivity of all fractures and its calculating are basis on the orientation, aperture and density of fractures.
- None of the methods that were used in this study allows one to consider fractures as barriers to fluid flow. A more realistic simulation should consider fractures like stylolites and filled veins as barriers. This could have affected the anisotropy of the hydraulic conductivity tensor, since the flow would be preferential along other pathways.

CHAPTER 5: ASSESSMENT OF THE VULNERABILITY TO POLLUTION OF THE AQUIFER

5.1 Introduction

Groundwater protection is an issue of global interest since water is an essential natural resource for the survival of the planet, human life and economic development. Aquifers, which take place in permeable geologic formations, are the stores of this important resource. Natural protection of aquifers to the pollution coming from the surface is provided by layers which cover the aquifer. These layers acts like filters of the contaminants lessening their impact on groundwater. Thus, the effective groundwater protection in an aquifer depends on the thickness of the protected layers and on the hydraulic conductivity of the material (Kirsch, 2006). Lobo-Ferreira (1999) defines the concept of vulnerability of an aquifer as *"the sensitivity of groundwater quality to an imposed contaminant load, which is determined by the intrinsic characteristics of the aquifer*". This concept differs of the risk concept since the latter considers the vulnerability and potential human threats for a system (Kirsch, 2006). In territorial planning both concepts are used to establish the land use and for the environmental protection. The typical tools to represent these concepts and to evaluate development plans are zoning maps. Vulnerability to pollution maps can represent hidrogeological parameters, and allow the prevision of the risk (Vías *et al.*, 2010) and make better decisions for the management of an aquifer. Different models to asses the vulnerability to pollution have been developed. In the case of *Monte Conero* vulnerability to pollution was assessed with DRASTIC model (Aller *et al.*, 1987), an index composed of seven hydrogeological parameters with different theoretical weights or importance levels and defined as "*a standardized system for*

evaluation ground water pollution potential using hydrogeologic settings". This model is described bellow.

5.2 Methods

The DRASTIC model was developed by the U.S. Environmental Protection Agency (EPA) and was designed under four assumptions (Aller *et al.*, 1987):

1. The contaminant is introduced at the ground surface;
2. The contaminant is flushed into the ground water by precipitation;
3. The contaminant has the mobility of water; and
4. The area evaluated using DRASTIC is 100 acres or larger

This method was elaborated with the purpose to "*create a methodology that will permit the ground-water pollution potential of any hydrogeologic setting to be systematically evaluated with existing information anywhere in the United States*" (Aller *et al.*, 1987). The system is based on the integration of hydrogeological settings, represented by the following seven parameters or factors: **D**epth to Water, (Net) **R**echarge, **A**quifer Media, **S**oil Media, **T**opography (Slope), **I**mpact of the Vadose Zone Media and **C**onductivity (Hydraulic) of the Aquifer. The following are the definitions and significances given by Aller *et al.* (1987) for each parameter:

- **D – Depth to Water**: This is the vertical distance from the topography until the water table. This is important because the larger the deep to water level, the greater the chance for attenuation of a contaminant coming from the surface.

- **R – (Net) Recharge**: It represents the amount of water per unit area of land which penetrates the ground surface and reaches the water table. This is important because this water is able to transport contaminants vertically and horizontally, determining the dispersion and dilution of the contaminant in the vadose and saturated zones.
- **A – Aquifer Media**: It corresponds to the type of consolidated or unconsolidated rock which serves as an aquifer. This is important because the flow system within the aquifer is affected by the aquifer medium. The larger the grain size and the more fractures or openings within the aquifer, the higher the permeability and the lower the attenuation capacity of the aquifer media.
- **S – Soil Media**: It is the uppermost portion of the vadose zone characterized by significant biological activity. This is important because soil has a significant impact on the amount of recharge which can infiltrate into the ground and hence on the ability of a contaminant to move vertically into the vadose zone. The presence of fine-textured materials can decrease relative soil permeabilities and restrict contaminant migrations
- **T – Topography (Slope)**: It is referred to the slope and slope variability of the land surface. This is important because helps to control the likelihood that a pollutant will run off or remain on the surface in one are long enough to infiltrate. Slopes which provide a greater opportunity for contaminants to infiltrate will be associated with higher ground-water pollution potential.
- **I – Impact of the Vadose Zone Media**: The vadose zone is defined as that zone above the water table which is unsaturated or discontinuously saturated. The type of vadose zone media determines the attenuation characteristics of the material below the typical soil horizon and above the water table.

- **C – Conductivity (Hydraulic) of the Aquifer**: It is referred to the ability of the aquifer materials to transmit water and it is important because controls the rate at which ground water will flow under a given hydraulic gradient. The rate at which the ground water flows also controls the rate at which a contaminant moves away from the point at which it enters the aquifer.

The DRASTIC index is composed of weights and ratings for each one of these parameters. Each rating is defined according to ranges. The characteristics of each of these components are described bellow.

- **Weight**: It represents the relative importance of each parameter with respect to the other. The values range from 1 to 5, being the least significant parameter that with weight of 1 and the most significant that with weight of 5.
- **Ranges**: They represent significant media types of each parameter which have an impact on pollution potential.
- **Ratings**: They represent the relative significance of each range with respect to pollution potential. Rating values vary from 1 to 10; the rating 1 is assigned to the least important range and the rating 10 to the most important range. The parameters 'A' and 'I' have a "typical" rating and a variable rating. The variable rating allows adjust the value according to more specific knowledge.

Tables of ranges and ratings for each parameter are included in the Appendix of this thesis.

The equation to calculate the DRASTIC index is the following:

$$D_R \cdot D_W + R_R \cdot R_W + A_R \cdot A_W + S_R \cdot S_W + T_R \cdot T_W + I_R \cdot I_W + C_R \cdot C_W = Pollution\_Potential$$

Equation 5-1

Where:

R : Rating

W : Weight

Replacing the weight values of each parameter in Equation 5-1, we obtain:

$$D_R \cdot 5 + R_R \cdot 4 + A_R \cdot 3 + S_R \cdot 2 + T_R \cdot 1 + I_R \cdot 5 + C_R \cdot 3 = Pollution\_Potential$$

Equation 5-2

To determine the range of each parameter, the data and source enounced in Table 5-1 were used.

Table 5-1: Information used for determining the DRASTIC's parameters

Parameter	Data considered	Source
Depth to water	Estimated by modelling	Ghyben-Herzberg equation
(Net) **R**echarge	= Pp – PET	LocClim (FAO, 2002)
Aquifer media	Massive limestone	Geomorphological and geological maps, fieldwork
Soil media	Thin or absent, gravel	Geomorphological map
Topography (slope)	DEM with percent slope	Contour shapefile (courtesy of the company LAC, Italy)
Impact of the vadose zone	Limestone, Karst limestone, Gravel	Fieldwork and geological map
Conductivity (Hydraulic) of the aquifer	Estimated by modelling and literature	Oda method (1985, 1986) and literature

In ArcGIS, one layer was generated for each parameter, using the information obtained as is indicated in Table 5-1. Zoning in each layer varied depending on the type of information. Each layer represents a rating component in the Equation 5-2. This equation was entered in the Map Calculator tool of ArcGIS to overlay the seven layers obtained. The result was a vulnerability map which was classified in five level of vulnerability to pollution: ‘low’, ‘moderately low’, ‘moderate’, ‘moderate high’ and ‘high’. The GIS process was repeated for three scenarios described in the Chapter 4.

5.3 Results of DRASTIC Application

The results of the determination of DRASTIC’s parameters are described bellow:

The parameter ‘Depth to water’ varies as far as the height of the water table changes in the different zones of the study area. Theoretically, this parameter might vary with the increase of fracturing, since fractures may facilitate or block access of water to the aquifer. However, this parameter was estimated with the Ghyben-Herzberg equation (Chapter 2, Section 2.2) and the results indicated that it depends principally on the topography, since the water table is about 2 metres above sea level. This method of estimation does not allow to consider the effect of fractures on the variation of the water table level. Ratings assigned according to the DRASTIC method are the lowest (vary between 1 and 2).

The parameter ‘Net Recharge’ is variable throughout the year, since it is calculated as the algebraic difference between the inputs and outputs of the water balance in the system. In this study the recharge was estimated using LocClim (Chapter 2, Section 2.2),

calculating the difference between precipitation and potential evotranspiration. The rating for this parameter is high (8) equivalent to about 188 [mm/year] (about 7 inch/year).

The aquifer of *Monte Conero* was evaluated as an unconfined aquifer and the parameter 'Aquifer Media' is constant among scenarios because it is dependent on the characteristics of the aquifer. The media of the aquifer was considered as massive limestone with a equivalent rating of 6.

The parameter 'Soil Media' is constant among the different scenarios but varies among the zones of the study area. For *Monte Conero* this parameter belongs to the ranges 'Thin or Absent' and 'Gravel', which have the same value of rating (10), generating a homogeneous layer of information.

The parameter 'Topography' changes among zones in the study area but is constant among scenarios. Its values vary from 1 to 10 but it is predominant in the lowest values (1, 3 and 5) which are associated to the highest slope. In these areas contaminants are less likely to enter in the aquifer. The slope was estimated using a Digital Elevation Model (DEM) of the Province of *Ancona*.

The parameter 'Impact of the Vadose Zone Media' in *Monte Conero* has surface areas belonging to three different categories of this parameter: 'bedded limestone' (typical rating of 6), 'gravel' (rating 8) and 'karst limestone' (rating 10). There are not literature which indicates the location and characterization of karst zones in *Monte Conero*. We have represented in the maps those zones observed during fieldwork. The ratings of the range 'Bedded Limestone' can vary between 4 and 8, according to particular characteristics of a zone, or take the typical value (6). We have assigned the ratings according to fracture

density in the scenarios. Thus, for the scenario 0 the lowest value (4) was assigned, for the scenario 1 the highest value (8) was assigned, and for the scenario 2 the typical value was assigned (6).

Finally, the parameter 'Hydraulic Conductivity of the Aquifer' was defined according to the results of the Discrete Fracture Network models and the Oda's method. In the three scenarios, the hydraulic conductivity varies from 0 [m/s] in zones of massive (unfractured) limestone to 0.0014 [m/s] in karst zones (theoretical value indicated by Davis, 1969), with equivalent ratings from 1 to 10 (the higher the hydraulic conductivity, the higher the vulnerability of the system). To other materials in *Monte Conero* were assigned the following theoretical values: landslides 0.00035 [m/s] (Baker & Pavlik, 1990), gravel 0.00051 [m/s] (Adams & Gelhar, 1992) and alluvium 0.00019 [m/s] (Robson, 1974).

The DRASTIC index of vulnerability for *Monte Conero* ranges from 109 to 202; in a global context, these values might be considered as a vulnerability to pollution from moderate to high intensity. These ranges are based on the extreme values of the index: minimum 23 and maximum 230. With these values we can define five categories of equal intervals:

- Values from 23 to 64.4 as low vulnerability to pollution
- Values from 64.5 to 105.8 as moderately low
- Values from 105.9 to 147.2 as moderate
- Values from 147.3 to 188.6 as moderately high
- Values from 188.7 to 230 as high

In the local context the categories (Figure 5-4) were defined according to the local minimum (109) and maximum (202); thus, it was possible to distinguish between areas

with varying vulnerability to pollution. The vulnerability maps were made considering these categories of vulnerability.

The three scenarios analyzed show different results, although the changes are minimal between the vulnerability maps of scenario 2 and 3 (Figure 5-4), including both fractures.

In the Scenario 0 or “base scenario” (Figure 5-1) the hypothetical situation of *Monte Conero* without fractures is represented. Under these conditions the zones that are vulnerable to pollution are karst areas (high vulnerability), detritic areas and high slope areas (moderately high vulnerability) and landslide areas (moderate vulnerability).

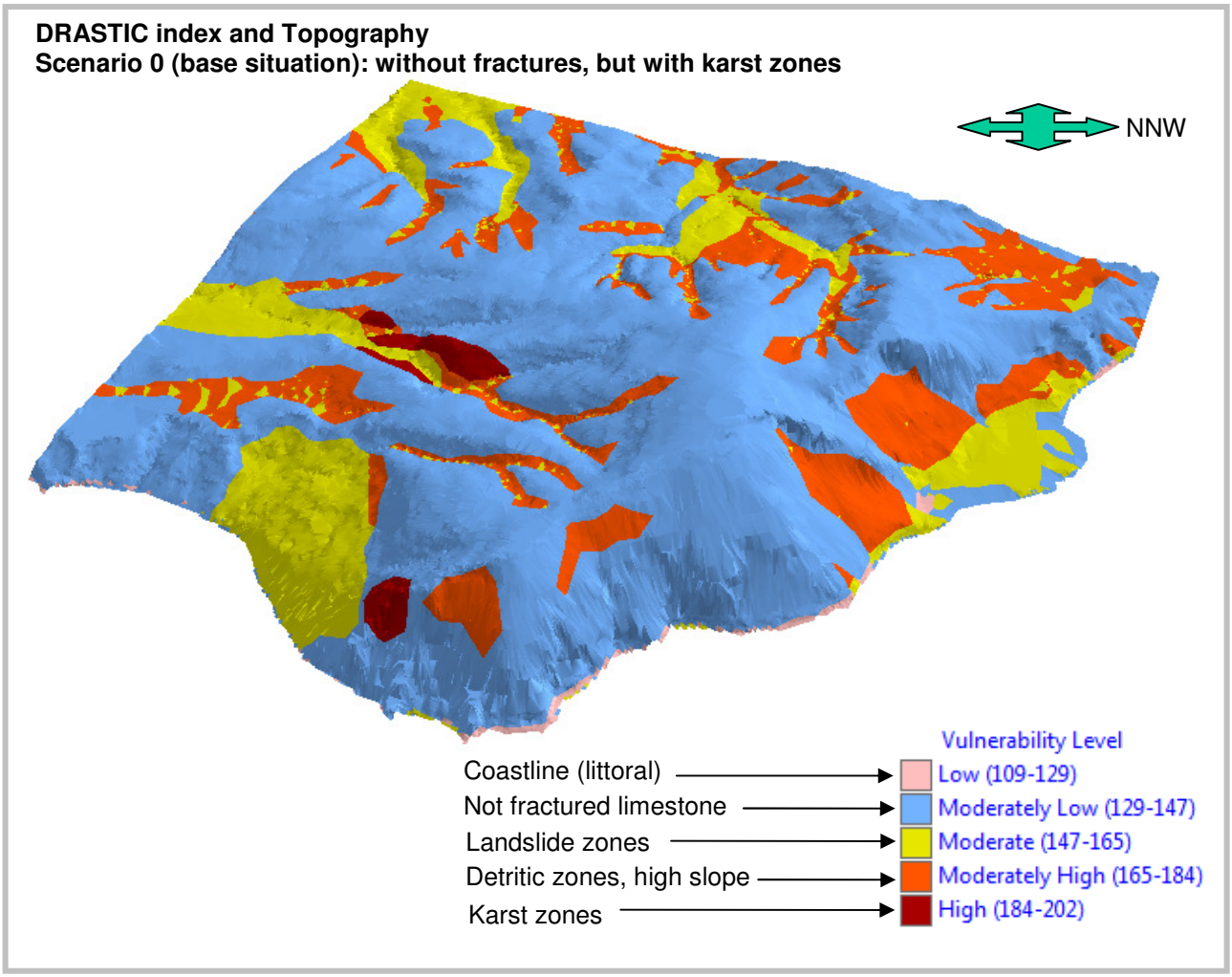

Figure 5-1: Vulnerability digital model for Scenario 0

Scenario 1 (Figure 5-2), which considers all systematic fractures measured, shows 'moderate' to 'moderately high' vulnerability in all zones where a high/moderate fracture density was observed. The 'moderately high' vulnerability to pollution occurs principally along the coastline (zone of *Le Due Sorelle*). This vulnerability level is result of the combination of parameters with high importance in hydraulic conductivity in a zone of potential landslide zone. Karst areas are as also under this scenario the areas with higher vulnerability. The consideration of only open fractures does not cause important changes in the vulnerability map (scenario 2, Figure 5-3). In this scenario the hydraulic conductivity of the aquifer decreased and detritic areas became important, like in scenario 0. For this

reason some zones located in the hillside around the valley have ‘moderately-high’ vulnerability, in contrast to scenario 1.

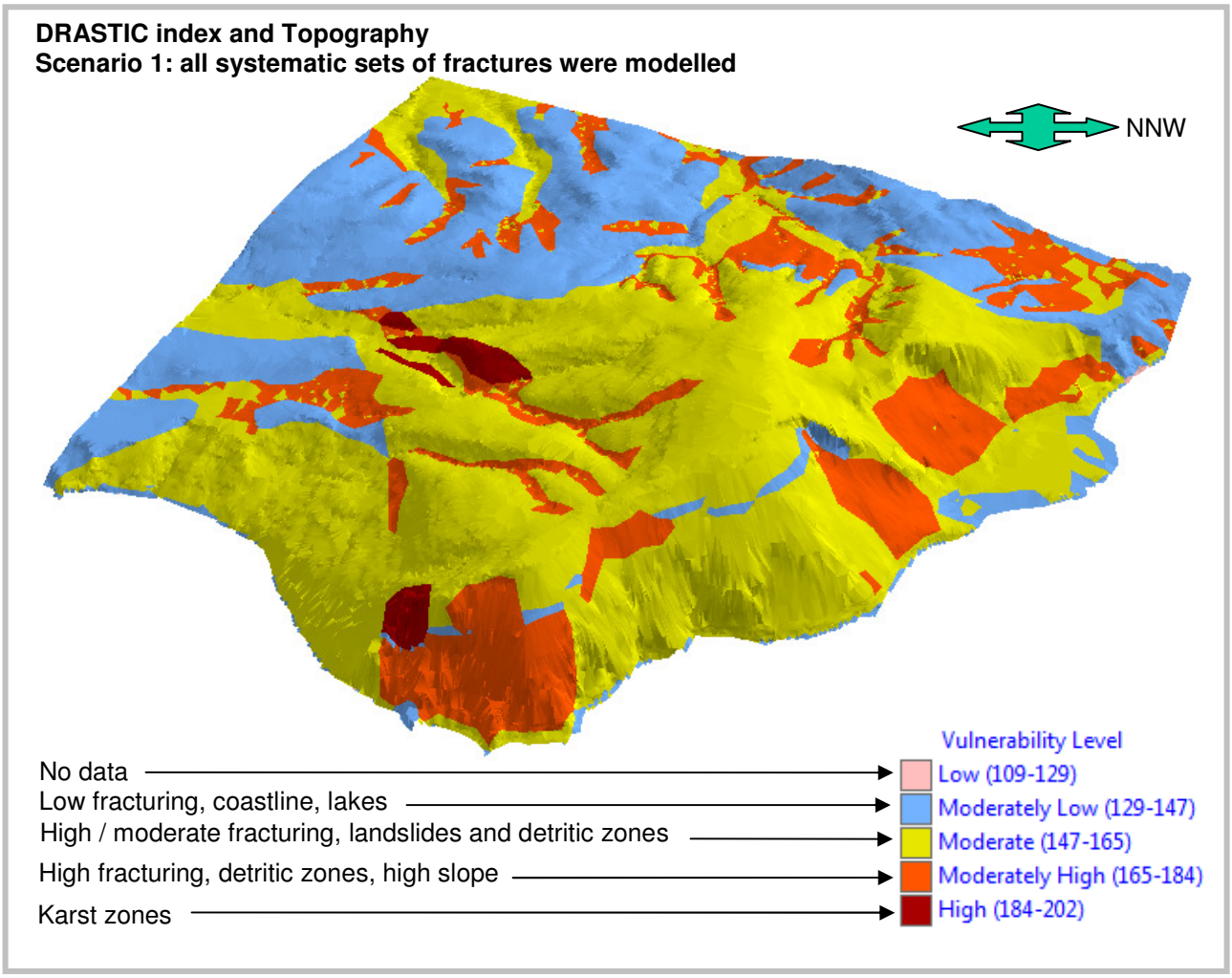

Figure 5-2: Vulnerability digital model for Scenario 1

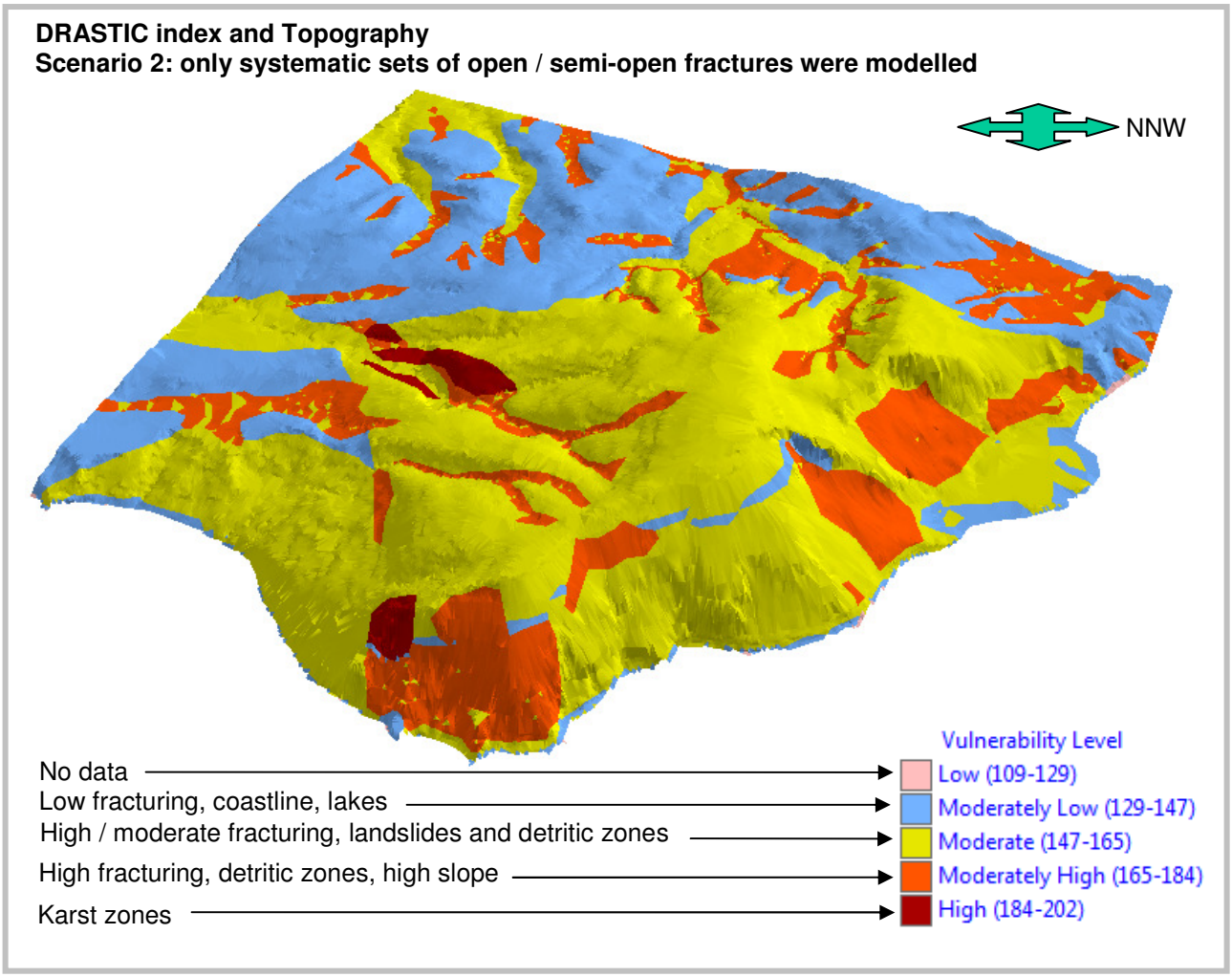

Figure 5-3: Vulnerability digital model for Scenario 2

Figure 5-4 shows a scheme comparing the three scenarios simulated. Simultaneously, these results are contrasted with the maps of the hydraulic conductive parameter. This parameter represents the effects of fractures in the territory.

In the Scenario 0, the zones with highest values of hydraulic conductivities are reproduced in the vulnerability map, where the same zones show the highest level of vulnerability. The red arrows indicate the zone in which Scenario 1 changed in relation with Scenario 0. This zone increased its vulnerability level after the integration of fractures in the system, passing from a 'Moderately Low' vulnerability to a 'Moderate' level or 'Moderately High' level. In the Scenario 1, due to the incorporation of fractures, the results

of the hydraulic conductivity are increased with respect to the Scenario 0. The changes are identified in all zones with medium and high fracture density. These increases in the hydraulic conductivity causes the increases of vulnerability indicated above. The blue arrows in the vulnerability map of Scenario 1, indicate the specific areas where the hydraulic conductivity have influence. In Scenario 2, the map of the hydraulic conductivity shows a decrease of at least one unit in the rating of importance due to the decrease in the number of fractures. However, this diminution is not reflected in the vulnerability map and in relation with Scenario 1, the changes are minimal. The green arrow indicates the points where the changes can be appreciate. These changes are attributed to the parameters ‘Topography’ and ‘Impact to Vadose Zone Media’, which became more vulnerable zones of low slope and gravel.

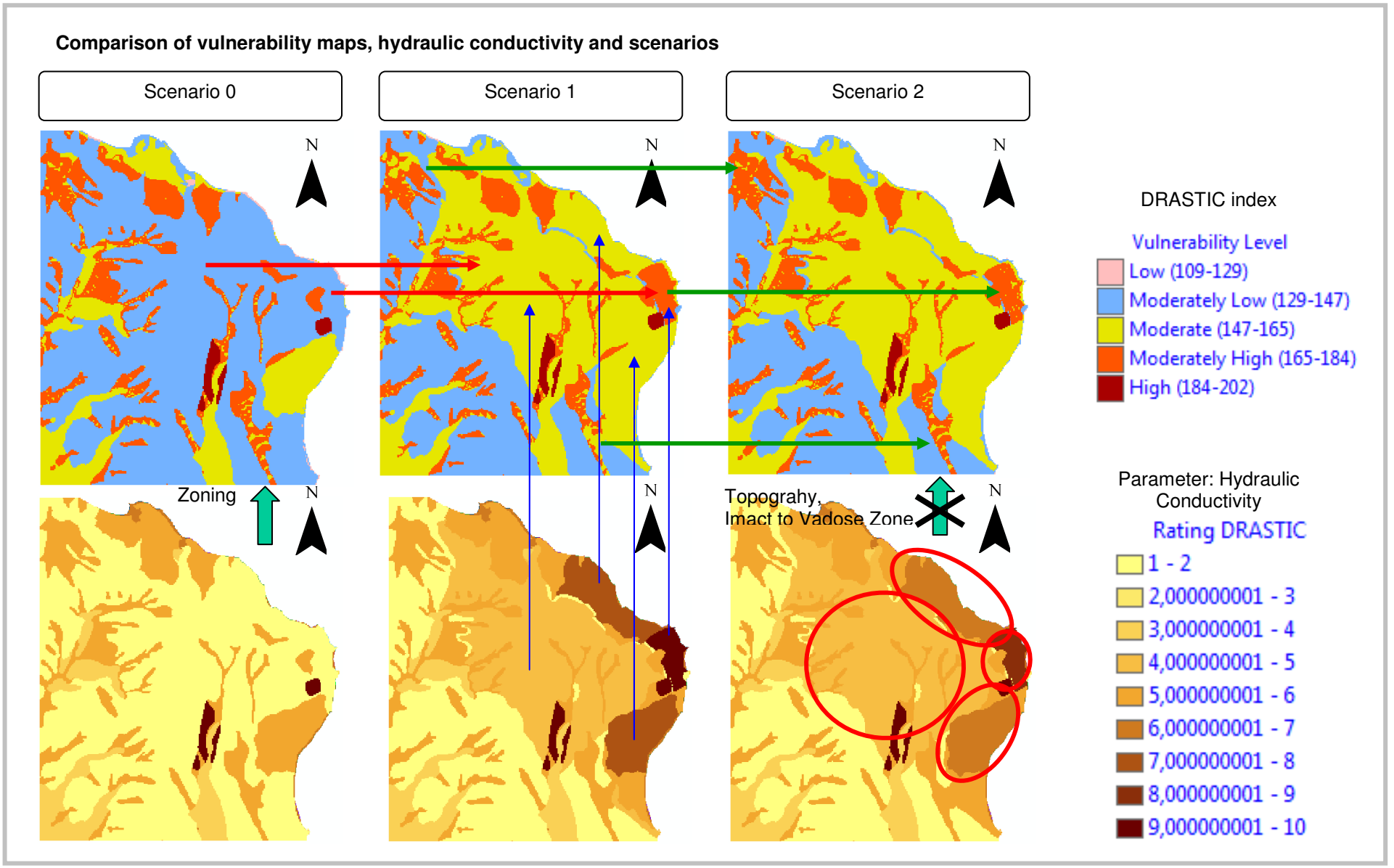

Figure 5-4: Scheme of comparison among vulnerability maps, hydraulic conductivity and scenarios

5.4 Discussion of the Chapter

The calculated DRASTIC index showed that the zones that are more vulnerable to vertical pollution in *Monte Conero* are the karst areas, the landslide areas, the areas covered with detritic material and the fractured areas. Karst areas are typically located along gullies and riverbeds whereas landslides and detritic material are typically along slopes with a dip greater than 30º. The coastal areas have the highest fracture density because the folding of the layers.

The changes among scenarios are explained considering the contribution of each parameter to the vulnerability maps obtained. Table 5-2 shows the variability of each parameter of DRASTIC in *Monte Conero*. The only parameters that vary among scenarios are 'Impact of the vadose zone' and 'Hydraulic Conductivity'.

Table 5-2: Variability of DRASTIC's parameters in *Monte Conero*

Parameter	The value is…	
	Constant in	Variable in
Depth to water	Scenarios*	Zones
(Net) **R**echarge	Scenarios*	Seasons of the year
Aquifer media	Scenarios, zones	-
Soil media	Scenarios	Zones (but the rating is constant)
Topography (slope)	Scenarios	Zones
Impact of the vadose zone	-	Scenarios, Karst, gravel zones
Conductivity (Hydraulic) of the aquifer	-	Scenarios, Karst, gravel, limestone zones, fracture density

* Parameters which, theoretically, might vary among scenarios due to fracturing

The parameter ‘Depth to water’ does not have a significant contribution to the vulnerability maps. This parameter is closely correlated with the ‘Topography’ parameter and then it provides no additional information to the model. Despite being one of the most important parameters in the DRASTIC index (weight equal to 5), its value remained constant among the three scenarios and then, it does not contribute to the assessment of the influence of fractures in the vulnerability maps.

The high theoretical importance of the parameter ‘Net Recharge’ in the model (weight equal to 4) is not distinguishable in the resulting vulnerability maps. In addition, the estimated recharge is valid only during the winter and autumn seasons. Moreover, the values obtained are estimated at provincial scale, due to the availability of the meteorological information. The parameter might vary because of fractures. For example, fractures like stylolites and filled veins may provide traps, where the water recharged may be concentrated and can achieve a greater thickness. However, the estimation method does not allow include in the parameter the effects of the variation in fracture density, and it became the parameter constant for the three scenarios.

The parameter ‘Aquifer Media’ has a medium importance (weight equal to 3) into the index and its results are not shown in the vulnerability maps. This parameter must be equal in the whole study area, since is not possible to evaluate more than one aquifer at a time (Aller *et al.*, 1987).

The parameter ‘Soil Media’ has a small contribution to the total index (weight equal to 2). Both ranges assigned, thin or absent soil and gravel material, are

considered as the most vulnerable media to pollution since they are less capable of filtering one contaminant coming from the surface. Due to this parameter is constant in the whole study area, its results does not influence the vulnerability maps.

The parameter 'Topography' is the least important in the entire index (weight equal to 1) and its values are rather low. Despite this, the influence of this parameter is reflected in the vulnerability maps, because this is one of the few parameters that shows a significant variation from one zone to another in our study area.

In the 'Impact of the Vadose Zone Media' the three categories of range and the assignations of ratings for the range 'Bedded Limestone' generated diversity in the map of the parameter. Along with this, the importance of this parameter in the DRASTIC index (weight equal to 5) influenced the resulting vulnerability maps. Limestone, despite having low matrix permeability, is considered to be prone to fracturing and then it is valuated to have a moderate rating value. Karst limestone is considered to have the highest vulnerability rating since karst aquifers may have very large pathways for contaminants.

The last parameter to be analyzed is 'Hydraulic Conductivity of the Aquifer' which is variable among scenarios and zones in *Monte Conero*. This parameter is the most important for our study because is the only one which reflects directly the influence of fractures. Unfortunately, this parameter is unable to represent the anisotropy of the hydraulic conductivity. This parameter has a moderate importance in the index (weight equal to 3). The coastal areas are the most fractured areas and

thus have the highest ratings of hydraulic conductivity (according to the Oda's method estimations).

In summary, the two parameters have the largest influence on the vulnerability to vertical pollution of *Monte Conero* are the 'Impact of the Vadose Zone Media' and the 'Hydraulic Conductivity'. Instead the parameter 'Topography' has the largest variability in the study area although it doesn't influence the vulnerability as much. The contrast of result between the hydraulic conductivity maps and the vulnerability maps (Figure 5-4) suggest that the incorporation of fractures in the system increases de vulnerability of this. However, a decrease in the number of fractures incorporated does not affect considerably the levels of vulnerability, because other parameters become more relevant.

All previous interpretations should be contrasted with a sensitivity analysis to evaluate the influence of each parameter in quantitative terms and based on statistical analysis of the parameters (for example, Napolitano & Fabbri, 1996). The importance of parameters depends of the characteristic of the area where DRASTIC was applied, as we have analyzed in this study and how other studies have demonstrated. For example, Ducci (2010) found out that the parameters 'Aquifer Media' and 'Hydraulic Conductivity are quite correlated, whereas Rosen (1994) concluded that all DRASTIC parameters are independent and relevant for his study area.

In terms of risk to pollution of the aquifer of the *Monte* Conero, that mean including the location of possible sources of pollution, the results of DRASTIC have another interpretation. In *Monte Conero* a potential source for pollution along the coast is seawater. However DRASTIC only considers possible contamination sources from above and so pollution by seawater cannot be evaluated by DRASTIC. GALDIT, for example, is a specialized method to asses the vulnerability to saltwater intrusion (Chachadi & Lobo-Ferreira, 2001). In our study area, there is a small probability for vertical pollution since the territory is covered by a forest, part of a nature reserve and not easy to access. Unless the source of contamination comes from the air, for example as contaminated rain, these zones will not be contaminated. Furthermore, considering our hydrogeological model presented in the section 2.2 (Chapter 2), the aquifer would be protected from lateral pollution coming from the sea by the impermeable thin layer of the *Marne a Fucoide* Fm. Potential sources of pollution for the part of the Monte Conero that is away from the coast are the agricultural areas. Agricultural or flatter areas tend to change their land use. Therefore, the protection of the aquifer of *Monte Conero* should be focused on the hinterland when devising a territorial development plan.

Standard methods like DRASTIC, never can be completely standardized for all cases, because each study area has particular characteristics. Several authors have made modifications to the DRASTIC index, for example SINTACS (Civita, 1994) and DRASTIC-Fm (Denny *et al*., 2007). SINTACTS is the Italian version of DRASTIC that allows for changes in the weight according to the conditions of a zone in a study area. DRASTIC-Fm adds an eighth parameter to include the effect of fractures in the

analysis. We choose the DRASTIC model because is a complete index which involves a wide range of hydrogeological factors that are influential in the aquifer vulnerability, in contrast with other methods like GOD (Foster, 1987), AVI (Van Stempoort *et al.*, 1993), EPIK (Doerfliger *et al.*, 1999) and PI (Goldscheider *et al.*, 2000) which consider only three or four parameters of the aquifer. We preferred the original definition of the DRASTIC index because of the type of information that was available for the calculation. Even if we would have included the Fractured media (Fm) parameter as defined in DRASTIC-Fm, it would not have affected our results, since in our study the fracture orientation, fracture length and fracture intensity are already considered in the estimation of the hydraulic conductivity (through the Discrete Fracture Network models). In consequence, the Fm parameter would be correlated with the 'Hydraulic Conductivity' parameter. In addition, DRASTIC-Fm was developed for a macro-scale and the ranges and the rating of the index were modified on the basis of local information.

The scale of our study area influences the results. DRASTIC was designed for an area of minimum of 100 acres (about 0.4 Km^2) and *Monte Conero* is about 7.5 Km^2. Some parameters were estimated for a larger area, for example 'Net Recharge'. DRASTIC works well over large areas, for example at regional scale, where parameters, such as land cover, geology and soil, vary considerable. In our study area in the end, these parameters do not vary so much and, therefore, it is difficult to identify areas that are more or less vulnerable to pollution.

We did not apply the SINTACS method for our study area but due to the characteristics of the parameters in *Monte Conero* and the characteristics of this method, it is possible that the vulnerability would be higher than with the DRASTIC method, but the relative vulnerability could be kept. An increase in the vulnerability value does not have a representative mean. Our interest using this type of index is to establish a reference between zones in *Monte Conero*, in that sense, DRASTIC and SINTACS can give similar results.

The last consideration is referred to the availability of data for this research. Conditions like the absence of previous hydrological studies in *Monte Conero*, scientific researches and availability of historical data from wells and springs; as well as, the absence of infrastructure like wells, have made difficult the research work, particularly the characterization of the hydrological settings. This research has contributed to the increase the scientific information in the zone and represents a first approach for future researches in this thematic and undoubtedly leave open question to be resolved, particularly referred to the improving of the determination of the petrophysical parameters, using technical methods like drills, geophysics, etc. to obtain more accurate results. Other questions that can not be resolved with this research are, for example, Why some veins could become in small faults and why not all kinds of veins observed had the same behaviour? What is the quantitative influence of fractures to saltwater pollution? What protection techniques can be effective to lower the levels of vulnerability? Are the coastal aquifers more vulnerable to pollution than hinterland aquifers? What type of fractured structure (anticline,

syncline, etc) is more vulnerable to pollution? What would be the results of the application of a physical model of contaminant transport in *Monte Conero*?

CHAPTER 6: CONCLUSIONS

This research was carried out to determine the influence of fractures on the vulnerability to pollution in the fractured aquifer of *Monte Conero*. The study considered fracture characterization on outcrops during fieldwork and thin section analysis, designing of conceptual models for the aquifer and fault development, stochastic simulation of fractures using Discrete Fracture Networks (DFNs) models, analytic modelling of the petrophysical properties of the aquifer, and vulnerability assessment using the DRASTIC index.

Fractures may influence the fluid circulation in an aquifer in different ways, acting as pathways or as barriers, depending on the type of mechanical fracture and kind of host rock. Therefore, an important part of the research was dedicated to identifying the various types of mechanical fractures, exposed in the limestone rocks of *Monte Conero*.

The fractures occurring in the outcrops of *Monte Conero*, consist of veins, stylolites, joints, faults and breccias that occur both in as elongated zones and in pockets. Veins and stylolites are the most occurring fractures and the highest fracture density occurs in outcrops along the coastline. Veins and stylolites are arranged in various geometries (e.g. en-echelon) which influence the connection with other fractures. Different types of veins (filled, open) and faults (normal, reverse) were observed during the fieldwork.

Veins and stylolites play a fundamental role in the fault development process. *Maiolica* and *Scaglia Rossa* Fm. have different processes of fault development. The initial phase of fault development consists in both formations by shearing along pre-existing veins and the connection of veins by tail-joints. These tail joints brecciate the rock in between overlapping segments of veins. In the *Maiolica* Fm. the process includes a greater number of phases than in *Scaglia Rossa* Fm., generating phase after phase increasingly large breccias and pockets of breccias. Stylolites at the tail of faults accompany the process in the *Maiolica* Fm. whereas tail-cracks are formed at the end of veins in the *Scaglia Rossa* fault development.

The relationship and episodes of fracture development observed at the micro-scale are similar to the one observed at the outcrop-scale. At least 3 different geological episodes were identified, the first that formed a set of veins, the second that formed sets of stylolites and the third that caused the slip along veins, reactivating the veins as faults.

The micro-structure analysis revealed that breccia zones are the principal fractures which can contribute to the fluid flow in Monte Conero, with an estimated porosity of 2% and a permeability of 7 [mD], much higher that the values of the host rock, a mudstone with porosity near to 0%. Currently the veins do not contribute to fluid circulation, because they are completely or partially filled with calcite crystals. Some stylolites are found to be open, but faults and open veins do not contribute to an effective porosity since they are not connected. Due to these factors, the influence

of fractures to vulnerability to pollution was analyzed assuming three different scenarios. Scenario 0 idealizes the *Monte Conero* without fractures. Scenario 1 represents *Monte Conero* with all the different fracture sets observed assuming that all the fractures were open to fluid flow; and Scenario 2 represents the *Monte Conero* assuming that only those fractures are open to fluid flow, that are observed to be open

Discrete Fracture Network models were generated using the code FracSim3D. The simulations showed that these types of models are a useful tool for the representation of a fractured aquifer in 2D and 3D and complete the missing information not possible to measure during fieldwork. However, the code used had some difficulties to represent accurately specific fractures and geometries, like breccia zones and en-echelon veins, connectivity, fractures as barriers. The use of different techniques is necessary for representing different mechanical types of fractures in a realistic way. The best results were obtained using the uniform statistical distribution and domains of different sizes that were defined based on fracture density.

The hydraulic conductivity tensors obtained with bi-dimensional Discrete Fracture Networks models and Oda's methods has the highest value in its component X, which vary from 8.66 x 10^{-7} to 8.59 x 10^{-4} [m/s] for the scenario 1 and from 8.03 x 10^{-7} and 3.46 x 10^{-4} for the scenario 2. The highest values occur in the *Maiolica* Fm. and the lowest values in the hinterland of the *Scaglia Rossa* Fm. These values are higher than the hydraulic conductivity estimated for the breccia zone with the point

counting and binary image methods, whose values vary from 5.33 x 10^{-8} [m/s] to 2.45 x 10^{-7} [m/s]. The results show that at outcrop scale, not only breccias contribute to fluid flow but also other fractures like open veins and joints if they are organized as a network. The fracture network increases the porosity of the limestone of *Monte Conero* from 0% to up to 2%. This analysis confirms that for fluid flow the most important properties are the aperture of fractures and their connectivity as a network.

The variability of the hydraulic conductivity in the territory of *Monte Conero* was crucial for defining a zoning and for the determination of the vulnerability of the aquifer. The assessment of the aquifer vulnerability of the *Monte Conero* was made employing the empirical index DRASTIC, elaborated by the U.S. Environmental Protection Agency (EPA). This model considers seven hydrogeological parameters in the calculation of the index: Depth to water, net Recharge, Aquifer media, Soil media, Topography, Impact of vadose zone, and hydraulic Conductivity. The resulting map obtained from the application of the DRASTIC method suggests that the coastal zones of *Monte Conero* are the most vulnerable but due to the characteristics of these zones we propose that the protection efforts should be focused on the hinterland zones, especially those affected by the karst phenomenon. The resulted model serves as a guide and a first approach for environmental and territorial assessment and planning in the fractured aquifer of *Monte Conero* and we hope that this thesis work will provide directions for future research and the *Monte Conero* results may be used to predict the behaviour of analogue aquifers.

In summary, fractures influence petrophysical properties increasing the porosity and conductivity of a limestone aquifer (micrite). However, fractures are not the only factor to be considered for the evaluation of vulnerability to pollution in an area. Therefore, in an integrated multi-factor evaluation system, the level of influence of fractures depends heavily on the other system components, in *Monte Conero*, the presence of kart limestone, landslides and detritic zones, and the material of the vadose zone.

ACKNOWLEDGMENTS

First of all, I would like to thank to the Programme Eramus Mundus External Cooperation Windows, especially to Ms. Carmen Martín (UVA) and Ms.Catharina Solano (UNIBO) who were my referees during my stay at the University of Bologna. Thanks to the Programme for giving me this opportunity to grow as person and as professional. This opportunity that allowed me to learn about other disciplines and that opened me the doors towards the investigation world. Thanks for the opportunity to know other part of the world, other cultures and meet new people.

I want to thank the Integrated Geosciences Research Group of the CIRSA-Ravenna, to Professor Giovani Gabbianelli for accepting me into the group; to Pauline Mollema for guiding my research, correcting my advances and taking responsibility of my work during my whole stay at the UNIBO; to Professor Marco Antonellini for his teaching, advices and support in my research; to Professor Enrico Dinelli for his advices and support as the Ph.D. coordinator and for his unconditional sympathy; to my colleagues, especially to Mario Laghi and Nicolas Greggio for all the favours and personal advices that they gave me.

I want to thank to all external people to the University, who help me with my research: Dr. Xu for his support with FracSim3D, Dr Ilaria Mosca (ISPRAM), Professor Torquato Nanni (Università delle Marche) and Mr. Serafino Angelini (LAC cartografia) for the information and database given. I want to give an especial acknowledgment to Mr. Stefano Rosoni for all his uninteresting help and hospitality during my stay in Ancona and in Monte Conero.

Finally, I thank to my mum and family that allow me live this experience and understood our physical distance during almost three years. I thank infinitely to Nico, to my little Dalir, and to God for staying with me in all moment and place, for always give me good moments, for making me laugh even in the most difficult situations, for all their unconditional support and for loving me …

Sincerely,
Elizabeth

REFERENCES

Ahlm C, Wallin K, Lundkvist A, Elgh F, Juto P, Merza M, Tärnvik A. 2000. Serologic evidence of Puumala virus infection in wild moose in northern Sweden. Am J Trop Med Hyg 62:106-11.

Allen L.J., Langlais M. and C.J. Phillips (2003) The dynamics of two viral infections in a single host population with applications to hantavirus. Mathematical Biosciences 186 191–217.

Adams, E.E., Gelhar, L.W. (1992). Field study of dispersion in a heterogeneous aquifer. Spatial moments analysis. Water Resour. Res., 28 (12), 3293-3307.

Agenzia Regionale per la Protezione Ambiental Le Marche – ARPAM (2011). Digital information: Shape files to use in Geographical Information Systems to elaboration of academic maps.

Alberti, M., Decandia, F.A., Tavarnelli, E. (1998). Kinematic evolution of the outer zones of the northern Apennines, Italy: the contribution of sequential cross-section balancing techniques. Memorie Società Geologica Italiana, 52, 607-616,6ff.

Alexander, D. (1984). Building damage by landslide: The case of Ancona, Italy. Ekistics, 51: 308, 452-462.

Aller, L., Bennett, T., Lehr, J.H., Petty, R.J. (1985). DRASTIC: A Standardized System for Evaluating Ground Water Pollution Potential Using Hydrogeologic Settings. U.S. Environmental Protection Agency.

Alvino, R., Corniello, A., Ducci, D. (1998). Aquifer pollution vulnerability in the Roccamonfina Volcano area, southern Italy. Groundwater Quality: Remediation and Protection (Proceedings of the GQ'98 Conference held at Tübingen, Germany, September 1998). IAHS Publ. nº 250.

Angeli, M.G. (1991). Condizioni idrauliche di alcune frane nella argille marine del Plio-Pleistocene marchigiano. SCAI conference, Portonovo (AN), 10-12 May, 1989, 67-62.

Angeli, M.G., Barbarella, M., Dramis, F., Garzonio, C.A., Pontoni, F. (1990). A monitoring project for the definition of the geostructural model of Sirolo landslide (Italy). Proc. VI ICFL ALPS 90, Milano, September 12th, 1990, 175-186.

Angeli, M.G., Barbarella, M., Pontoni, F. (1992). Instability of a sea cliff: Sirolo landslide (Italy) Proc. VI ISL, Christchurch, 2: 1093-1100.

Antonellini, M. A., Aydin, A. (1994). Effect of faulting on fluid flow in porous sandstones: Petrophysical properties. The American Association of the Petroleum Geologists Bulletin vol. 78, 355-377.

Antonellini, M. A., Aydin, A. (1995). Effect of faulting on fluid flow in porous sandstones: geometry and spatial distribution. The American Association of the Petroleum Geologists Bulletin, v. 79, 642-671.

Antonellini, M. A., Aydin, A., Pollard, D. D. (1994). Microstructure of deformation bands in porous sandstones at Arches National Park, Utah. Journal of Structural Geology, vol. 16, 941-959.

Antonellini, M. A., Mollema, P.N. (2000). A natural analog for a fractured and faulted reservoir in dolomite: Triassic Sella Group, Northern Italy. The American Association of Petroleum Geologists Bulletin, vol. 84, 314-344.

Antonellini, M., Mollema, P, Giambastiani, B., Banzola, E., Bishop, K., Caruso, L., Minchio, A., Pellegrini, L., Sabia, M., Ulazzi, E., Gabbianelli, G. (2008). Salt water intrusion in the coastal aquifer of the southern Po-plain, Italy. Hydrogeology Journal, 16, 1541 – 1556. DOI 10.1001/s10004000803199

Argnani, A. (1998). Structural elements of the Adriatic foreland and their relationships with the front of the Apennine fold-and-thrust belt. Memorie della Società Geologica Italiana, 52, 647-654, 10 ff.

Aydin, A. (2000). Fractures, faults, and hydrocarbon entrapment, migration and flow. Marine and Petroleum Geology v.17, p.797-814.

Baghbanan, A., Jing, L. (2007). Hydraulic properties of fractured rock masses with correlated fracture length and aperture. International Journal of Rock Mechanics and Mining Sciences, 44, 704-719.

Baker, F.G., Pavlik, H.F. (1990). Characterization and modelling of groundwater flow in a heterogeneous aquifer system to evaluate contaminant migration. Fifth Canadian/American Conference on Hydrogeology, S. Bachu (Ed.), National Water Well Association.

Barchi, M.R., De Feyter, A., Magnani, M.B., Minelli, G., Pialli, G., Sotera, B.M. (1998). The structural style of the Umbra-Marche fold and thrust belt. Memorie della Società Geologica Italiana, 52, 557-578, 8 ff.

Bear, J.; Tsang, C.F., De Marsily, G. (ed.) (1993). Flow and contaminant transport in fractured rock. London: Academic Press, Inc.

Berkowitz, B. (2002). Characterizing flow and transport in fractured geological media: A review. Advances in Water Resources, 25, 861-884.

Birk, S., Liedl, R., Sauter, M., Teutsch, G. (2003). Hydraulic boundary conditions as a controlling factor in karst genesis: A numerical modeling study on artesian conduit development in gypsum. Water Resources Research, vol. 39, nº 1, 1004.

Bortolotti, V.; Castellarin, A.; Cita, M.B.; Dal Piaz, G.V.; Praturlon, A.;, Ricchetti, G.; Vanossi, M. (1994). Guide Geologiche Regionali, 15 itinerari Appennino Umbro-Marchigiano – Vol.1. Società Geologica Italiana. BE-MA ed. Pages 11-88, 207-218 and 289-301.

Bradbury, K.R., Muldoon, M.A. (1994). Effects of Fracture Density and Anisotropy of delineation of Wellhead-Protection Areas in Fractured-Rock Aquifers. Applied Hydrogeology, 3, 17 – 23.

Caprari, M., Folchi Vici d'Arcevia, C., Nanni, T., Siciliani, A., Vivalda, P. (2006). Carta idrogeologica dell'area comprasa tra I Fuimi Cesanoe e Potenza (Marche Centrali). Presented at an international workshop AVER 5, Parma, GNDCI-CNR.

Cello G., Coppola L. (1984). Assetto Geologico-Struttural dell'Area Anconetana e sua Evoluzione Plio-Quaternaria. Bolletino Società Geologica Italiana 103 (1984), 97-109, 6.

Chachadi, A.G., Lobo-Ferreira, J.P. (2001). Sea water intrusion vulnerability mapping of aquifers using GALDIT method. Proc. Workshop on modelling in hydrogeology, Anna University, Chennai, pp. 143 – 156, and in COASTIN A Coastal Policy Research Newsletter, nº4, March 2001. New Delhi, TERI, pp. 7 – 9, (cf. http://www.teriin.org/teri-wr/coastin/newslett/coastin4.pdf)

Chen, Z., Huan, G., Ma, Y. (2006). Computational Methods for Multiphase Flows in Porous Media. Philadelphia: Society for Industrial and Applied Mathematics.

Cherubini, C. (2008). A Modeling Approach for the Study of Contamination in a Fractured Aquifer. Geotech Geol. Eng., 26: 519-533.

Civita, M. (1994). Le carte della Vulnerabilità degli Acquiferi all'Inquinamento. Teoria I Pratica (Aquifer vulnerability maps to pollution). Pitagora Ed. (publisher), Bologna.

Coccioni, R., Moretti, E., Nesci, O., Savelli, D., Tramontana, M., Venri, F., Astracedi, M. (1997). Carta Geologica con itinerari escursionistici, scala 1:20.000. Parco Regionale del Conero, S.E.L.C.A., Firenze, Italia.

Colosimo, P., Crescenti, U. (1972). Carta geolitologica ad orientamento geotecnico e della franosità della zona del Monte Conero (Comuni di Ancona, Numana e Sirolo). Memories Società Geologica Italiana, 12: 317-334.

Colosimo, P., Crescenti, U., Tommasoni, D. (1973). Studi di conservazione territoriale in Provincia di Ancona: I movimenti franosi lungo il litorale tra Numana e Sirolo. Boll. Econ. C.C.I.A.A., 9: 1-26.

Conti, S. (1998). Caratteri Geomorfologici e Idrogeologici dell'Area Costiera di Portonovo (Ancona). Undergraduate thesis, Faculty of Scienze Matematiche, Fisiche e Naturali, University of Bologna. 80 p.

Corniello, A., Ducci, D., Monti, G.M. (2003). Aquifer pollution vulnerability in the Sorrento peninsula, southern Italy, evaluated by SINTACS method. Geofísica Internacional, vol. 43, nº 4, pp. 575-581.

Cucchi, F., Marinetti, E., Potleca, M., Zini. L. (2001). Influence of Geostreutural Conditions on the Spelogenesis of the Trieste Karst (Italy). Geologica Belgica, vol. Karst & Tectonics, 4/3, 241 – 250.

Cumin, G. (1936). Il promontorio del Conero. Boll. Società Geologica Italiana, 14 (7); pp. 360-391. Roma.

Davis, S.N., Porosity and permeabiliy of natural materials. Flow through porous media, ed. R.J.M. De Wiest, Academic Press, New York, 54-89, 1969.

Denny, S.C., Allen, D.M., Journeay, J.M. (2007). DRASTIC-Fm: A modified vulnerability mapping method for structurally controlled aquifers in the Gulf Island, British Columbia, Canada. Hydrogeology Journal, 15, 483 - 493.

Dershowitz, W, Doe, T. (1997). Analysis of heterogeneously connected rock masses by forward modeling of fractional dimension flow behaviour. Int. J. Rock Mech. & Min. Sci., 34, 3 – 4, paper nº 061.

Dershowitz, W.S., La Pointe, P.R., Doc, T.W. (2004). Golder Associates Inc. http://www.cluin.org/products/siteprof/2004fracrockconf/cdr_pdfs/indexed/group1/882.pdf

Dershowitz, W.S., Lee, G., Geier, J., Hitchcock, S., La Pointe, P. (1993). User documentation: Fracman driscrete feature data analysis, geometric modelling and exploration simulations. Seattle: Golder Associates.

Doerfliger, N., Jeannin, P.Y., Zwahlen, F. (1999). Water vulnerability assessment in karst environments: a new method of defining protection areas using a multi-attribute approach and GIS tools (EPIK method). Environ Geol, 39(2), 165 – 176.

Dramis, F., Garzonio, C.A., Leopardi, S., Nanni, T., Pontoni, F., Rainone, M. (1988). Damage due to landslides in the ancient village of Sirolo (Marche, Italu): preliminary analysis of risk mitigation on the historical site. Proc. IAEG Int. Symp. 'The Engineering Geology of Ancient Works, Monuments and Historial Sites. Atene, 217-224.

Ducci, D. (2010). Aquifer Vulnerability Assessment Methods: The Non-Independence of Parameters Problem. Journal Water Resource and Protection, 2, 298-308.

Fan, Y., Bras, R. (1995). On the Concept of a Representative Elementary Area in Catchment Runoff. Hydrological Processes, vol. 9, 821-832.

Fancelli, R., Radrizzani, S. (1964). Foglio 118 Ancona. Note III. Carta Geologica d'Italia, 42, Roma.

Fancelli, R., Radrizzani, S. (1964). Note Illustrative della Carta Geologica d'Italia alla scala 1:100.000, Foglio 118, Ancona. Ministero dell'Industria e del Commercio, Direzione Generale delle Miniere, Servizio Geologico d'Italia. Libreria dello Stato, Roma.

Fetter, C.W. (2001). Appied Hydrogeology (Fourth Edition). New Jersey: Prentice-Hall Inc.

Foster, S. (1987). Fundamental concepts in aquifer vulnerability, pollution risk and protection strategy. In: Van Duijven-booden, W., Van Waegeningh, H.G. (eds), Vulnerability of soil and groundwater to pollutants. Proc Inf TNO Comm Hydrol Res, The Hague, 38, 69 – 86.

Fouché, O., Diebolt, J. (2004). Describing the geometry of 3D fracture systems by correcting for linear sampling bias. Matematical Geology 36 (1), 33-63.

Goldscheider, N., Klute, M., Sturm, S., Hötzl, H. (2000). The PI method – a GIS-based approach to mapping groundwater vulnerability with special consideration on karst aquifers. Z Angew Geol, 46(3), 157 – 166.

Harstad, H., Teufel, L.W., Lorenz, J.C., Brown, S.R. (1996). Characterization and Fluid Flow Simulation of Naturally Fractured Frontier Sanstone, Green River Basin, Wyoming. Sandia National Laboratories. United States. pp. 32 – 36.

Harstad, H., Teufel, L.W., Lorenz, J.C., Brown, S.R. (1996). Characterization and Fluid Flow Simulation of Naturally Fractured Frontier Sandstone, Green River Basin, Wyoming. Sandia National Laboratories, United States. pp 32-36.

Hyndman, R.J. (1995). The problem with Sturges'rule for constructing histograms. Department of Econometrics and Business Statistis, Monash University, Clayton, Victoria, Australi, 3168.

Jing, L. (2003). A review of thechniques, advances and outstanding issues in numerical modelling for rock mechanics and rock engineering. International Journal of Rock Mechanics & Mining Sciences 40, 283-353, p. 315-318.

Kaufmann, G., Braun, J. (2000). Karst aquifer evolution in fractured, porous rocks. Water Resources Research, vol. 36, nº 6, pages 1381-1391.

Kirsch, R. (2006). Groundwater protection: vulnerability of aquifers. Groundwater Geophysics, A Tool for Hydrogeology. Springer Berlin Heidelberg, pp 459 – 471.

Lavecchia, G., Minelli, G., Pialli, G. (1988). The Umbria-Marche arcuate fold belt (Italy). Tectonophysics, 146, 125-137.

Lobo-Ferreira, J.P. (1999). The European Union experience on groundwater vulnerability assessment and mapping. COASTIN A Coastal Policy Research Newsletter, 1, 8 – 10.

Marsico, A., Giuliano, G., Pennetta, L., Vurro, M. (2004). Intrinsic vulnerability assessment of the south-eastern Murge (Apulia, sourthern Italy). Natural Hazards and Earth System Sciences, 4: 769-774.

Massart, B., Paillet, M., Herion, V., Sausse, J., Dezayes, C., Genter, A., Bisset, A. (2010). Fracture Characterization and Stochastic Modeling of the Granitic Basement in the HDR Soultz Project (France). Proceedings Worl Geothermal Congress 2010. Bali, Indonesia, 25-29 April 2010.

Mollema, P. N., Antonellini, M. A. (1996). Compaction bands: a structural analog for anti-mode I cracks in Aeolian sandstone. Tectonophysics, vol. 267, 209-228.

Mollema, P. N., Antonellini, M. A. (1999). Development of strike-slip faults in the Dolomites of the Sella Group, Northern Italy. Journal of Structural Geology, vol. 21, 273-292.

Mollema, P., Antonellini, M. (1998). Influence of fault architecture on fluid flow: a comparison between faults in dolomite and Aeolian sandstone. AAPG Annual Convection Abstract. Salt Lake City, Utah. May 17-28, 1998.

Mollema, P., Aydin, A. (1997). Fracture Patterns and Fault Architecture in the East Kaibab Monocline. Natural Fracture Systems.

Montanari, A.,Sandroni, P. (1995). Le Rocce del Conero Raccontano, una breve guida geoescursionistica. Parco del Conero. Ed. Aniballi, Ancona. 63 pp.

Nanni, T. (2011). Personal Interview. Nanni, T. is a professor at the Università delle Marche and expert in the hydrogeology of the area.

Nanni, T., Vivalda, P. (2005). The aquifers of the Umbria-Marche Adriatic region: relationships between structural setting and groundwater chemistry. Boll. Società Geologica Italiana, 124: 524-542, 24 ff., 1 tab.

Nanni, T., Vivalda, P. (2009). Idrogeologia degli acquiferi carbonatici terrigeni ed alluvionali tra i fuimi Cesano e Potenza Marche Centrali – Sintesi dei risultati. Ed. La Nuova Lito, Firenze.

Napolitano, P., Fabbri, A.G. (1996). Single-parameter sensitivity analysis for aquifer vulnerability assessment using DRASTIC and SINTACS. HydroGIS 96:

Application of Geografic Information Systems in Hydrology and Water Resources (Proceeding of the Vienna Coneference, April 1996). IAHS Publi. no. 235.

Oda, M. (1985). Permeability tensor for discontinuous rock masses. Géotechnique 35, nº 4, 483-495.

Oda, M. (1986). An Equivalent Continuum Model for Coupled Stress and Fluid Flow Analysis in Jointed Rock Masses. Water Resources Research, vol. 22, nº 13, 1845-1856.

Oude Essink, G.H.P. (2001). Improving fresh groundwater supply – problems and solutions. Ocean & Coastal Management, Volume 44, Issues 5-6, pp. 429-229

Parco del Conero (2011). Itinerari Geologici del Parco del Conero – Il Trave e il Monte dei Corvi. Information panel. (http://www.noseonline.org/pdf/pannelli/pannello_Trave.pdf)

Park, W.C., Schot, E.K., (1968). Stylolites: Their nature and origin. Journal of Sedimentary Petrology, 38: 175-191.

Pashin, J., Jin, G., Zheng, C., Chen, S., Mcintyre, M. (2008). Discrete Fracture Network models for risk assessment of carbon sequestration in coal, Final Technical Report. Geological Survey of Alabama.118p. (http://www.gsa.state.al.us/CO2/DFNModeler/dfnm_files/Final%20report%2005NT42435.pdf)

Petracchini, L., Antonellini, M., Billi, A., Scrocca, D. (2012). Fault development through fractured pelagic carbonates of the Cingoli anticline, Italy: Possible analog for subsurface fluid-conductive fractures. Journal of Structural Geology, in press, 1-17.

Polemio, M., Casarano, D., Limoni, P.P. (2009). Karstic aquifer vulnerability assessment methods and results at a test site (Apulia, southern Italy). Natural Hazards and Earth System Sciences., 9, 1461-1470.

Rabinowitz, D.D., Gross, G.W. (1972). Environmental tritium as a hydrometeorologic tool in the Roswell Basin, New Mexico, Tech. Completion Rep. OWRR:A-037-NMEX, N. M. Water Resour. Res. Inst., Las Cruces.

Regione Le Marche (2010). Piano del Parco del Conero, Uso del Suolo attuale rilievo 2005. Ufficio Cartografia.

Regione Le Marge (2011). Piano tutela acque. Servizio Ambientale e Paesaggio. Information personally received from the cartography office.

Robson, S.G. (1974). Feasibility of Digital water quality modeling illustrated by application of Barstow, California, U.S. Geol. Surv. Water Resourc. Invest., 46-73.

Schultz, R.A., Fossen, H. (2008). Terminology for structural discontinuities. Geologic note. AAPG Bulletin, v. 92, no. 7 (July 2008), pp. 853-867.

Shackleton, J.R., Cooke, M.L., Verges, J., Simo, J.T. (2011). Temporal constraints on fracturing associated with fault related folding at Sant Corneli Anticline, Spanish Pyrenees Journal of Structural Geology, vol. 33, 5-19, doi:10.1016/j.jsg.2010.11.003

Tondi, E., Antonellini, M., Aydin, A., Marchegiani, L., Cello, G. (2006). The role of deformation bands, stylolites and sheared stylolites in fault development in carbonate grainstones of Majella Mountain, Italy. Journal of Structural Geology 28, 376-391.

Vacher, H.L. (1988). Dupuit-Ghyben-Herzberg analysis of strip-island lenses. Geological Society of America Bulletin, v. 100, p. 580 – 591.

Van Stempoort, D., Ewert, L., Wassenaar, L. (1993). Aquifer Vulnerability Index (AVI): A GIS compatible method for groundwater vulnerability maping. Can Water Res J., 18, 25 – 37.

Vías, J., Andreo, B., Ravbar, N, Hötzl, H. (2010). Mapping the vulnerability of groundwater to the contamination of four carbonate aquifers in Europe. Journal of Environmental Management, 91, 1500-1510.

Wang, X., Ghassemi, A. (2011). A three-dimensional stochastic fracture network model for geothermal reservoir stimulation. PROCEEDINGS, Thirty-Sixth Workshop on Geothermal Reservoir Engineering. Stanford University, Stanford, California, January 31 – February 2, 2011. SGP-TR-191.

Worthington, S.R.H., Ford, D.C. (2009). Self-Organized Permeability in Carbonate Aquifers. Ground Water, vol. 47, nº 3, pages 326-336.

Worthington, S.R.H., Gunn, J. (2009). Hydrogeology of Carbonate Aquifers: A Short History. Ground Water, vol. 47, nº 3, pages 462-467.

Xu, C., Dowd, P. (2010). A new computer code for discrete fracture network modelling. Computers & Geosciences 36, 292-301.

Yeo, I.W., Ge, S. (2005). Applicable range of the Reynolds equation for fluid flow in a rock fracture. Geosciences Journal. Vol. 9, Nº. 4, p. 347 – 352.

Yu, C., Yao, Y., Hayes, G., Zhang, B., Zheng, C. (2010). Quantitative assessment of groundwater vulnerability using index system and transport simulation,

Huangshuihe catchment, China. Science of the Total Environment, 408, 6108-6116.

APPENDIX

Table 0-1: Ranges and ratings for Depth to Water

Depth to water [Feet] (Weight: 5)	
Range	**Rating (D_R)**
0 – 5	10
5 – 15	9
15 – 30	7
30 – 50	5
50 – 75	3
75 – 100	2
100+	1

Table 0-2: Ranges and ratings for Net Recharge

Net Recharge [Inches] (Weight: 4)	
Range	**Rating (R_R)**
0 – 2	1
2 – 4	3
4 – 7	6
7 – 10	8
10+	9

Table 0-3: Ranges and ratings for Aquifer Media

Aquifer Media (Weight: 3)		
Range	**Rating (A_R)**	**Typical Rating (A_R)**
Massime Shale	1 – 3	2
Metamorphic/Igneous	2 – 5	3
Weathered Metamorphic/Igneous	3 – 5	4
Glacial Till	4 – 6	5
Bedded Sandstone, Limestone and Shale Sequences	5 – 9	6
Massive Sandstone	4 – 9	6
Massive Limestone	4 – 9	6
Sand and Gravel	4 – 9	8
Basalt	2 – 10	9
Karst Limestone	9 – 10	10

Table 0-4: Ranges and ratings for Soil Media

Soil Media (Weight: 2)	
Range	**Rating (S_R)**
Thin or Absent	10
Gravel	10
Sand	9
Peat	8
Shrinking and/or Aggregated Clay	7
Sandy Loam	6
Loam	5
Silty Loam	4
Clay Loam	3
Muck	2
Nonshrinking and Nonaggregated Clay	1

Table 0-5: Ranges and ratings for Topography

Topography [percent slope] (Weight: 1)	
Range	**Rating (T_R)**
0 – 2	10
2 – 6	9
6 – 12	5
12 – 18	3
18 +	1

Table 0-6: Ranges and ratings for Impact of the Vadose Zone Media

Impact of the Vadose Zone Media (Weight: 5)		
Range	**Rating (I_R)**	**Typical Rating (I_R)**
Confining Layer	1	1
Silt / Clay	2 – 6	3
Shale	2 – 5	3
Limestone	2 – 7	6
Sandstone	4 – 8	6
Bedded Limestone, Sandstone, Shale	4 – 8	6
Sand and Gravel with significant Silt and Clay	4 – 8	6
Metamorphic / Igneous	2 – 8	4
Sand and Gravel	6 – 9	8
Basalt	2 – 10	9
Karst Limestone	8 – 10	10

Table 0-7: Ranges and ratings for Hydraulic Conductivity

Hydraulic Conductivity [GPD/FT^2] (Weight: 3)	
Range	**Rating (C_R)**
1 – 100	1
100 – 300	2
300 – 700	4
700 – 1000	6
1000 – 2000	8
2000 +	10